GFZ

Helmholtz-Zentrum
POTSDAM

Sebastian Breitenbach

Changes in Monsoonal Precipitation and Atmospheric Circulation During the Holocene Reconstructed from Stalagmites from Northeastern India

Scientific Technical Report STR10/06

www.gfz-potsdam.de

HELMHOLTZ
| GEMEINSCHAFT

Sebastian Breitenbach

Changes in Monsoonal Precipitation and Atmospheric Circulation During the Holocene Reconstructed from Stalagmites from Northeastern India

Dissertation
zur Erlangung des akademischen Grades
Doktor der Naturwissenschaften (Dr. rer. nat.)
in der Wissenschaftsdisziplin Geologie

eingereicht an der Mathematisch-Naturwissenschaftlichen Fakultät
der Universität Potsdam

März 2009

Scientific Technical Report STR10/06

Changes in Monsoonal Precipitation and Atmospheric Circulation During the Holocene Reconstructed from Stalagmites from Northeastern India

DISSERTATION
ZUR ERLANGUNG DES AKADEMISCHEN GRADES
DOKTOR DER NATURWISSENSCHAFTEN (DR. RER. NAT.)
IN DER WISSENSCHAFTSDISZIPLIN GEOLOGIE

EINGEREICHT VON

SEBASTIAN BREITENBACH

AN DER MATHEMATISCH-NATURWISSENSCHAFTLICHEN FAKULTÄT DER UNIVERSITÄT
POTSDAM

MÄRZ 2009

Abstract

Recent years witnessed a vast advent of stalagmites as palaeoclimate archives. The multitude of geochemical and physical proxies and a promise of a precise and accurate age model greatly appeal to palaeoclimatologists. Although substantial progress was made in speleothem-based palaeoclimate research and despite high-resolution records from low-latitudinal regions, proving that palaeoenvironmental changes can be archived on sub-annual to millennial time scales our comprehension of climate dynamics is still fragmentary. This is in particular true for the summer monsoon system on the Indian subcontinent. The Indian summer monsoon (ISM) is an integral part of the intertropical convergence zone (ITCZ). As this rainfall belt migrates northward during boreal summer, it brings monsoonal rainfall. ISM strength depends however on a variety of factors, including snow cover in Central Asia and oceanic conditions in the Indic and Pacific. Presently, many of the factors influencing the ISM are known, though their exact forcing mechanism and mutual relations remain ambiguous. Attempts to make an accurate prediction of rainfall intensity and frequency and drought recurrence, which is extremely important for South Asian countries, resemble a puzzle game; all interaction need to fall into the right place to obtain a complete picture. My thesis aims to create a faithful picture of climate change in India, covering the last 11,000 ka.

NE India represents a key region for the Bay of Bengal (BoB) branch of the ISM, as it is here where the monsoon splits into a northwestward and a northeastward directed arm. The Meghalaya Plateau is the first barrier for northward moving air masses and receives excessive summer rainfall, while the winter season is very dry. The proximity of Meghalaya to the Tibetan Plateau on the one hand and the BoB on the other hand make the study area a key location for investigating the interaction between different forcings that governs the ISM.

A basis for the interpretation of palaeoclimate records, and a first important outcome of my thesis is a conceptual model which explains the observed pattern of seasonal changes in stable isotopes (δ^{18}O and δ^2H) in rainfall. I show that although in tropical and subtropical regions the amount effect is commonly called to explain strongly depleted isotope values during enhanced rainfall, alone it cannot account for observed rainwater isotope variability in Meghalaya. Monitoring of rainwater isotopes shows no expected negative correlation between precipitation amount and δ^{18}O of rainfall. In turn I find evidence that the runoff from high elevations carries an inherited isotopic signature into the BoB, where during the ISM season the freshwater builds a strongly depleted plume on top of the marine water. The vapor originating from this plume is likely to 'memorize' and transmit further very negative δ^{18}O values. The lack of data does not allow for quantification of this 'plume effect' on isotopes in rainfall over Meghalaya but I suggest that it varies on seasonal to millennial timescales, depending on the runoff amount and source characteristics.

The focal point of my thesis is the extraction of climatic signals archived in stalagmites from NE India. High uranium concentration in the stalagmites ensured excellent age control required for successful high-resolution climate reconstructions. Stable isotope (δ^{18}O and δ^{13}C) and grey-scale data allow unprecedented insights into millennial to seasonal dynamics of the summer and winter monsoon in NE India. ISM strength (i. e. rainfall amount) is recorded in changes in δ^{18}O$_{stalagmites}$. The δ^{13}C signal, reflecting drip rate changes, renders a powerful proxy for dry season conditions, and shows similarities to temperature-related changes on the Tibetan Plateau. A sub-annual grey-scale profile supports a concept of lower drip rate and slower stalagmite growth during dry conditions.

During the Holocene, ISM followed a millennial-scale decrease of insolation, with decadal to centennial failures resulting from atmospheric changes. The period of maximum rainfall and enhanced seasonality corresponds to the Holocene Thermal Optimum observed in Europe. After a phase of rather stable conditions, ∼4.5 kyr ago, the strengthening ENSO system dominated the ISM. Strong El Niño events weakened the ISM, especially when in concert with positive Indian Ocean dipole events. The strongest droughts of the last ∼11 kyr are recorded during the past 2 kyr.

Using the advantage of a well-dated stalagmite record at hand I tested the application of laser ablation-inductively coupled plasma-mass spectrometry (LA-ICP-MS) to detect sub-annual to sub-decadal changes in element concentrations in stalagmites. The development of a large ablation cell allows for ablating sample slabs of up to 22 cm total length. Each analyzed element is a potential proxy for different climatic parameters. Combining my previous results with the LA-ICP-MS-generated data shows that element concentration depends not only on rainfall amount and associated leaching from the soil. Additional factors, like biological activity and hydrogeochemical conditions in the soil and vadose zone can eventually affect the element content in drip water and in stalagmites. I present a theoretical conceptual model for my study site to explain how climatic signals can be transmitted and archived in stalagmite carbonate. Further, I establish a first 1500 year long element record, reconstructing rainfall variability. Additionally, I hypothesize that volcanic eruptions, producing large amounts of sulfuric acid, can influence soil acidity and hence element mobilization.

Zusammenfassung

Stalagmiten erfuhren in den letzten Jahren vermehrt Aufmerksamkeit als bedeutende Paläoklima-Archive. Paläoklimatologen sind beeindruckt von der grossen Zahl geochemischer und physikalischer Indikatoren (Proxies) und der Möglichkeit, präzise absolute Altersmodelle zu erstellen. Doch obwohl substantielle Fortschritte in der speleothem-basierten Klimaforschung gemacht wurden, und trotz hochaufgelöster Archive aus niederen Breiten, welche zeigen, das Umweltveränderungen auf Zeitskalen von Jahren bis Jahrtausenden archiviert und rekonstruiert werden können, bleibt unser Verständnis der Klimadynamik fragmentarisch. Ganz besonders gilt dies für den Indischen Sommermonsun (ISM) auf dem Indischen Subkontinent. Der ISM ist heute als ein integraler Bestandteil der intertropischen Konvergenzzone verstanden. Sobald dieser Regengürtel während des borealen Sommer nordwärts migriert kann der ISM seine feuchten Luftmassen auf dem Asiatischen Festland entladen. Dabei hängt die Stärke des ISM von einer Vielzahl von Faktoren ab. Zu diesen gehören die Schneedicke in Zentralasien im vorhergehenden Winter und ozeanische Bedingungen im Indischen und Pazifischen Ozean. Heute sind viele dieser Faktoren bekannt. Trotzdem bleiben deren Mechanismen und internen Verbindungen weiterhin mysteriös. Versuche, korrekte Vorhersagen zu Niederschlagsintensität und Häufigkeit oder zu Dürreereignissen zu erstellen ähneln einem Puzzle. All die verschiedenen Interaktionen müssen an die richtige Stelle gelegt werden, um ein sinnvolles Bild entstehen zu lassen. Meine Dissertation versucht, ein vertrauenswürdiges Bild des sich wandelnden Holozänen Klimas in Indien zu erstellen.

NE Indien ist eine Schlüsselregion für den östlichen Arm des ISM, da sich hier der ISM in zwei Arme aufteilt, einen nordwestwärts und einen nordostwärts gerichteten. Das Meghalaya Plateau ist das erste Hindernis für die sich nordwärts bewegenden Luftmassen und erhält entsprechend exzessive Niederschläge während des Sommers. Die winterliche Jahreszeit dagegen ist sehr trocken. Die Nähe zum Tibetplateau einerseits und der Bucht von Bengalen andererseits determinieren die Schlüsselposition dieser Region für das Studium der Interaktionen der den ISM beeinflussenden Kräfte. Ein Fundament für die Interpretation der Paläoklimarecords und ein erstes wichtiges Ergebnis meiner Arbeit ist ein konzeptuelles Modell, welches die beobachteten saisonalen Veränderungen stabiler Isotope (δ^{18}O und δ^{2}H) im Niederschlag erklärt. Ich zeige, das obwohl in tropischen und subtropischen Regionen meist der amount effect zur Erklärung stark negativer Isotopenwerte während starker Niederschläge herangezogen wird, dieser allein nicht ausreicht, um die Isotopenvariabilität im Niederschlag Meghalaya's zu erklären. Die Langzeitbeobachtung der Regenwasserisotopie zeigt keine negative Korrelation zwischen Niederschlagsmenge und δ^{18}O. Es finden sich Hinweise, das der Abfluss aus den Hochgebirgsregionen Tibets und des Himalaya eine Isotopensignatur an das Oberflächenwasser der Bucht von Bengalen vererbt. Dort bildet sich aus isotopisch stark abgereicherten Wässern während des ISM eine Süßwasserlinse aus. Es ist wahrscheinlich, das Wasserdampf, der aus dieser Linse stammt, ein Isotopensignal aufgeprägt bekommt, welches abgereicherte δ^{18}O weitertransportiert. Der Mangel an Daten lässt es bisher leider nicht zu, quantitative Aussagen über den Einfluss dieses 'plume effect' auf Niederschläge in Meghalaya zu treffen. Es lässt sich allerdings vermuten, das dieser Einfluss auf saisonalen wie auch auf langen Zeitskalen variabel ist, abhängig vom Abfluss und der Quellencharacteristik.

Der Fokus meiner Arbeit liegt in der Herauslösung klimatischer Signale aus nordostindischen Stalagmiten. Hohe Urankonzentrationen in diesen Stalagmiten erlaubt eine exzellente Alterskontrolle, die für hochauflösende Klimarekonstruktionen unerläßlich ist. Die stabilen Isotope (δ^{18}O und δ^{13}C), sowie Grauwertdaten, erlauben einmalige Einblicke in die Dynamik des Sommer und auch des Wintermonsun in NE Indien. Die ISM Stärke (d. h. Niederschlagsmenge) wird in Veränderungen in den $\delta^{18}O_{stalagmites}$ reflektiert. Das δ^{13}C Signal, welches Tropfratenänderungen speichert, dient als potenter Indikator für winterliche Trockenheitsbedingungen. Es zeigt ähnlichkeit zu temperaturabhängigen Veränderungen auf dem Tibetplateau. Das sub-annuell aufgelöste Grauwertprofil stärkt das Konzept, das verminderte Tropfraten und langsameres Stalagmitenwachstum eine Folge von Trockenheit sind. Während des Holozäns folgte der ISM der jahrtausendelangen Verringerung

der Insolation. Es finden sich aber ebenso rapide Anomalien, die aus atmosphärischen Veränderungen resultieren. Die Phase des höchsten Niederschlages und erhöhter Saisonalität korrespondiert mit dem Holozänen Thermalen Maximum. Nach einer Phase einigermaßen stabilen Bedingungen begann vor ca. 4500 Jahren ENSO einen zunehmenden Einfluss auf den ISM auszuüben. Starke El Niño Ereignisse schwächen den ISM, besonders wenn diese zeitgleich mit positiven Indian Ocean Dipole Ereignissen auftreten. Die stärksten Dürren des gesamten Holozäns traten in den letzten 2000 Jahren auf.

Um zusätzliche Informationen aus den hervorragenden Proben zu gewinnen nutzte ich die Vorteile der laser ablation inductively coupled plasma mass spectrometry (LA-ICP-MS). Diese erlaubt die Detektion sub-annueller bis sub-dekadischer Elementkonzentrationsveränderungen in Stalagmiten. Mittels einer neu entwickelten Ablationszelle konnten Proben von maximal 22 cm Länge untersucht werden. Jedes analysierte Element ist ein potentieller Träger einer Klimainformation. Die Kombination der früheren Ergebnisse mit denen der LA-IPC-MS zeigt, das die Elementkonzentrationen nicht nur von Niederschlagsveränderungen und assoziiertem Auswaschen aus dem Boden abhängen. Zusätzlich können auch die biologische Aktivität und hydrogeochemische Bedingungen in der vadosen Zone Einfluss auf die Elementzusammensetzung im Tropfwasser und in den Stalagmiten haben. Darum entwickelte ich ein theoretisches Modell für meinen Standort, um zu klären, wie Klimasignale von der Atmosphäre in die Höhle transportiert werden können. Ein anschliessend rekonstruierter 1500 Jahre langer Proxyrecord zeigt Niederschlagsvariabilität an. Zudem besteht die Möglichkeit, das Vulkaneruptionen, welche große Mengen an Schwefelsäure produzieren, eine Bodenversauerung verursachen und damit die Elementmobilisierung verstärken können.

Contents

List of Figures

List of Tables

Acknowledgements

Gerald Haug – you believed in my enthusiasm and let me go caving for palaeoclimate! Your perpetuating support made possible what otherwise would have ended as a mere idea. Thank you so much for introducing me to these other enthusiasts Jess Adkins and Detlef Günther and for re-alignment whenever I started to drift.

Jess Adkins – I always remember my very first experiences in a (your) clean lab! My visit at CalTech was one of the most exciting experiences in my life. You opened my geographical mind for analytical work. I am deeply indebted and grateful for your support, teaching, and interest in my work. Thank you!

Birgit Plessen! **THANK YOU** I cannot express how much your support, your experience and discussions pushed me! But most importantly you friendship helped me to keep going. Your faith in my strange ideas and your curiosity gave me self-confidence and optimism whenever it was critically necessary!

Hedi Oberhänsli, thank you for long and not always easy discussions! There were many helpful critics and I learned to see things from different angles.

Detlef Günther – you not only invited me to work with your group, but you spread so much positive energy that I perceived you as a 'idea-source', very similar to ion sources that so greatly help element analysis. Your non-traditional way of pushing ideas forward is highly inspiring, not to say infective.

Norbert (Dr. M.) Marwan – without your Matlab-Magic much would have been excessively difficult, even more would have proven impossible. I already wait for the next session at your command line! **Diego Fernandez** – you always had some precious time for many stupid questions. It was great pleasure for me to work with you!

Many others supported my work at GFZ and AWI Potsdam. **Andreas Hendrich** and **Manuela Dziggel** – your skills proved invaluable when it came to improve figures and solving graphic problems! Thank you very much! Without the help of **Peter Dulski**, **Rudolf Naumann**, **Sylvia Köhler**, **Petra Meier**, **Christine Gerschke**, **Gabi Arnold**, **Michael Köhler** and **Dieter Berger** many questions would still remain unanswered. You answered to my 'special requests' (almost) always with a smile. Ich bin gut

präpariert worden bei euch. **Hanno Meyer** helped with extremely rapid analyses and (together with **Thomas Opel** and **Lutz Schirrmeister**) many inspiring discussions. **Thank you all!**

Iris, **Susanne**, **Clara**, **Christian**, **Hans**, **Stefan**, **Gergana**, **Sascha** and **Andreas**! We had a lot of fun after work and whenever it came to social activities – I had a lovely time with you!

The **Günther Group**, especially **Mattias** and **Beni**! Your cheerful adsorption was overwhelming! Thank you again for all work and not-work activities... It was a wonderful experience to work and discuss with you, and to take part in wonderful social activities. I hope we will have much more of all this in near future!

Much support came from the **Speleoclub Berlin**. Your world-wide map-making activities make science possible in the first place and our active help during field work is highly appreciated. It's a pleasure to belong to such bunch of nerds! I especially thank **Denis Rayen**, **Brian Kharpran Daly** and **Herbert Daniel Gebauer**, as they shared their experiences and caves with me and supported all my sampling efforts in an invaluable way! Without you Daniel I would still search for the proper sample! I also thank the international speleo-community for manyfold informal support. **KEEP CAVING!**

My parents **Veronika** and **Andreas** always supported my wanderlust and my curiosity. Without your love and belief and also financial help I would not be where I am!

Ola my **Lieblings-Łabądź**! Your patience and love made this a 'mission possible'. I look forward to years of wonder and excitement with you!

YES WE CAN!

1 Introduction

"Wo nach leitenden Ideen das Studium chemischer Verbindungen erweitert wird, kann auch aus den engen Räumen unserer Laboratorien sich ein helles Licht über das weite Feld der Geognosie, über die große unterirdische, Gestein bildende und Gestein umwandelnde Werkstätte der Natur verbreiten."

(von Humboldt, 1845)

— Kosmos, p. 268 —

One of the most exciting questions in palaeoenvironmental sciences is how fast ecological changes can occur. What are their controlling mechanisms? What is their impact on human societies? Environmental perturbations may evolve at different pace: Sea-level fluctuations or alterations in the hydrological cycle, for example, can develop gradually over time periods of decades to millennia. Such variations are related to global climate conditions, and because of their relatively slow changes it would seem these were easier to adapt to.

Palaeoclimate archives prove however, that abrupt high-amplitude climatic swings occurred repeatedly in the past (Petit et al., 1999; NGRIP members*, 2004). When certain tipping points are surpassed, the Earth's climate system can react unpredictable and very fast, with serious ecological and economic consequences. It appears that in comparison to the last glacial cycle, the climate variability during the Holocene was significantly reduced (Petit et al., 1999). Yet again climate archives document that the Holocene climate was nothing but stable; gradually following orbitally-paced insolation changes it was interrupted by several significant events (Cullen et al., 2000; Fleitmann et al., 2008; Mayewski et al., 2004). Inter-annual variations of the monsoon system incessantly thread the Asian economies with droughts and floods (Thompson et al., 2000).

Such dynamics can challenge human adaptation abilities. Did these gradual and rapid changes have a direct influence on the human habitat? To what extent has climate variability to be taken into account when interpreting the history of past civilizations? Up to date, a number of studies, coupling palaeoclimate information with archaeological data, linked exceptional climate conditions to descent and collapse of ancient cultures (Cullen et al., 2000; Haug et al., 2003; Yancheva et al., 2007; Zhang et al., 2008). In this light, deciphering the climatic past does not only offer the means to understand climate dynamics at different timescales. It also allows unraveling the fate of historical societies in a changing environment.

The Asian tropics and sub-tropics with their rich history deserve special attention, as these societies have long suffered the direct consequences of changing climatic conditions. There has been a lively debate amongst palaeoclimatologists and archaeologists on the role of climate on the downfall of the Indus culture (Brooks, 2006; Madella and Fuller, 2006; Possehl, 1997; Staubwasser et al., 2003; Weiss et al., 1993). Still, evidence from available Holocene palaeoclimate records from the Indian sub-continent is insufficient to constrain

any compelling hypothesis. Regional to global comparisons are hampered by sub-optimal time-resolution and chronological uncertainties of the available records (Enzel et al., 1999; Gupta et al., 2003; Ramesh, 2001). The use of stalagmites takes advantage of absolute U-series dating routines that allow very high accuracy and precision. Such terrestrial high resolution multi-proxy reconstructions will shed light on the timing and spatial variability of climate dynamics on the Indian sub-continent.

1.1 Motivation of research

Focusing on regions dominated by monsoonal influence, and particularly on the Indian sub-continent, I comprehend palaeoclimate reconstructions as a 3-dimensional problem issuing space, timescales and quantitative approach.

First, a spatial dimension in palaeoclimate research is obvious: too few high-resolution records are available to understand monsoonal variability. In general, palaeodata coverage is sub-optimal for many of the key monsoonal regions. For example, the relationship between the hydrological budget of NE India and adjacent regions like the Indian mainland and Indonesia is still unclear. A second dimension concerns the chronology and timescales. Precisely dated high-resolution records are crucial for inter-comparison between palaeo-climate archives. On the other hand, to fully understand teleconnections and possible thresholds for rapid climate shifts, longer time series are required. A third dimension pertains to the quantitative reconstruction of climate change. Multi-proxy, multi-archive approaches are crucial to extract information from palaeo-records. However, we need to understand the relationship between modern sediments and meteorological parameters in order to obtain quantitative data, which are essential for testing climate model predictions. The appropriate strategy to remedy above mentioned issues involves not only the common multi-proxy approach but calls for an extensive networking between different scientific disciplines.

The first and second steps can be reached by integrating information from terrestrial archives, such as stalagmites, tree ring and well-dated lake sediments. Developing novel climate proxies and broadening the scope of applied methods will surely facilitate this task. Transects, connecting several locations, could help to understand the spatial connections between the Indian summer monsoon (ISM) and other important components of the climate system like the Tibetan High or the North Atlantic. Moreover, long-term ISM changes can be revealed using replicated and stacked records. Such long profiles will offer answers about the co-variability and magnitude of climatic changes on glacial-interglacial timescales. Last but not least as stalagmites and tree rings can be dated using both, absolute and radioisotope methods, paired dating could contribute to the ^{14}C and ^{10}Be calibration. The solution of the third issue lies in a combination of study site monitoring and the development of transfer functions. First, monitoring of hydro-chemical parameters enables the calibration of different properties against meteorological and hydrological observations (Mattey et al., 2008a). Then, the application of transfer functions, extrapolat-

ing these relations down-core will ultimately provide quantitative estimates of past climate change. Keeping in mind potential difficulties, I tried throughout my PhD project to address this 3-dimensional problem. When I started my search for suitable samples the large number of caves in Meghalaya (Gebauer, 2008; Kharpran Daly, 2006) and Gebauer (personal communication), a heart region of Indian summer monsoon, immediately caught my interest. Working with a particular site (southern Meghalaya) and archive (stalagmites), and within a particular time-frame (the last 11,000 years) I was able to focus on more specific questions. Some of the enquiries were clear from the very beginning; others were born as a side effect of the interpretation process. Eventually all of them refer to the complex nature of palaeoclimate records and provide a red line so much needed to understand it:

- What are the main factors influencing sub-tropical stalagmite isotope records? Is it possible to determine and distinguish between the 'amount effect' and site-specific effects, like for example moisture source dynamics?

- Can stable isotope (δ^{18}O, δ^{13}C) records from Meghalayan speleothems be explained in terms of climate variability? If so, to what extent does this variability reflect ISM changes?

    – What is the natural variability of the ISM on millennial to sub-decadal timescales? Is the ISM vulnerable to changes of other atmospheric features, like the Tibetan High? Is there a significant relation between ISM and large-scale climate modes, such as the Indian Ocean Dipole (IOD) and El Niño/Southern Oscillation (ENSO)?

    – Can we constrain the details of the relation between ISM and Asian summer monsoon (ASM)? The ISM comprises the Bay of Bengal (BoB) and the Arabian Sea branch. How closely are these two branches interconnected, and do they act in parallel?

    – How fast evolved ISM changes in the past? How dynamic was the system of the ISM? Did it respond gradually, or rather rapidly?

- During stalagmite growth abundant trace elements are incorporated into the carbonate lattice. What mechanisms are responsible for the element deposition? Can concentrations of some of these elements be used as novel palaeoclimate proxies?

1.2   Study area

Located in NE India (25.0°– 26.15°N, 89.45°– 92.47°E), Meghalaya (1000–1500 m above sea level (a.s.l.)) represents the first mountain barrier for northward moving clouds that leave the BoB (Fig. 1.1). It is the steep gradient from the lowlands of Bangladesh (∼20 m a.s.l.) that leads to excessive rainfall during the ISM on the Plateau (Fig. 1.2). Indeed, the

Figure 1.1: Map, depicting Asia and the major circulation features. The westerlies are shown as brown, the Indian and Chinese summer monsoons as blue arrows. The dashed blue line represents the mean boreal summer position of the ITCZ.

worldwide highest amount of rainfall has been recorded at Cherrapunji (26,461 mm, Murata et al. (2008); Prokop and Walanus (2003)). The rainfall is very unevenly distributed over the seasons; less than 100 mm/month are recorded between December and March, while >1000 mm/month fall during the ISM (late May to September). This seasonality of the rainfall causes severe flooding in the adjacent lowlands of Bangladesh (Murata et al., 2008) and a shortage of water during the dry season on the Plateau. The use of caves as underground water reservoirs (Breitenbach and Gebauer, 2007; Gebauer, 2008) is a visible expression of this penury.

Up to ∼900–1000 m a.s.l., the Plateau's flora is characterized by sub-tropical dense broadleaved forest. At higher altitudes, the vegetation is represented by pine forest (*Pinus kesiya*). Both, intense agricultural development and coal mining activity lead to extensive deforestation, which in turn results in rapid nutrient loss and soil degradation (Khiewtam and Ramakrishnan, 1993; Ramakrishnan and Ram, 1988). At the Plateau's southern rim highly karstified Eocene limestone is found, often covered by several meters of sandstone, interbedded by coal seams (Singh and Singh, 2000). Detailed accounts on the limestone geology of Meghalaya are compiled in Gebauer (2008). To date, several hundred caves have been registered in Meghalaya (Gebauer, 2008; Kharpran Daly, 2006), including the longest cave of India (Liat Prah Cave, 29,774 m; Gebauer, personal communication).

For palaeoclimate studies I selected Krem Umsynrang cave (Fig. 1.1; 25°13' N, 92°21' E; 825 m a.s.l., ∼25 km SE of Jowai, near Chieruphi, Frank and Becher (1998)). It is located
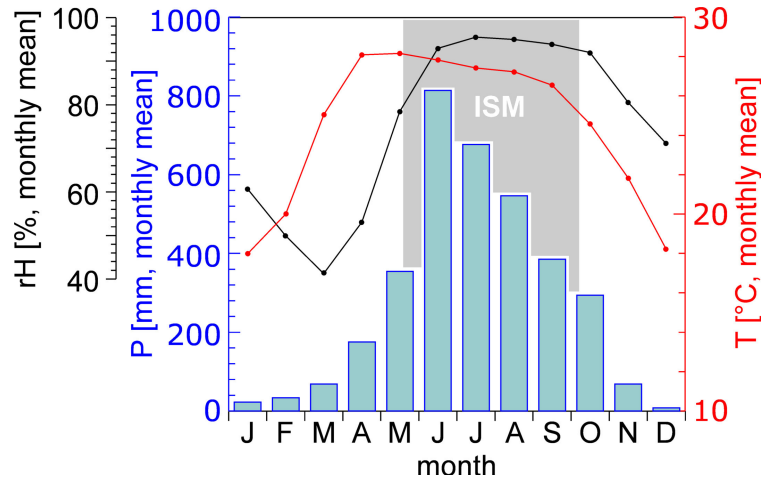
Figure 1.2: Climate conditions at Jowai, ∼25 km NW of Krem Umsynrang Cave (25°25'59.9" N, 92°12'1.7" E, 1334 m a.s.l.). T and rH data (monthly means for the period 1961–1990) are taken from NCEP/NCAR (Kalnay et al., 1996), rainfall data (mean monthly values for the period 1901–1930, $\Sigma_{1901-1930}$= 3445.2 mm) from KNMI (`http://climexp.knmi.nl/start.cgi?someone@somewhere`). The shaded area depicts the ISM season in the area.

in a relatively less populous area and richly decorated with a variety of speleothems. The cave's network of passages developed in limestone, which is overlain by ∼40 m of sandstone. The sandstone is intercalated by a 50 cm thick coal seam. The entire hostrock suite belongs to the Lakadong member of the Shella formation (middle Eocene, Jaintia group) (Gebauer, 2008; Singh and Singh, 2000). The sub-horizontal passages of Krem Umsynrang cave have been mapped to a length of 5.6 km (Kharpran Daly, 2006). Three passage levels are developed, the lowermost of which is actively eroded by a small rivulet (Fig. 1.3). Many active and inactive stalagmites can be found on all of the cave levels. The presence of broken, cant over stalagmites likely documents the seismic activity of the region. The mean cave air temperature of 20.6±0.6°C is somewhat lower than the mean air temperature at the surface (∼25°C at Jowai, Fig. 1.2). Both, grassland and tropical evergreen forest are found above the cave, the latter being restricted to shadowy dolines which retain moisture over the dry season. It is likely that this situation reflects human influence, rather than natural vegetation distribution.

1.3 Modern ISM conditions

For the Indian sub-continent, the ISM is the most important climate feature in terms of recurring seasonal winds and rainfall. The monsoon over India is developed as two separate arms, the Arabian Sea and the BoB branch, reaching from the Indian Ocean into the sub-continent (Fig. 1.1). The ISM depends to some extent on the snow conditions in Central Asia and the Himalaya in the preceding spring (Blanford, 1884; Gadgil, 2003; Walker, 1918). The extent of snow cover and the timing of snow melt reflect the strength
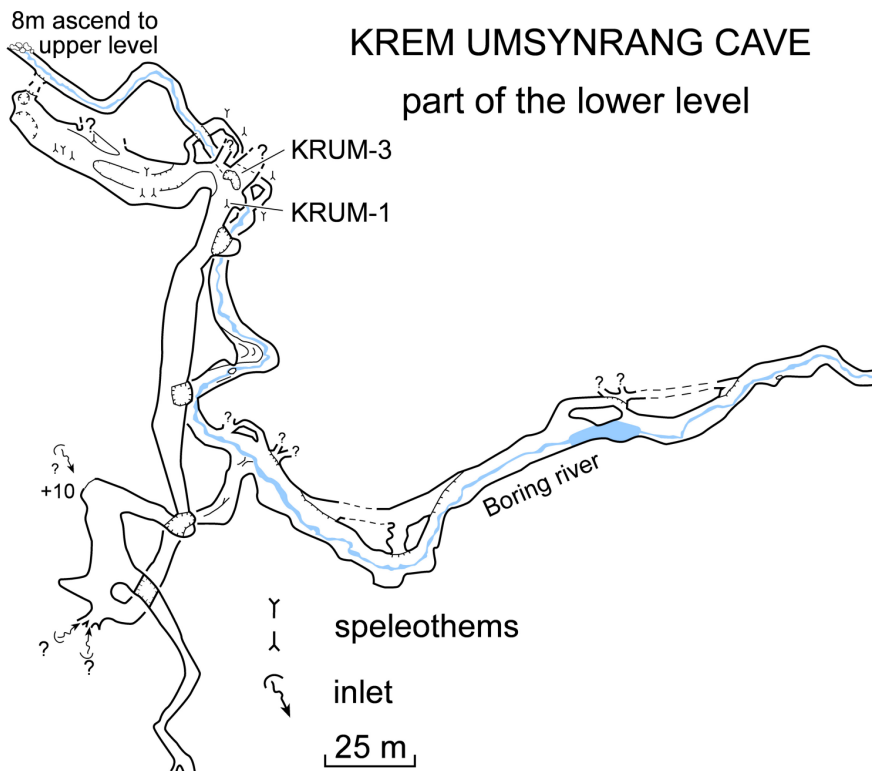
Figure 1.3: Plan view of a part of Krem Umsynrang Cave. The position of installed data loggers is the same as the assigned stalagmite samples (adopted 2009, after Gebauer, personal communication).

of the winter high pressure conditions over the Central Asian region (Dash et al., 2005). Only when this high pressure system decays, the northward-migrating ITCZ (Fig. 1.1) can push the ISM into the Indian sub-continent. The seasonal northward migration of the ITCZ seems to be one major factor that determines the strength of the ISM. Today, the summer monsoon is understood as an integral part of the ITCZ (Fleitmann et al., 2007). Still, other influencing factors, which are not sufficiently understood, modify the ISM behavior. For example, the amount of monsoonal rainfall over India is modulated by the oceanic conditions in the Indian and Pacific Oceans. Consequently, the ISM is dependent on the IOD (Abram et al., 2007; Saji et al., 1999) and ENSO, factors that govern the surface ocean conditions in the equatorial Indian Ocean and in the Pacific respectively. Both, IOD and ENSO alter the ISM, but their role varies with time and is not fully understood (Krishna Kumar et al., 1999). Furthermore, the ISM is influenced by the westerlies (Dash et al., 2005) which are in turn closely related to North Atlantic climate conditions. The extent of this influence also remains ambiguous.

Meteorological work has been centered mainly on the core region of ISM rainfall (ISMR), excluding NE India and the Himalaya (Gadgil, 2003; Goswami et al., 2006; Yadav, 2009). However, central Indian climate records are likely not representative for regions such as Bangladesh and NE India. Although important advances in meteorology have been made

during the past century, the ISM is still unpredictable. Individual years receive enormous water masses, for example, in 1998 ∼70 % of Bangladesh was inundated (Bates et al., 2008). Other years (e.g. 2001) are dangerously deficient in rainfall, with drought in its wake (Agrawala et al., 2001). Much of the attention of meteorologists and modelers was therefore focused on ISM forecasting, as a successful prognosis is of great economic value (Krishna Kumar et al., 2006; Singh and Singh, 2007; Webster et al., 1998). The timely onset and strength of ISM determine the crop yield in countries around the BoB (Krishna Kumar et al., 2006).

Unfortunately, the input data for models is largely restricted to available meteorological recordings of (at best) 150 years. These latest centuries are influenced by anthropogenic factors and probably not representative for the natural conditions. If we are to understand the natural long-term variability of the ISM much longer (palaeoclimate) records are required.

1.4 Palaeoclimate information on Indian climate – State of the art

Archives that record past climate of the Indian sub-continent unequivocally and over long time periods are rare (Fleitmann et al., 2007). There are manifold reasons for this scarcity. Marine sediments offer sub-optimal information about climate on the continents. Often, they represent wind-proxies and do not give insight into rainfall variations (Staubwasser, 2006). Lakes, containing long undisturbed sediment records, are seldom found in this region, and/or their chronology is less well constraint (Prasad and Enzel, 2006; Staubwasser, 2006). As India is a densely populated country, lake archives are often disturbed by human activity during several hundreds, if not thousands of years. Ice core records from Tibet (Aizen et al., 2006; Thompson et al., 2000; Yang et al., 2008) document climate conditions at high altitudes, but are not necessarily representative for the tropical and sub-tropical lowlands. Drought and flooding are however features of the coastal regions with extremely high population density, e. g. Bangladesh with estimated 1002.2 people/km^2 (EEDRB, 2006).

To find a remedy for many of these above mentioned issues, cave deposits from carefully selected sites provide excellent climate archives. Caves are distributed over ∼15 % of the continental area, including the Indian sub-continent (Ford and Williams, 2007). Stalagmites and flowstones are often found undisturbed by human and record climate-dependent parameters on timescales from seasons to tens of thousands of years (Dorale et al., 2007; Fairchild et al., 2007). Stephen Burns and his group traced the Holocene monsoon history in Oman using stable isotope records from stalagmites (Burns et al., 2003; Fleitmann et al., 2007, 2003a; Neff et al., 2001). They found several centennial-scale events of ISM weakening during the Holocene, superimposed on a gradual millennial-scale shift to weaker ISM conditions (Fleitmann et al., 2007, 2008). This weakening has been associated with
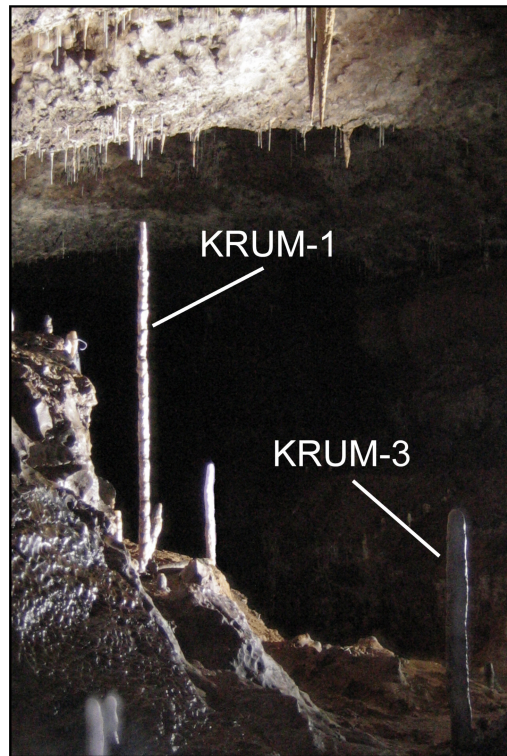
Figure 1.4: Krem Umsynrang Cave. The photograph depicts the two stalagmite samples KRUM-1 and KRUM-3, both collected in 2006. KRUM-1 is ~185 cm, KRUM-3 is ~64 cm long.

changes in insolation and a subsequent southward mean position of the ITCZ (Fig. 1.1). The results from Oman are essential for the reconstruction of the variability of the Arabian Sea branch of the ISM. Yet it remains unknown if they are equally valid for the BoB branch of the ISM. Central India only recently came into focus of speleothem-based palaeoclimate studies (Sinha et al., 2007; Yadava and Ramesh, 2005). These works underline the importance of detailed tracing of ISM history, and the quality of stalagmites as climate archives. Unfortunately, these records reach only back into the late Holocene and leave questions about the spatial characteristics of ISM dynamics unanswered.

Continuous well-dated high-resolution records from the Indian periphery can fill this gap of knowledge on ISM variability. In addition, NE India is a key-region for tracing air-mass transport from the BoB into south China and onto the Tibetan Plateau. Understanding the contribution of the ISM to rainfall in China can help to reduce forecasting uncertainties. Clearly, there are large gaps in spatial coverage of high-resolution records in the eastern Indian Ocean and adjacent lands.

1.5 Sample material and methods

The sampling site in Krem Umsynrang is located several hundred meters inside the cave at the second (middle) level (Figs. 1.3 and 1.4), which is inaccessible to local people and not

affected by flooding and measurable air movements. Stalagmites KRUM-1 ($\sim$185 cm long) and KRUM-3 ($\sim$64 cm long) were both wet when collected, hence presumably actively growing. Both stalagmites are composed of aragonite, revealed by micro X-ray diffraction (μXRD) analyses. Several other stalagmite samples were collected, but most contain too few uranium to be dated accurately. Sample KRUM-1 grew on a sandy-clayey terrace remnant, while KRUM-3 grew $\sim$4 m apart on limestone host rock.

Although this study focuses on the stable isotopic signature (δ^{18}O, δ^{13}C) in the stalagmites, a variety of accompanying methods has been employed to answer questions regarding mineralogy, chronology, element concentration and variability, and annual banding (Fig. 1.5). Parallel to the palaeoclimate studies, rainwater monitoring was started in 2007 near the study area. Modern observations allow us to interpret the variability of the isotopic signature in precipitation and subsequently in the stalagmites.

The flow diagram of Figure 1.5 gives a comprehensive overview on the methods that I utilized. To facilitate transport after collecting, the whole stalagmites were broken into several pieces. In the laboratory, the samples were cut lengthwise. μXRD is a non-destructive method that allows the qualitative identification of individual mineral phases (Hardy and Tucker, 1988). In the case of stalagmites, it differentiates the mineral phases of calcium carbonate (calcite and aragonite) that occur under natural conditions in caves. Knowledge about the mineralogy is crucial as co-occurrence of both mineral phases may render a sample futile for isotopic studies, because isotopic fractionation occurs in the calcite-aragonite system (Kim et al., 2007).

Further, I took sub-samples from both stalagmites for uranium concentration analysis using inductively coupled plasma mass spectrometry (ICP-MS). With known uranium concentration the optimal sample size for U/Th dating can be calculated (Dorale et al., 2007). In a further step, samples were drilled for multi-collector ICP-MS (MC-ICP-MS) U/Th dating and stable isotope analyses. With the advantage of highly precise and accurate isotope ratio analysis and higher sample-throughput compared to thermal ionization mass spectrometry, MC-ICP-MS is now widely used for uranium-series dating (Dorale et al., 2007). Sample preparation includes sample dissolution and spiking, chemical separation of uranium and thorium using ion-exchange resin columns, followed by isotope ratio mass spectrometry. Linear interpolation between discrete dates is used to determine ages for the various proxy samples. Growth banding is revealed by microscopy or high-resolution imaging. Near-UV blue light microscopy was used in search for organic inclusions, known to fluoresce at certain excitation and emission wavelengths (Shopov, 2005). KRUM-3 was scanned at high resolution (4800 dpi) for grey-scale analysis. The counting of individual dark and bright layers and comparison with the U/Th model confirmed that the layers are annual. Therefore, layer counting was performed to establish an independent chronology for sample KRUM-3.

The stable carbon and oxygen isotope ratios (δ^{18}O, δ^{13}C) are routinely analyzed using
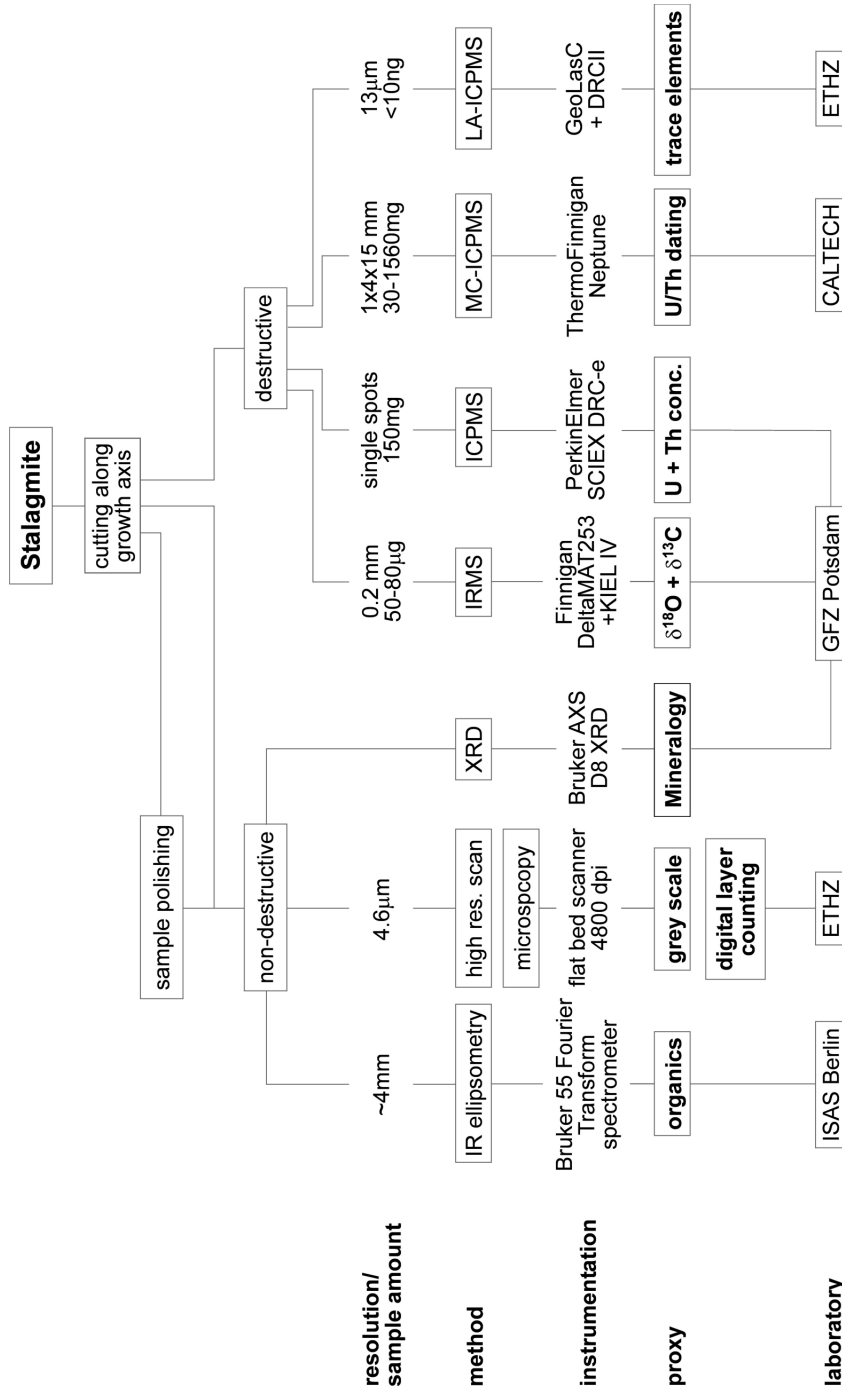
Figure 1.5: The different methods used in this thesis are shown together with the spatial resolution and/or sample amount, the instruments used, the proxies, and the different laboratories.

isotope ratio mass spectrometry (IRMS) with an attached carbonate preparation device. We used a Finnigan DeltaMAT253 + Kiel IV device for analyzing the stalagmite carbonates. The isotope ratios (^{18}O/^{16}O and ^{13}C/^{12}C) are reported in δ-notation[1] relative to the Vienna Pee Dee Belemnite (‰ VPDB) standard. The isotopic variability in KRUM-3 and KRUM-1 reflects changes of ISM strength during the entire Holocene.

Laser ablation ICP-MS (LA-ICP-MS) analysis is increasingly used to gain highest time-resolution (sub-annual to sub-decadal). However, before analyzing large stalagmite samples a new ablation cell had to be designed. LA-ICP-MS allows for quasi-simultaneous analysis of up to 50 isotopes, including major, minor, trace, and rare earth elements. Laser ablation work was accompanied by micro-X-ray fluorescence (μXRF) studies to validate concentration changes of selected major elements. These latter analyses were conducted on an EAGLE III XXL[2].

In an experimental study, infra red (IR) ellipsometry was tested as a method for non-destructive analysis of organic compounds in stalagmites. Ellipsometry is used to study the molecular composition of ultra-thin surfaces by analysis of the absorption characteristics (Hinrichs et al., 2005). While IR-ellipsometry is useful for investigating mineral phases, much pioneering work is required before this method can be applied for analysis of organic matter in speleothems, which is beyond the scope of this thesis.

1.6   Organisation of manuscripts

The manuscripts my thesis is based upon are structured as follows:

Manuscript #1 gives an overview on stable isotopes in precipitation and the factors influencing the isotopes (δ^{18}O and δ^2H) in rainwater over the BoB and adjacent northeastern India. This paper provides a detailed insight into the seasonal dynamics of the isotopic signature at the moisture source (the BoB) for the precipitation over the cave. This work is regarded as an introduction into the stable isotopy of rainwater in NE India.

Manuscript #2 is the main outcome of my PhD and focuses on changes in δ^{18}O, δ^{13}C, and grey scale values in two stalagmites from NE India. The stalagmites comprise the first well-dated continuous high-resolution palaeoclimate records from the BoB region that cover the entire Holocene. The record proves the dependence of the ISM on the mean position of the ITCZ and a gradual weakening of the strength of the ISM during the Holocene. Centennial and decadal-scale excursions point to severe droughts in the climate history of India. The last two millennia experienced enhanced ISM variability, with conditions often much drier than today.

Manuscript #3 is an attempt to interpret a variety of elements, analyzed using LA-ICP-MS, in a palaeoclimatological sense. The high resolution of this method allows the reconstruction of sub-annual to sub-decadal element concentrations changes. The climatic interpretation however is hampered by the complex nature of influencing factors. To es-

---

[1]δ=((R$_{sample}$)/R$_{standard}$)-1)$\times$1000
[2]I appreciate the support by the Landesmuseum Affoltern, Switzerland!

tablish elements as useful tracers for (palaeo-) climate signals, one must have thorough knowledge of their sources and sinks (Beer et al., 2002). Here, the origin of the majority of elements analyzed is not clear. The unknown pathway of the percolating water from the soil to the cave may mask the climate signal on its way into the stalagmite. Such deficiencies have to be seized before an unequivocal interpretation can be made. The manuscript 3 gives an account on various parameters influencing element concentration changes. A conceptual model explains how climate signals may be transfered into the cave environment. I compare the LA-IPC-MS results with instrumental records from the region. Furthermore, the comparison of element concentrations with data from ice cores provides evidence that volcanic eruptions might by recorded in stalagmites. The various influencing factors however do not allow at this point to quantitative reconstructions and will be part of future studies.

2 Strong Influence of Water Vapor Source Dynamics on Stable Isotopes in Precipitation Observed in Southern Meghalaya, NE India

Sebastian F. M. Breitenbach[1,2,], Hanno Meyer[3], Norbert Marwan[4], Kanikicharla Krishna Kumar[5], Jess F. Adkins[6], Gerald H. Haug[2,7]*

[1] *Helmholtz Zentrum Potsdam, Deutsches GeoForschungsZentrum, 5.2 Climate Dynamics and Landscape Evolution Section, 14473 Potsdam, Germany*

[2] *DFG-Leibniz Center for Surface Process and Climate Studies, Institute for Geosciences, Potsdam University, 14476 Potsdam, Germany*

[*] *corresponding author: sebastian.breitenbach@gfz-potsdam.de, tel: ++47(0) 331 288 1347, fax: ++47(0) 331 288 1302*

[3] *Alfred Wegener Institute for Polar and Marine Research, Telegrafenberg, Potsdam, Germany*

[4] *Potsdam Institute for Climate Impact Research (PIK), 14412 Potsdam, Germany*

[5] *Indian Institute for Tropical Meteorology, Pune, India*

[6] *California Institute of Technology, GPS Division, E. California Blvd. 1200, CA 91125, USA*

[7] *Geological Institute, Department of Earth Sciences, ETH Zürich, 8092 Zürich, Switzerland*

Abstract

To understand the moisture regime over the northern Bay of Bengal (BoB) we analyze $\delta^{18}O$ and $\delta^{2}H$ of rainwater, collected in 2007 and 2008 in NE India. To delineate potential moisture source regions, we use backward and forward trajectory computations. $\delta^{2}H$ values range from +18.5‰ to -144.4‰, while $\delta^{18}O$ varies between +0.8‰ and -18.8‰. The isotopic variability is explained to relate to moisture source dynamics. The Local Meteoric Water Line (LMWL) is found close to the Global Meteoric Water Line (GMWL). Late Indian summer monsoon (ISM) rainfall exhibits lowest $\delta^{18}O$ and $\delta^{2}H$ values during September–October, and is interpreted to reflect isotopic changes in the northern BoB. We propose a seasonally developing freshwater plume in the northern BoB, due to runoff from Tibet. Seasonal variability of the isotopic composition of BoB surface water influences the isotopic signature of ISM rainfall. Evidently we need to be cautions interpreting $\delta^{18}O$ and $\delta^{2}H$ time series only in terms of the 'amount effect' in subtropical regions. Regional effects such as a large freshwater plume need to be considered when strong seasonal runoff changes are observed in the source region of the water vapor. Possible effects due to

variable source vapor can further complicate interpretation. Palaeoclimatic stable isotope records from speleothems from NE India likely reflect both, a subordinate amount effect and the isotopic composition of the BoB freshwater plume.

2.1 Introduction

Northeastern India and Bangladesh are both characterized by seasonal recurrence of the summer monsoon, associated with heavy cyclones and annual floods. The variability of the Indian summer monsoon (ISM), its onset, duration, and failure has clear impacts on regional societies and agriculture (Butler, 1908; Mukherjee et al., 2007). To better understand and forecast monsoonal dynamics researchers dedicate much attention to reconstruct past climate conditions, linking terrestrial proxy records (e.g. stalagmites, lake sediments) to hydrological and meteorological conditions (Fleitmann et al., 2003b, 2007; Gupta et al., 2003; Sinha et al., 2007; Staubwasser and Weiss, 2007; Wang et al., 2005, 2008; Yancheva et al., 2007; Zhang et al., 2008).

Delineating the relationship between vapor source, amount effect (Dansgaard (1964), see below), and evaporation on synoptic timescales may help to understand the factors that lead to observed rainfall dynamics. In order to calibrate and quantify these dynamics modern regional hydrological conditions have to be known. Whereas Europe or Northern America are covered with a dense network of meteorological and hydrological stations, publicly available meteorological and hydrological data for NE India are limited. Early regional isotope studies (Bhattacharya et al., 1985; Krishnamurthy and Bhattacharya, 1991) give only short term results, whereas uninterrupted long-term records are lacking. Hitherto, stable isotope variability of Indian monsoonal precipitation has been characterized for few Indian stations (Araguaś-Araguaś et al., 1998; Bhattacharya et al., 2003; Datta et al., 1991).

The isotopic signature of precipitation provides valuable information about vapor source and atmospheric circulation pattern, and can therefore be used to reconstruct past climate conditions. δ^{18}O and δ^2H in precipitation show a distinct empirical relationship, described by the Global Meteoric Water Line (GMWL, δ^2H $= 8 \times \delta^{18}$O$+10$). This relation was first introduced for fresh surface waters, and later adopted for precipitation (Craig, 1961; Rozanski et al., 1993). Comparing precipitation isotope data with the GMWL helps to understand the precipitation history. On a local scale, several effects (such as moisture re-cycling, evaporation, and condensation) can lead to deviations from the GMWL, and the δ^{18}O–δ^2H relationship is then better described by a Local Meteoric Water Line (LMWL). This paper highlights initial isotopic results from rainwater samples, collected near Cherrapunji during 2007 and 2008. The purpose of sampling is the development of a long-term isotope curve for understanding seasonal and long-term variability of precipitation characteristics in this ISM key-region. A LMWL is constructed and results compared with published data from the region. A strong coupling is proposed between river runoff from the Tibetan Plateau, and the isotopic composition of sea surface water and subsequent

precipitation. A minor contribution by source and amount effects might be superimposed on moisture source dynamics. Seasonal isotope variations of the BoB freshwater plume seem to dominate observed changes of stable isotopes in precipitation in NE India.

The amount effect

A factor that strongly affects the isotopic composition of rainfall (δ^{18}O and δ^2H) in tropical and subtropical regions is the amount effect. Dansgaard (1964) was the first to note a negative correlation between δ^{18}O and mean monthly rainfall, leading to a distinct seasonality in stable isotopes in precipitation. He and later Rozanski et al. (1993) recognized several mechanisms responsible for this effect. First, with increasing convection intensity and higher cloud build-up, vapor cooling in the cloud will lead to depleted δ-values of the condensate. As the condensation also increases with cooling, a negative relationship can be observed between δ-values and the condensation amount. Second, smaller drops from light rainfall will earlier reach isotopic equilibrium with the vapor below the cloud. Third, evaporation of droplets in low humidity air increases the δ-values in the remaining droplet. Thus, dry season rainfall is likely enriched in ^{18}O and ^{2}H. Fourth, isotopic depletion of water vapor and subsequent rainfall with time is more likely in heavy showers. Dansgaard (1964) concluded that low δ-values in heavy tropical rainfall are the result of deep convectional cooling and reduced influence of enrichment processes. Risi et al. (2008) show that the amount effect is governed by processes related to fall and re-evaporation of droplets rather then processes occurring during air ascent in the cloud. This finding is similar to results of a numerical model for the amount effect, designed by Lee and Fung (2007) who conclude that the amount effect depends on drop size and degree of equilibration with the sub-cloud atmospheric layer.

The processes described above have different characteristic timescales at which they are effective. Thus, the question arises at what timescales the amount effect is best observed? Dansgaard (1964) and Rozanski et al. (1993) refer to monthly mean values for observing the amount effect. Risi et al. (2008) also suggest that the amount effect is optimally observed at intra-seasonal or longer timescales. The amount effect can be observed also on timescales of days in single storm events (Rozanski et al., 1993) but the above mentioned prolonged timescale has implications for the interpretation of the data presented here.

2.2 Geographical setting

The sampling site (825 meter above sea level (m a.s.l.), N 25°13'09", E 91°39'46") is located ∼500 m below and just south of the meteorological station at Cherrapunji (WMO station #42515 at 25.25' N, 91.73' E, 1313 m a.s.l., Fig. 2.1) at the south-facing ridge of the Meghalaya Plateau. Meghalaya receives enormous amounts of moisture from the BoB, the major moisture source during the whole year. The air masses coming from the south are split into a NE and a NW arm in front of the Himalaya. The orographic barriers of the Meghalaya Plateau and the Himalaya (Bookhagen et al., 2005), together with lifting of
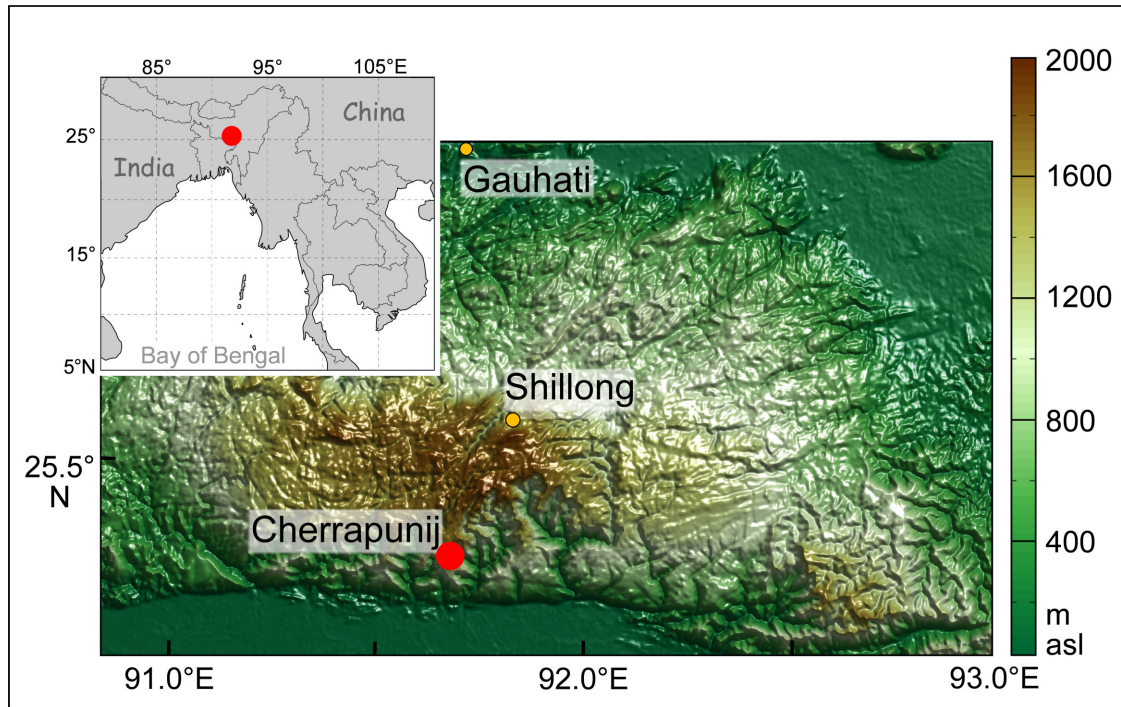
Figure 2.1: Map of the study area showing the Meghalaya Plateau as a digital elevation model (SRTM elevation data courtesy of the U. S. Geological Survey, http://seamless.usgs.gov/). The southern border shows the sharp contrast between the lowlands of Bangladesh and the Plateau.

unstable upstream air (Murata et al., 2008) lead to excessive windward rainfall. Located close to the Tropic of Cancer, this area experiences a strongly seasonal climate (Fig. 2.2). The meteorological year can be divided into three seasons: pre-monsoon (January to May), ISM (June to mid-October), and post-monsoon (mid-October to December) (similar to Mukherjee et al. (2007)). In the pre-monsoon season, local convectional storms add some moisture to the season's rainfall. During the ISM, the study area receives >80 % of its annual rainfall (Fig. 2.2). The ISM is governed by deep convection and cyclonic activity over the eastern and northwestern BoB, transporting large vapor masses to Meghalaya and onto the southeastern Tibetan Plateau (Tian et al., 2001a,b; Zhou and Yu, 2005; Yoon and Chen, 2005). Orographic rise leads to adiabatic cooling of the northward moving air masses and subsequently to heavy rainfall. For the rest of the year, relatively drier conditions prevail. During post-monsoon, occasional rainfall might occur, associated with atmospheric disturbances over the BoB. Very strong isotopic seasonality in precipitation, with very low ^{18}O and ^{2}H values during ISM, has been reported for N India and Nepal (Gajurel et al., 2006). The precipitation isotope signal in the study area is governed by seasonal changes of the vapor source and possibly by the amount effect (Aggarwal et al., 2004; Araguaś-Araguaś et al., 1998; Dansgaard, 1964; Mukherjee et al., 2007; Zhang et al., 2006). The GNIP mean oxygen isotopic composition of precipitation modeled for February falls between -2‰ to +2‰ VSMOW (Vienna Standard Mean Ocean Water) and for September -14‰ to -10‰ VSMOW (data from the International Atomic Energy
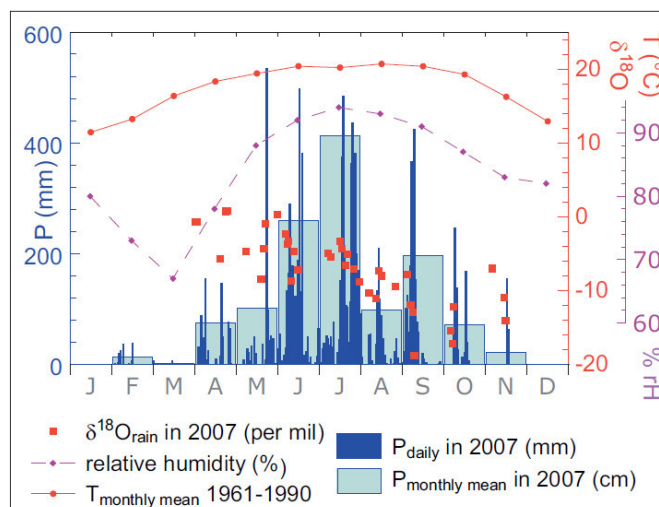
Figure 2.2: Climate diagram of Cherrapunji meteorological station (WMO station #42515) showing long term monthly temperature (T) mean and relative humidity (rH), monthly precipitation (P) for the year 2007, and all individual $\delta^{18}O$ (‰ VSMOW) measurements on rainwater in 2007. Annual rainfall exceeds 10,700 mm. Clearly seen is the strong seasonality, with excessive rainfall during the summer monsoon. Daily precipitation data is provided by the Pune Institute of Tropical Meteorology, temperature data is based on WMO data (`http://climexp.knmi.nl/data/t42515.dat`). Relative humidity data after Takahashi and Arakawa (1981).

Agency Global Network for Isotopes in Precipitation GNIP; IAEA/WMO (2001)). A temporal offset between highest rainfall and most negative ^{18}O is found at New Delhi, Mumbai, Shillong, in SW China, and Myanmar (Datta et al., 1991; Araguaś-Araguaś et al., 1998; Rozanski et al., 1993; Zhang et al., 2006). Strong seasonal changes are recorded in the BoB surface water, due to fluvial runoff of the Ganges-Brahmaputra river system, with subsequent changes in sea surface salinity (Delaygue et al., 2001) (Fig. 3). Salinity and ^{18}O variability exhibit a linear relationship, with both reacting on evaporational enrichment, runoff and rainfall depletion, and oceanic mixing (Delaygue et al., 2001). Additionally, Lawrence et al. (2004) show that in the tropics, the $^{18}O_{vapor}$ is only near equilibrium with sea water during quiescent weather, while it is not in equilibrium with seawater during stormy weather condition, but rather depleted by up to 15‰. They explain this effect by the exposure of water vapor to rainfall. Subsequent rainfall from such depleted vapor will be even more depleted.

2.3 Methods

2.3.1 Sampling and analysis

68 rainwater samples have been collected over the period from March 2007 to October 2008 (Tab. 2.1). One to twelve samples per month were collected, each representing snap-shots of individual rainfall events. Due to logistical restrictions, we conducted event-sampling
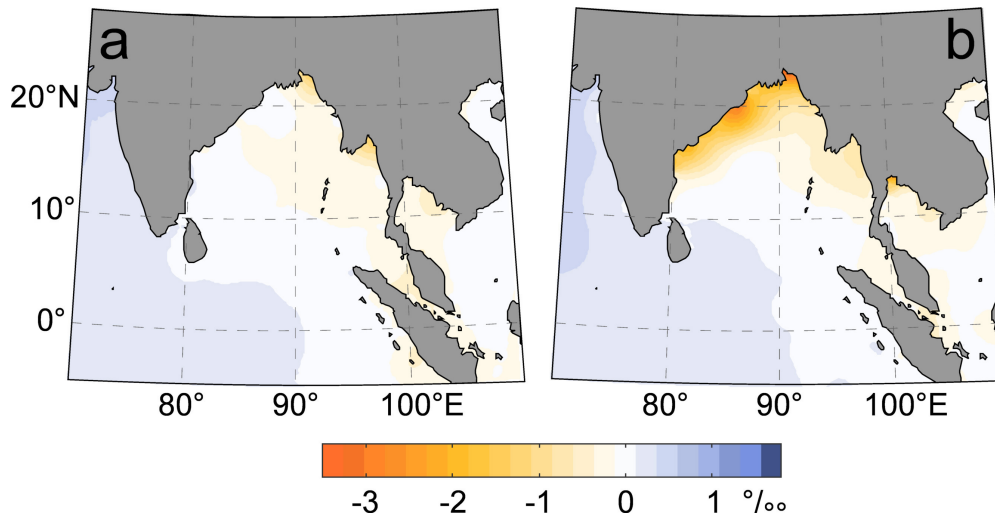
Figure 2.3: Contour map of the BoB showing strong seasonal variations of $\delta^{18}O_{surfacewater}$, inferred from the $\delta^{18}O$/salinity relationship alone; a proposed additional inherited $\delta^{18}O$ signal from the runoff water is not considered here. The $\delta^{18}O$ values were calculated using the relation $\delta^{18}O=0.18\times S$-5.9 (Delaygue et al., 2001) and sea surface salinity values given by NOAA (2005). **a) April** shows minimum runoff dilution effects, due to reduced runoff. **b) September** clearly reflects BoB $\delta^{18}O_{surfacewater}$ changes due to runoff from the Ganges-Brahmaputra river system. Minimal seasonal changes are seen in the Arabian Sea.

only, without volume and/or time integration. Some rain fall at the sampling site when no rainfall was recorded at the meteorological station Cherrapunji. The rainwater samples presented here have been collected mainly during pre-monsoon and the ISM, with very few samples representing the post-monsoon period. No samples were obtained between December 2007 and March 2008, and after October 2008. This unavoidably leads to a bias that has to be taken into account when interpreting the results. Samples of a volume of 60 ml were stored in sealed air-tight Nalgene® polypropylene bottles. Aliquots were analyzed for their stable isotope composition (δ^2H and $\delta^{18}O$, referring to the international standard VSMOW (Vienna Standard Mean Ocean Water)) at the Alfred Wegener Institute for Marine and Polar Research (AWI) Potsdam, Germany. A Finnigan MAT Delta-S mass spectrometer equipped with two equilibration units has been used for the online determination of hydrogen and oxygen isotopic composition. The external errors of long-term standard measurements for hydrogen and oxygen are better than 0.8‰ and 0.1‰ respectively (Meyer et al., 2000).

2.3.2 Trajectory computations

To deduce the probable source of the air masses from which our water samples derived, we generated backward trajectories based on the Hybrid Single-Particle Lagrangian Integrated Trajectories (HYSPLIT) ARL trajectory tool database of the National Oceanic and Atmospheric Administration (NOAA) (Fig. 2.4).

Table 2.1: δ^{18}O, δ^2H, and d excess in rainwater collected in 2007 and 2008.

Sample	Sampling date	Season†	Lab. Nr.	δ^{18}O (‰)‡	δ^2H (‰)‡	d excess
1	02.–03.04.2007	P	5756	-0.66	7.9	13.1
2	03.04.2007	P	5758	-0.65	5.5	10.7
3	20.04.2007	P	5759	-5.71	-28.8	16.9
4	24.04.2007	P	5760	0.72	18.0	12.2
5	25.04.2007	P	5764	0.76	18.5	12.4
6	09.05.2007	P	5765	-4.66	-20.7	16.6
7	20.05.2007	P	5766	-8.39	-54.8	12.3
8	22.05.2007	P	5768	-4.34	-15.7	19.0
9	23.05.2007	P	5769	-0.93	5.5	12.9
10	01.06.2007	M	5771	0.28	10.1	7.9
11	07.06.2007	M	5772	-2.35	-5.4	13.4
12	08.06.2007	M	5773	-3.73	-14.5	15.4
13	09.06.2007	M	5774	-3.33	-10.7	15.9
14	11.06.2007	M	5776	-8.71	-61.3	8.4
15	13.06.2007	M	5777	-4.64	-22.6	14.5
16	16.06.2007	M	5778	-7.23	-44.1	13.7
17	08.07.2007	M	5802	-4.94	-26.9	12.7
18	10.07.2007	M	5804	-5.43	-30.7	12.7
19	17.07.2007	M	5805	-3.35	-14.3	12.5
20	18.07.2007	M	5806	-4.37	-21.7	13.3
21	21.07.2007	M	5879	-6.56	-40.2	12.3
22	22.07.2007	M	5880	-5.06	-28.6	11.8
23	27.07.2007	M	5881	-7.07	-43.6	12.9
24	31.07.2007	M	5883	-8.78	-55.5	14.8
25	07.08.2007	M	5884	-10.35	-70.8	12.0
26	12.08.2007	M	5886	-11.07	-76.8	11.8
27	14.08.2007	M	5887	-7.31	-47.9	10.5
28	16.08.2007	M	5888	-8.01	-51.6	12.5
29	26.08.2007	M	5889	-9.39	-61.1	14.1
30	04.09.2007	M	5891	-7.87	-49.3	13.6
31	06.09.2007	M	5892	-11.92	-86.4	9.0
32	07.09.2007	M	5893	-11.98	-86.8	9.1
33	08.09.2007	M	5894	-12.97	-94.2	9.5
34	09.09.2007	M	5896	-18.82	-144.4	6.2
35	07.10.2007	M	5897	-15.43	-115.9	7.5
36	08.10.2007	M	5898	-17.19	-123.7	13.8

Tab. 2.1 – continued...

Sample	Sampling date	Season[†]	Lab. Nr.	$\delta^{18}O$ (‰)[‡]	δ^2H (‰)[‡]	d excess
37	09.10.2007	M	5971	-12.19	-83.3	14.2
38	06.11.2007	PM	5972	-7.00	-46.7	9.3
39	15.11.2007	PM	5973	-10.91	-78.5	8.8
40	16.11.2007	PM	5975	-14.06	-99.5	13.0
41	29.04.2008	P	14814	-3.31	-9.7	16.7
42	18.05.2008	P	14815	0.62	14.5	9.5
43	20.06.2008	M	14816	-3.07	-12.9	11.6
44	30.06.2008	M	14817	-4.01	-22.5	9.6
45	01.07.2008	M	14819	-5.21	-32.8	8.9
46	15.07.2008	M	14820	-5.57	-33.9	10.7
47	16.07.2008	M	14821	-4.53	-29.5	6.8
48	20.07.2008	M	14822	-4.85	-27.4	11.4
49	22.07.2008	M	14824	-3.92	-18.5	12.9
50	16.08.2008	M	14825	-5.10	-32.4	8.4
51	16.08.2008	M	14826	-6.66	-42.1	11.1
52	17.08.2008	M	14827	-6.71	-48.7	5.0
53	18.08.2008	M	14829	-5.90	-37.7	9.5
54	19.08.2008	M	14830	-7.96	-54.0	9.6
55	25.08.2008	M	14831	-6.92	-43.0	12.3
56	27.08.2008	M	14837	-4.94	-27.1	12.4
57	27.08.2008	M	14838	-6.61	-40.6	12.3
58	28.08.2008	M	14839	-8.45	-55.4	12.2
59	29.08.2008	M	14840	-9.27	-64.1	10.0
60	30.08.2008	M	14842	-6.40	-38.5	12.8
61	31.08.2008	M	14843	-2.58	-16.6	4.0
62	02.09.2008	M	14844	-5.95	-35.6	12.0
63	04.10.2008	M	14845	-12.71	-89.2	12.4
64	09.10.2008	M	14847	-5.64	-27.4	17.7
65	09.10.2008	M	14848	-5.57	-29.4	15.1
66	09.10.2008	M	14849	-4.15	-23.0	10.2
67	27.10.2008	PM	14850	-11.90	-80.9	14.3
68	28.10.2008	PM	14852	-15.00	-104.6	15.4
Average				**-6.73**	**-42.0**	**11.9**
STDEV				**4.25**	**34.4**	**2.9**

[†] P = pre-monsoon, M = monsoon, PM = post-monsoon. [‡] vs. SMOW

Trajectories for time periods of 56 to 98 hours were computed for 500, 1500, and 2500 m a.s.l., for rainfall is expected to originate from the latter altitudes. This exercise helped
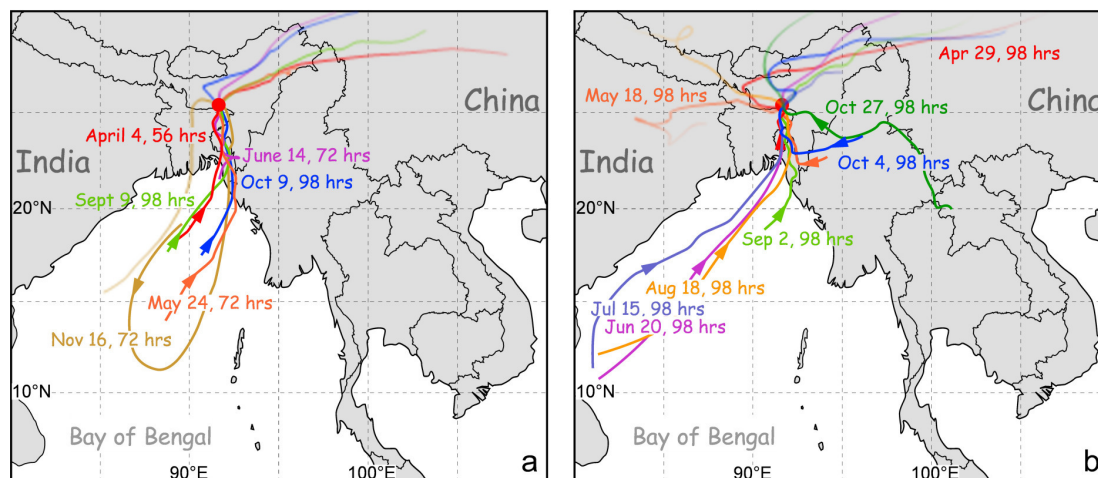
Figure 2.4: Trajectories (backward and forward) are plotted for the different months in which the water samples were collected. The computed trajectories (for 56 to 98 hours) faint in the direction the air masses advanced. GDAS1 meteorological data has been used for trajectory calculation. Trajectory labels show the month, day, and the length of the backward calculation (in hours). Trajectories were computed for 500 m (shown here), 1500, and 2500 m a.s.l. (not shown), using resources on the NOAA ARL website (http://www.arl.noaa.gov/ready/hysplit4.html).
a) In 2007 the source region did not change, as reflected by the comparison of the different trajectories. Air masses start over the BoB and head northeastward to Bangladesh before reaching Cherrapunji (red dot). The air is then transported NE-ward into southern China. Only with the onset of the post-monsoon period, the air is circled back to the BoB, due to strengthening of the Tibetan High.
b) In 2008 the ISM trajectories stem from the BoB, but several late ISM samples have their origin in South Asia. Mostly, the air is transported further NE, similar to 2007, but some trajectories show pathways northwestward along the Himalaya mountain chain.

to locate the likely major source region for the water vapor of our samples. Noteworthy, backward trajectory analysis indicates only the synoptic situation, and can only be treated as an approximation of the general origin of an air mass. Minor local moisture sources cannot be excluded. The trajectories were calculated for every rainwater sampling day. For the sake of clarity, only a representative selection of the computed trajectories is shown in Figure 2.4.

2.4 Results and Interpretation

2.4.1 Stable isotope variations in precipitation

The δ^2H values range from +18.5‰ to -144.4‰ (Fig. 2.5a) and the δ^{18}O values range from +0.8‰ to -18.8‰, with a large variability in our time series (Fig. 2.5b). Highest δ^2H and δ^{18}O values are found in April and May and the lowest values in September and October. The isotope values show a gradual decrease between April and October, after which they start to return to higher values. Generally, values are higher during pre-monsoon months compared to months of monsoonal precipitation. Lowest values are observed during the
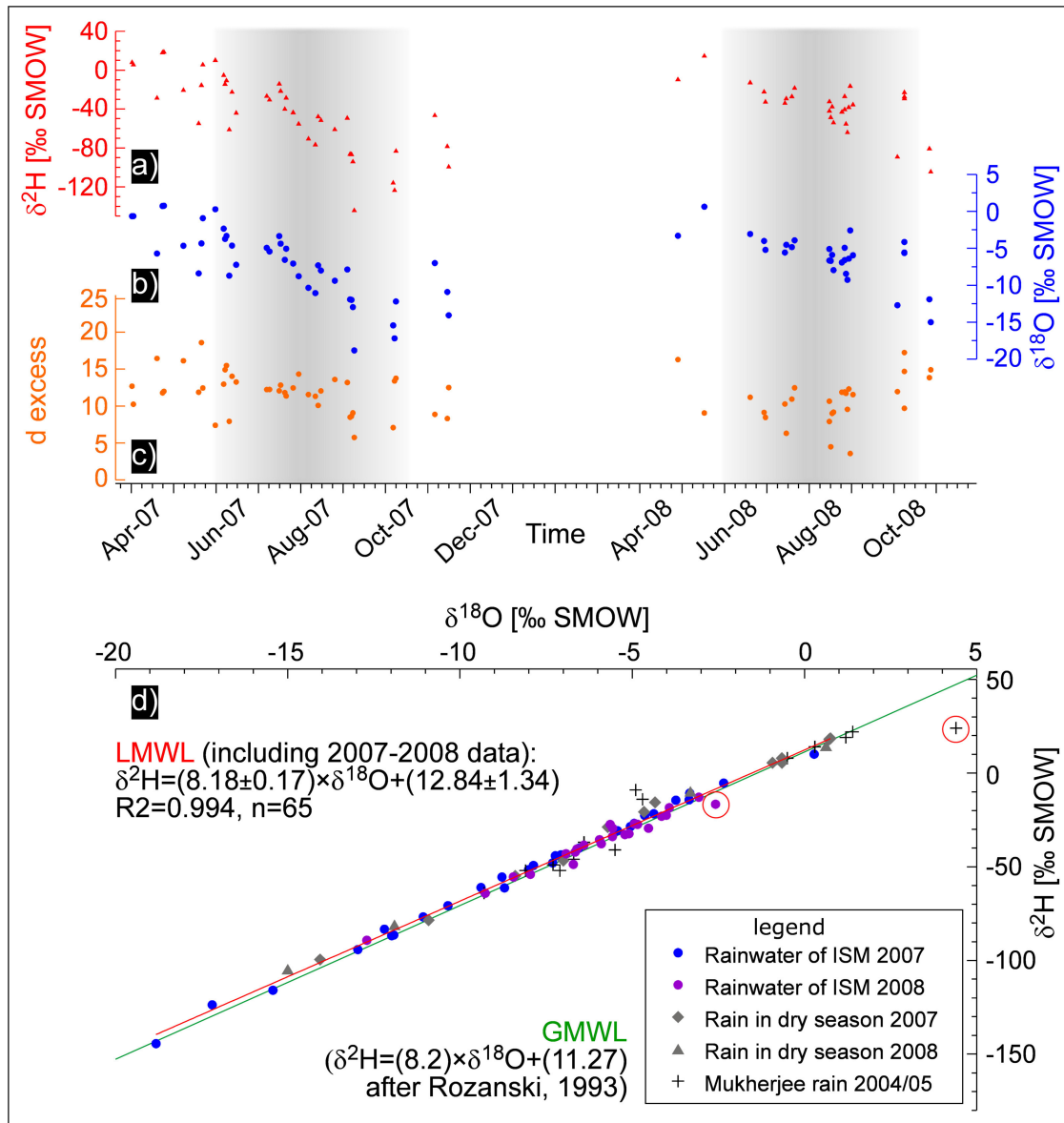
Figure 2.5: Plots of seasonal variation of **a)** δ^2H , **b)** $\delta^{18}O$, and **c)** d excess based on rainwater isotopes collected 2007–2008 near Cherrapunji. $\delta^{18}O$ and δ^2H are depleted during ISM (shaded) and its aftermath. d excess shows only slightly lower values during late ISM. **d)** is a $\delta^{18}O$–δ^2H diagram of water samples collected for this study and in West Bengal in 2004/05 (black crosses) (Mukherjee et al., 2007). The highlighted samples (red circles) are prone to evaporational effects. The red linear fit indicates the LMWL, based on the samples presented in this study. The GMWL with $\delta^2H=8.2\times\delta^{18}O+11.27$ (Rozanski et al., 1993) is plotted for reference.

late monsoon period (September – October, Fig. 2.5). It has been shown for New Delhi, Mumbai, Rangoon, and Shillong that isotope enrichment occurs during the dry period, due to evaporation from falling drops (Clark and Fritz, 1997; Rozanski et al., 1993; Datta et al., 1991). Dansgaard (1964) attributed this phenomenon to the amount effect. A similar situation has been described for southern China (Zhang et al., 2006). The Cherrapunji $\delta^{18}O_{rainfall}$ samples show no clear negative correlation to rainfall amount. This observation led us search for another factor that influences the isotopic signal in precipitation over Meghalaya. Volume-integrated monthly mean samples are required to clarify the amount effect. Below, we discuss how the isotopic signal of source water and vapor, originating in the northern BoB, can influence the stable isotopes in rainfall and hence potentially in terrestrial isotope proxy records.

2.4.2 Deuterium excess d

The excess of deuterium (d excess: $d=\delta^2H-8\times\delta^{18}O$) has been defined by Dansgaard (1964). This excess d is used as a measure for non-equilibrium conditions during primary evaporation, and depends mainly on relative humidity (rH) and partly sea surface temperature (SST) in the source region. A lower d excess in precipitation should result from lowered evaporation at high rH over the primary source region (BoB) during the ISM. This is consistent with regional meteorological conditions. Highest rH over the BoB is reached during ISM (e.g. Port Blair, Andaman Islands) while during the dry season (post- and pre-monsoon) dry air is transported from the southern Tibetan Plateau.

More importantly, a runoff effect originating from an inherited d excess signature of fluvial runoff from the high-altitude Tibetan Plateau with d excess closer to 10 during the late ISM is expected (Tian et al., 2001a). The strong d excess seasonality on the Tibetan Plateau affects the d excess of the freshwater plume in the northern BoB via fluvial runoff during the ISM. This in turn leads to a seasonality of d excess in the source water, with low d excess during ISM and vice versa.

D excess varies between 4.0‰ during ISM and 19.3‰ in the dry season (Fig. 2.5c), reflecting high rH (>85 %) during ISM, and lowered rH during post- and pre-monsoon (∼70–80 % rH) (Fig. 2.2). At the sampling site, highest annual values for d are found in April and May, the lowest in August–September (Fig. 2.5c); with relatively low variability during the ISM in the two-year period (average=11.9±2.9‰, n=68, Tab. 2.1). Slightly higher variability during the dry season and a small decrease during summer are observed. In order to test the significance of the d excess decrease, we applied a simple test based on surrogates for each of the sampling years. The null hypothesis is that there is no linear (anti-) correlation between d excess and time. By simply shuffling the order of the d values, we generate a new series (surrogate) which would not be correlated with time, i. e. would not reveal a decrease over time. Repeating this shuffling many times (Monte Carlo simulation), we estimate the distribution of the regression coefficient of d excess on time. Using this distribution we are able to find the significance level for which we have to reject the null hypothesis, i. e. for which the found linear correlation is still significant. In this Monte

Carlo simulation we used 10,000 runs. Based on this test we find that the decrease of the d excess is significant (p=0.05) in 2007, but not in 2008. If the same test is applied for both years, the decrease is less significant (p=0.1). We assume that the sparse sampling, together with the different number of monthly samples affect this calculation. A longer and denser sampling will strengthen the interpretation of seasonal variation of the d excess.

Low annual SST variability in the BoB (NOAA, 2005) might contribute only to a lesser extent to observed d excess variability. Tian et al. (2001a) relate higher d excess in precipitation during Tibetan winter to lower cloud temperature during high-elevation precipitation and enhanced supply of recycled terrestrial moisture, and lower d values during ISM to enhanced moisture supply from the marine BoB region. However, more data for the dry season is critical for a robust interpretation.

2.4.3 Local Meteoric Water Line

Modern rainwater isotope data has been scarce for Meghalaya (Bhattacharya et al., 1985). δ^2H and δ^{18}O, measured on Meghalayan rainwater samples, collected in 2007 and 2008, show a linear relationship (Fig. 2.5d). For the first time, a tentative (as limited with the number of samples) LMWL is generated for Meghalaya, based on linear regression analysis of the δ^2H and δ^{18}O data presented, described with the least squares fit:

$$\delta^2 H = (8.12 \pm 0.16) \times \delta^{18}O + (12.84 \pm 1.34) \tag{2.1}$$

, with r^2=0.994 and n=65. Three samples (#2, #16, and #21) from our dataset are possibly affected by evaporation and were therefore excluded from LMWL calculations. Due to the intercept of 12.84, the constructed LMWL is slightly above of the GMWL. The 95 % confidence intervals of the regression parameters were estimated, based on the variances of the residuals (Sachs, 1984). This LMWL compares well to the GMWL δ^2H=8.2×δ^{18}O+11.27 (Rozanski et al., 1993), but has slope and intercept higher than the LMWL for West Bengal (δ^2H=7.2×δ^{18}O+7.7, n=14) (Mukherjee et al., 2007). Most of the difference between the data provided by Mukherjee and co-workers and the data presented here disappears if their most enriched sample (rainwater sample #1, marked in Fig. 2.5d) is not included into the calculation of their LMWL. This sample is likely prone to evaporation and a much better fit of their LMWL (δ^2H=8.07×δ^{18}O+12.60) to the GMWL (and our LMWL) is found if the sample is excluded from calculation.

The slope, s, depends on rH during secondary sub-cloud evaporation, so that evaporation of droplets after condensation would lead to a slope <8 (Clark and Fritz, 1997). With 8.12, s is above 8 and only slightly smaller than for the GMWL, indicating little secondary evaporation effects and high rH in the source area (Datta et al., 1991). This finding would be expected for our sampling site, receiving rainfall at a very early stage of moisture transport and Rayleigh distillation, and thus is unlikely to reflect long-distance recycling and secondary evaporation effects. If only ISM samples for 2007 and 2008 are considered, the summer LMWL (δ^2H= (8.13±0.20)×δ^{18}O+(12.55±1.62), n=50, r^2=0.993) is determined by a higher slope value, compared to the dry season. The slope decreases during

pre-monsoon (δ^2H=(7.57±0.62)×δ^{18}O+(13.14±2.45), n=10, r^2=0.989) and post-monsoon (δ^2H=(7.26±0.83)×δ^{18}O+(3.39±10.04), n=5, r^2=0.993). This supports the interpretation that secondary evaporation is effective mainly during the dry season, and could point to a minor influence of the amount effect (Clark and Fritz, 1997; Dansgaard, 1964). Unfortunately, the possible influence of the amount effect remains ambiguous with a weakly determined dry season intercept. The large error estimates for the pre- and post-monsoon LMWL result from the low sample number, and possible seasonal changes of the LMWL cannot be taken as significant within this dataset.

2.4.4 Moisture sources

For each day of sampling, the history of the storm trajectories has been evaluated using backward trajectories, and representative days have been plotted (Fig. 2.4). This procedure allows us to examine the region the moisture likely originates from and the path it followed until it reached the sampling site. Furthermore, we evaluate the trajectories the air masses progressed on, making use of forward trajectories, based on the same database as for the backward trajectories (Fig. 2.4a and b). As a last step, backward trajectories were computed for selected days within the dry season (not shown) to test for possible other source regions.

Analysis of the backward trajectories for 2007 shows that the air masses relevant for our samples had their likely origin in the BoB, and were directed to the northern BoB, and to eastern Bangladesh before reaching Cherrapunji (Fig. 2.4a). This is in agreement with results from Zhou and Yu (2005). In 2008, the situation is very similar except that during the late ISM several samples originate from South Asia (Laos and Thailand) (Fig. 2.4b). Forward trajectories of the storm tracks show that the latter head towards NE India and further into S China. Exceptions occurred in November 2007, when the storm track circled directly over Meghalaya back to the BoB (Fig. 2.4a) and in May and August 2008, when the air masses were directed NW-ward along the Himalaya (Fig. 2.4b). This behavior may be related to advancing northeasterly air spells from the Tibetan Plateau. During the dry season all tested backward trajectories reflect air mass transport from either the Tibetan Plateau or the Ganges plains north-west of the Meghalaya Plateau (not shown). These air masses are generally dry and cold, with negligible effective precipitation.

2.5 Discussion

2.5.1 Moisture origin

The likely origin of the moisture has been traced using backward trajectory analysis. These computations reveal that for all ISM rainwater samples, the source region is most likely the BoB (Fig. 2.4). In 2007, no significant change in the vapor source is observed between the non-monsoon and monsoon seasons. Whereas the pre-monsoon and ISM trajectories are all directed towards the NE (SW China), as seen in the forward trajectory calculations,

this is not true for the early post-monsoon tracks that are pushed back into the BoB, as depicted in the November 2007 forward trajectory (Fig. 2.4a). In 2008, the situation is found to be more complex. Whereas the ISM water samples have their origin in the BoB as in 2007; the pre-monsoon and late ISM samples partly originate from South Asia. δ^2H and δ^{18}O values for rainwater, collected in late October 2008 are much depleted. The backward trajectories for the 4th, 27th, and 28th October also point to a source located in South Asia (Fig. 2.4b). The reason for the isotopic depletion of these 'South Asian' samples is likely the longer air transport over land and the high altitudes of the southern Tibetan Plateau. We assume that the abovementioned post-monsoonal air transport (the turn-back) is forced by the enhancement of the Tibetan High and associated retreat of the ITCZ during boreal autumn and winter. In the study area, ISM is related to the northward migration of the ITCZ and associated atmospheric circulation, with distinct depleted δ^2H and δ^{18}O signature (Araguaś-Araguaś et al., 1998). Dry season air masses originate mainly from the Ganges plains and the Tibetan Plateau. Both regions serve only as minor moisture sources. Air masses from the Tibetan Plateau are cold and dry and, while descending, will warm, enhance its moisture holding capacity, and prevent precipitation. Air originating from the Ganges plains could generally serve as minor source for rainfall, with likely isotopically enriched precipitation due to moisture recycling. However, we assume only a minimal contribution of this source on Cherrapunji precipitation, as the latter is located at the southern rim of the plateau and any rainfall from Ganges plains likely takes place on the NW flank of the Meghalaya Plateau. Furthermore, d excess in rain from the Ganges plains would presumably reflect minimum values in May, similar to New Delhi (Bhattacharya et al., 2003). Such pattern is not observed in Cherrapunji rainwater. Even during the dry season in 2007, several thunderstorms originating in the BoB reached the study site, associated with effective rainfall and a maritime isotope signature.

2.5.2   The BoB freshwater plume effect

It is clear from Figure 2.2 that the amount effect is not the only factor that influences the isotopic signal in rainfall over Meghalaya. The offset between highest rainfall and most negative $\delta^{18}O_{rainfall}$ has to be explained. With our limited dataset the details of the amount effect remain ambiguous. Tests of the significance of the $\delta^{18}O_{rainfall}$ correlation show that the data of our study is not comprehensive enough to clearly reflect the amount effect at the sampling site. We invoke a conceptual model to explain how the rainfall isotopic signal can be influenced by an isotopic signal that is inherited from the history of the BoB surface water. Although the main vapor source region changes only little over the year, the surface waters in the BoB do change their isotopic character in a seasonal cycle (Fig. 2.3). Seasonal changes in fluvial runoff amount and isotopy, with associated seasonal changes in BoB sea surface isotopy can influence the regional precipitation isotope signature. Figure 2.6 shows the different contributions of the runoff in summer and winter. During ISM, massive fluvial runoff from the large river systems of Ganges (Singh et al., 2007) and Yarlungzangbo-Brahmaputra-Padma (Sarma, 2008) follows the intense rains and
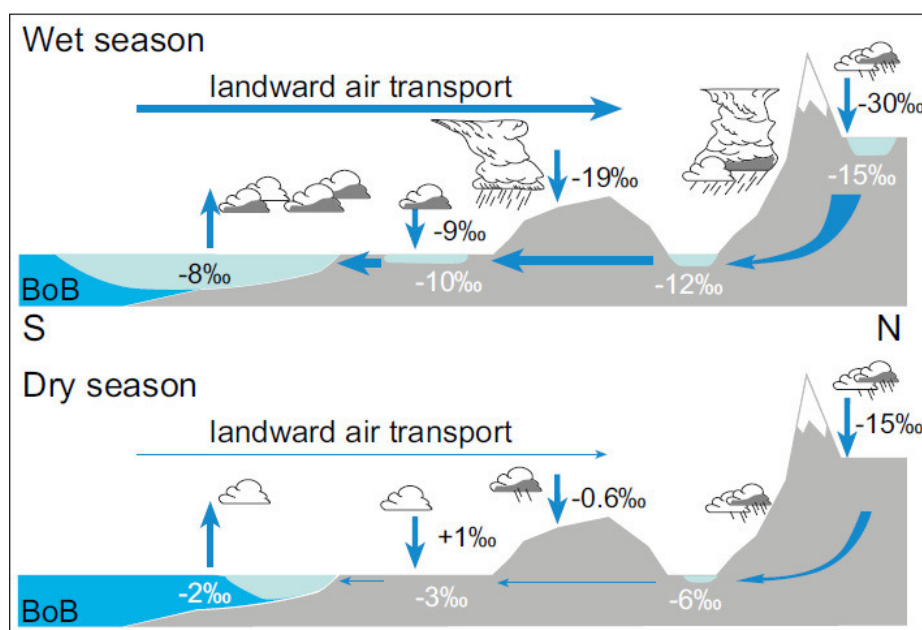
Figure 2.6: Conceptual model of the seasonal influence of an inherited stable isotope signature in the river runoff on rainwater samples in Meghalaya, NE India. The S–N transect is approximately along 90° E. Monsoonal runoff from the Tibetan Plateau develops a large freshwater plume in the northern BoB (upper panel). These waters carry an inherited isotope signal that is reflected in subsequent rainfall over Meghalaya. A minor plume effect is supposed for dry season precipitation (lower panel). Isotope data compiled from Liu et al. (2008a,b) and Tian et al. (2001a) (Tibet rain and river), (Lambs et al., 2005) (Brahmaputra river), (Mukherjee et al., 2007) (Bangladesh rain and rivers), (Kudrass et al., 2001) and (Delaygue et al., 2001) (N BoB surface water), (IAEA/WMO, 2001) and own rainwater analyses (Tab. 2.1).

snow-melt in the Himalaya. When the ISM arrives on the Tibetan Plateau, the isotopic composition of rainfall and subsequent fluvial runoff is depleted by altitude, rainout and amount effect (Liu et al., 2008a; Tian et al., 2001b). Meltwater from ice and snow add to the δ^2H and δ^{18}O depletion of the runoff, which leads to the build-up of a freshwater plume in the northern BoB (Sengupta and Ravichandran, 2001). The plume build-up is accompanied by isotope dilution in the surface water δ^{18}O pool (Fig. 2.6 upper panel; (Delaygue et al., 2001; Zhang et al., 2006). Because the main vapor source is likely located in the northern BoB (Zhou and Yu, 2005; Yoon and Chen, 2005) the inherited depleted δ^{18}O$_{runoff}$ will affect the δ^{18}O$_{surfacewater}$ values and likely result in a depleted isotopic signature of the initial vapor. The 'plume effect' on source vapor will be most effective during late ISM, while the early ISM is probably affected mainly by the amount effect. Additionally to the plume effect, we assume that progressively better cloud organization during the ISM leads to further depletion of δ^{18}O$_{rainwater}$, as found by Lawrence et al. (2004). The two effects together can explain both, the large range of δ^{18}O$_{rainwater}$ observed, and the delay of the δ^{18}O minima relative to maximum rainfall. Such scenario is certainly valid not only for the northern BoB, but also for the Myanmar coast, where seasonal floods of the Salween river system likely have a similar effect. This river also originates on the Tibetan Plateau

and has its highest runoff during the late ISM (GRDC, 2008). We stress that this concept is a special case bound to areas receiving enormous runoff, which in turn is fed by highly continental and/or high altitude regions.

During the dry winter season, the freshwater plume decays with diminished runoff, and the isotopic signature of the BoB surface water will be shifted to typical 'oceanic' values (Figs. 2.3 and 2.6 lower panel). A BoB surface water stable isotopic composition of -2‰ has been found in January/February (Delaygue et al., 2001). The observed high $\delta^{18}O_{rainwater}$ values during the dry season may reflect relatively quiescent conditions over the BoB, which would allow for vapor $\delta^{18}O$ closer to equilibrium values with the BoB surface water $\delta^{18}O$, similar to findings by Lawrence et al. (2004).

Additionally, isotopically depleted waters from the Himalaya regions are progressively enriched on their course through the Ganges plains due to high evapotranspiration (Krishnamurthy and Bhattacharya, 1991; Ramesh and Sarin, 1992). The evaporational counterbalancing process is effective for the Ganges River mainly during winter, when the rH over the Ganges plains is lowered. Similar observations have been reported for precipitation in the Tibetan Yarlungzangbo river basin (Liu et al., 2008b; Singh et al., 2007). There, infrequent winter precipitation $\delta^{18}O$ is derived mainly from the westerlies and recycled local vapor sources, isotopically enriched by evaporation. This finding confirms our interpretation of strong isotopic enrichment during the dry season with low runoff and recycled moisture. In the lower Brahmaputra basin evaporation is thought to be negligible, due to very high rH throughout the year (Sarma, 2008).

The hypothetic BoB 'plume effect' is a process that explains the depleted isotopic values during late ISM (Fig. 2.5). Occasional spells from the mountainous region of South Asia may serve as a second (minor) source for depleted rainfall (e.g. in October 2008, Fig. 2.4b). Our interpretation is corroborated by d excess variability in the data presented here (Fig. 2.5c). During winter, addition of recycled continental moisture to the atmosphere over the Tibetan Plateau shifts the d excess above the GMWL (Tian et al., 2001a). During the ISM, the moisture source on the Tibetan Plateau changes from continental recycled vapor to ISM moisture, with lower d excess values associated with monsoonal rainfall. Higher inherited d excess values are hence found in samples with likely Tibetan Plateau origin.

As shown above, the seasonal dynamics of the isotopic composition of river water leads to a depleted in ^{18}H, and ^{18}O, freshwater plume on top of the denser sea water in the northern BoB. With only little data available, we take the river isotopy during ISM (Fig. 2.7) as approximation, and suspect an isotopy of the freshwater plume of about -5‰ to -8‰, similar to the assumption by Kudrass et al. (2001). Additionally, we can take advantage of a proposed linear relationship between surface water $\delta^{18}O$ and salinity in the Indian Ocean (Delaygue et al., 2001) and use salinity data to visualize the seasonal character of the BoB freshwater plume ((NOAA, 2005), Fig. 2.3 and 2.7). In the northern BoB a seasonal salinity variation is apparent (Pati, 1980; Rashid et al., 2007), with very low salinity (<23 Practical Salinity Units (PSU)) during late ISM and post-monsoon (September – December) and higher values during the post- and pre-monsoon (January–May, ~34 PSU)
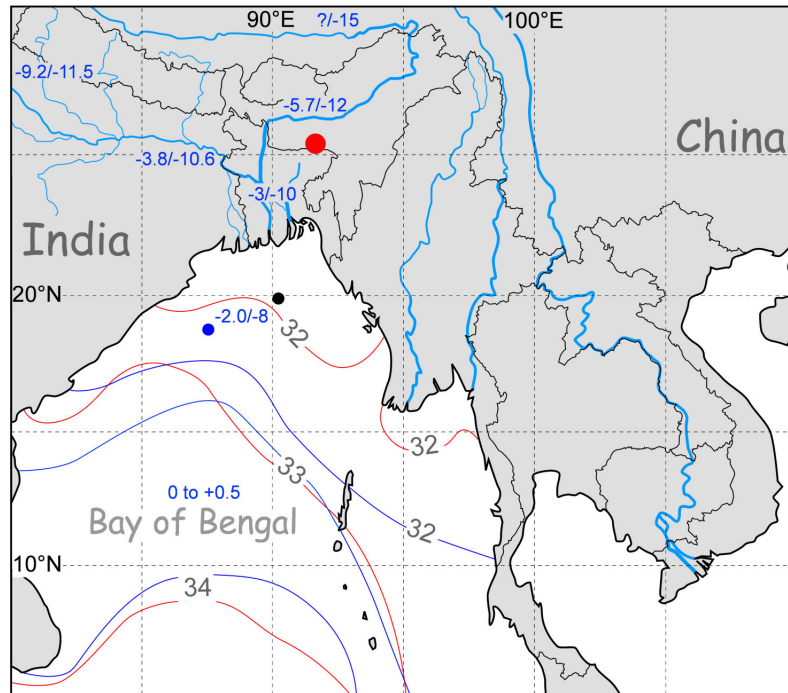
Figure 2.7: Map of the BoB, showing approximate (and conservative) isohalines of sea surface salinity (in PSU, after NOAA (2005)). Red lines depict salinity during the dry season (January to March), while blue lines depict late ISM conditions (October to December). Salinity values of 22 PSU have been found for the ISM season by Pati (1980) (blue dot). The development of freshwater plumes south of the Ganges-Brahmaputra river and the Irrawaddy and Salween deltas are reflected by southward extension of the 32 PSU isohaline during October. Rivers relevant for this study are shown with pre-monsoon, and ISM δ^{18}O values, respectively (in ‰ VSMOW, blue numbers) (Delaygue et al., 2001; Lambs et al., 2005; Ramesh and Sarin, 1992; Rozanski et al., 2001; Tian et al., 2001a). Ocean δ^{18}O values (in ‰ VSMOW, in blue) are given only for January–February (Delaygue et al., 2001) and ISM (black dot, Kudrass et al. (2001)).

(Fig. 2.7; Pati, 1980). A seasonal change in salinity of ∼8 PSU would however result in only a minor change in δ^{18}O of ∼1.4‰ – insufficient to explain the large isotopic changes proposed. Therefore, we assume that the freshwater isotopy must carry an inherited signal that is much more depleted. Together with Lawrence's observation of disequilibrium conditions between seawater and vapor during stormy periods (Lawrence et al., 2004), the large range of δ^{18}O$_{rainwater}$ can be explained.

The seasonal character of anticorrelation between fluvial runoff and BoB surface water isotopy (δ^{18}O and δ^2H) finds a long-term analogue and has been used to reconstruct glacial-interglacial differences in the Indian Ocean (Duplessy, 1982). We note, that the complex relationship between BoB surface water salinity and δ^{18}O is certainly influenced by hydrologic changes on longer (millennial) timescales, as found for the western Pacific (Oppo et al., 2007). Runoff into the BoB and the relative contribution of different headwaters changed significantly during the Holocene. Hence, the δ^{18}O$_{surfacewater}$ might have varied considerably with changing inherited δ^{18}O$_{runoff}$. Such variability is possible even if the total runoff into the Bay, and hence the salinity in the BoB, is assumed to have remained

unchanged. Lastly, during the early monsoon (June), when rH is reduced, rainfall falling on parched ground can suffer partial re-evaporation. This in turn could partly counter-balance the amount effect. In southwestern China, Zhang et al. (2006) find only a weak amount effect, but a strong inverse relationship between the precipitable water and $\delta^{18}O$ in precipitation. This relationship likely plays an additional role at our study site, but lack of relevant data hampers a detailed discussion. We propose that the 'plume effect' surmounts the amount effect. Because the observed late ISM $\delta^{18}O$ minimum is not associated with the highest rainfall amount, the $\delta^{18}O$ signal is likely linked to the extent of the proposed freshwater plume and hence moisture source isotopic composition (Fig. 2.6).

Rainwater samples collected during the ISM periods 2007/2008 are distributed (with few exceptions) along the GMWL (Fig. 2.5d), suggesting that no significant evaporational enrichment took place. Interestingly, samples from 2007 are distributed all along the LMWL, while the samples from 2008 are more clustered around higher $\delta^{18}O$ and δ^2H values (Fig. 2.6). Such feature may point to changes in the convective activity, with higher convection leading to condensation at lower temperatures and subsequently lower isotope values in the rainfall (Dansgaard, 1964). This may be interpreted as reflecting enhanced activity in 2007. The monitoring the stable isotopy over long periods would possibly allow for reconstruction of plume extent in the BoB and ISM convective activity. Such work is beyond the scope of this contribution and has to wait long-term observations.

The ISM samples of 2007 stem most probably from the same moisture source as non-monsoon samples, as they all are relatively closely distributed along the LMWL. Most ISM $\delta^{18}O$ values are between -3‰ to -18‰, similar to reported values from West Bengal (Mukherjee et al., 2007) and Myanmar (Araguaś-Araguaś et al., 1998). The slope of our LMWL (s=8.12) points to higher relative humidity and negligible secondary evaporational effects (Clark and Fritz, 1997).
Dry season samples show generally a tendency of isotope enrichment, compared to the ISM samples, except those that have their likely origin in South Asia. Evaporation is most effective during the dry season between November and March, causing strong re-evaporation (up to 100 %) of falling droplets. The remaining fraction of water reaching the ground will be enriched in $\delta^{18}O$ and δ^2H. Additionally, the proposed freshwater plume in the BoB with – compared to ocean water – depleted isotopic values, disappears during the dry season (as reflected in salinity changes, Fig. 2.7). Hence, BoB source waters are likely less isotopically depleted during pre-monsoon. However, too few samples for this time period are available. Only with extended surface water sampling, the proposed relations can be verified.

Due to the altitude effect a somewhat stronger depletion is expected in Meghalaya, when compared to West Bengal (Mukherjee et al., 2007). The altitude effect (-0.15‰ to -0.5‰/100 m, (Clark and Fritz, 1997)) could account for ∼-1.35‰ to -4.5‰ depletion in $\delta^{18}O_{precipitation}$ (with assumed ∼900 m forced orographic uplift from the Bengal lowlands

to our sampling site). Unfortunately, without data from two or more sites on an altitudinal transect, evaluation of this effect has to wait future monitoring. For a better understanding of the importance of humidity changes on isotopes in precipitation near Cherrapunji, long-term observations are needed.

2.6 Conclusions

A local meteoric water line and seasonal variations in the isotopic composition of precipitation for Meghalaya provide insight into the hydrological regime of northern Bangladesh and NE India. Our data suggest that the governing role on isotopes in precipitation is played by the strong seasonality of the isotopic composition of source vapor, aided by source region changes. With the present data we are not able to clearly track the influence of the amount effect on the stable isotopic signature of precipitation in Meghalaya. An amount effect can be traced only after extensive rainwater sampling, which is a matter of ongoing research.

We propose **a)** that seasonal runoff changes of the Ganges-Brahmaputra river system impacts the isotopic composition of the BoB surface water, and **b)** that this isotopic signature of the BoB influences the isotopy of subsequent rainfall over Meghalaya. During and after the ISM, high river runoff leads to a surface freshwater plume in the BoB. This results in a depleted isotopic composition of the evaporating surface water. The dry winter season is characterized by diminished freshwater runoff into the BoB and enhanced evaporation of recycled waters result in elevated $\delta^{18}O$ values in the BoB surface water. Consequently, $\delta^{18}O$ and δ^2H values of the water vapor, originating from the BoB, and in the winter rain are enriched. Although this 'plume effect' explains the lag between minimum $\delta^{18}O_{rainwater}$ and maximum rainfall, it can not fully explain the large range of observed $\delta^{18}O_{rainwater}$. Disequilibrium conditions between surface water and water vapor during stormy weather enhances the isotopic depletion, while quiet conditions result in near-equilibrium conditions, favoring $\delta^{18}O_{vapor}$ values closer to equilibrium with $\delta^{18}O_{seawater}$.

In 2007, the source region for all collected rainwater samples was likely the BoB, as revealed by backward trajectory computations. 2008 was characterized by a similar pattern, although several late ISM and post-monsoon samples had their likely origin in South Asia and not in the BoB. The air masses moved further in northeasterly directions into the SE Tibetan Plateau and SW China, or north-westward along the Himalaya. The trajectory analysis reflects the splitting of the BoB branch of the ISM, with a major fraction moving NE.

Stable isotopes measured in palaeoclimatic archives (e.g. stalagmites) fed by moisture from the BoB are likely to record seasonal changes in BoB surface water isotopic composition. Stronger ISM will lead to enhanced river runoff, a larger extent of the proposed BoB freshwater plume and consequently to more depleted $\delta^{18}O$ and δ^2H signatures in ISM precipitation. Such scenario should be valid on seasonal, but also on millennial and probably

on glacial-interglacial timescales. Isotopically depleted rainwater from South Asia is likely a minor component, as only few events bring effective moisture from this second source region.

Further investigation of the spatial and temporal dynamics of the proposed freshwater plume will allow for a better understanding of its influence on regional precipitation isotopy. Similar effects are expected in other regions with seasonal high runoff and high-altitude hinterland (e.g. Mekong (SE Asia) or Rio Grande de Santiago (Mexico)), but detailed analyses are needed to understand river runoff–surface ocean–atmosphere interactions and associated isotope characteristics. Future palaeo- rainfall reconstructions with palaeoclimate archives will benefit from a detailed understanding of the extent of its moisture source variability and impact on palaeoclimate records.

3 Holocene History of the Indian Summer Monsoon reconstructed from a Stalagmite from Meghalaya/Northeastern India.

Sebastian F. M. Breitenbach[1,2,], Birgit Plessen[1], David Lund[3], Norbert Marwan[4], Jess F. Adkins[3], Diego Fernandez[3,†], Hedi Oberhänsli[1], Gerald H. Haug[2,5]*

[1] *Helmholtz Zentrum Potsdam, Deutsches GeoForschungsZentrum, 5.2 Climate Dynamics and Landscape Evolution Section, 14473 Potsdam, Germany*

[2] *DFG-Leibniz Center for Surface Process and Climate Studies, Institute for Geosciences, Potsdam University, 14476 Potsdam, Germany*

[*] *corresponding author: sebastian.breitenbach@gfz-potsdam.de, tel: ++47(0) 331 288 1347, fax: ++47(0) 331 288 1302*

[3] *California Institute of Technology, GPS Division, E. California Blvd. 1200, CA 91125, USA*

[†] *present address: Department of Geology and Geophysics, University of Utah, UT 84112, USA*

[4] *Potsdam Institute for Climate Impact Research (PIK), 14412 Potsdam, Germany*

[5] *Geological Institute, Department of Earth Sciences, ETH Zürich, 8092 Zürich, Switzerland*

Abstract

We present the first stalagmite record documenting Indian summer monsoon (ISM) variability during the entire Holocene. Stable isotope (δ^{18}O and δ^{13}C) and grey-scale records from two stalagmites from Meghalaya (NE India) reflect ISM intensity, and winter aridity. The high-resolution δ^{18}O record suggests that ISM precipitation is likely coupled to the migration of the intertropical convergence zone (ITCZ). Wetter periods were associated with longer and deeper northward ITCZ penetration into the Asian continent. ISM rainfall leads to enhanced river runoff with depleted δ^{18}O, and subsequently to changes in the Bay of Bengal (BoB) surface water δ^{18}O, the source for Meghalayan rainfall and dripwater. Stalagmite δ^{13}C can trace aridity and points to severe droughts, lasting up to several years. δ^{18}O and δ^{13}C seem to be coupled only during extreme drought phases, e. g. during the Little Ice Age (LIA). Grey values show a negative relationship to δ^{18}O and point to a possible link between the ISM domain and Europe, with low grey values (drought conditions) contemporaneous with cold events in Europe. Decadal to centennial-scale periods of drought, superimposed on the long-term ISM trend, often coincide with Northern Hemisphere events. NE Indian droughts likely occur during positive Indian Ocean Dipole

(IOD) and El Niño events. The past ∼2 kyr experienced the driest and most variable ISM during the entire Holocene, with maximum drought conditions recorded ∼1600 AD.

3.1 Introduction

The monsoonal rainfall belt is one of the most important components of low-latitude climate. The Indian Summer Monsoon (ISM) variability, its onset, duration, and failure, strongly influences Indian agriculture (Fleitmann et al., 2003a; Krishna Kumar et al., 2006). Deficient rainfall over Southeast Asia causes drought, famine and civil unrest (Bhatia, 1991). Considering the importance of the ISM for the Indian subcontinent, it is surprising how little we know about its behavior on longer, as well as on shorter timescales. A crucial question to be answered is how rapidly or severely the ISM can change in near future. Understanding the relation between monsoonal rainfall and modern atmospheric circulation patterns like the El Niño-Southern Oscillation (ENSO) or the westerlies is of major importance for constraining global circulation models. Gadgil (2003) and Fleitmann et al. (2003a, 2007) suggested that the ISM is part of the intertropical convergence zone (ITCZ), and that ISM and Asian summer monsoon (ASM) act in parallel. To test such relationships requires continuous and well-dated high-resolution records, not only from the western but also the eastern part of the Indian subcontinent.

In India, early terrestrial reconstructions of Holocene climate concentrated on the analysis of lake sediments (Enzel et al., 1999; Bryson and Swain, 1981) and peat bogs (Sukumar et al., 1993; Phadtare, 2000). Marine records from Arabian Sea provide information on the Arabian Sea summer monsoon which is the western branch of the ISM (Fig. 1) (Staubwasser et al., 2002, 2003; Lückge et al., 2006; Gupta et al., 2003). Reconstructions of the Arabian Sea summer monsoon are supported by continental stalagmite δ^{18}O records from Oman (Fleitmann et al., 2003a), interpreted as rainfall amount proxy. Although of different resolution and duration, these records consequently point to ISM weakening starting ∼5 ka ago and likely following precessional insolation forcing (Fleitmann et al., 2007).

A major problem common to many of the mentioned archives is not well-constrained chronologies. Comprehensive summaries by Fleitmann et al. (2007) and Prasad and Enzel (2006) show, that a correlation of registered events is restricted. Additionally, observations valid for the Arabian Sea may not be representative for the Bay of Bengal (BoB) branch of the ISM, where only little is known about Holocene ISM conditions (Kudrass et al., 2001). This issue was raised by Staubwasser (2006), who identified three ISM domains; NW India, the Indian peninsula, and NE India, all of which are characterized by different ISM variability. Still, due to lack of reliable climate records, the interpretation of Arabian Sea ISM records is often extrapolated over the entire ISM domain.

High-resolution records from stalagmites with precise and accurate chronological control and a wealth of proxies make cave deposits very appealing climate archives (Overpeck and Cole, 2008). Studies on stalagmites from caves in Oman and China demonstrate the preservation of monsoon variability in speleothem records (e. g. Fleitmann et al. (2003a,

2004); Zhang et al. (2008); Hu et al. (2008); Wang et al. (2008)). Chinese stalagmites recorded ASM variability on sub-decadal to multi-millennial timescales (Wang et al., 2008; Zhang et al., 2008). From central India, Yadava et al. (2004) reconstructed the past three hundred years of monsoon variability, while Sinha et al. (2007) presented an oxygen record for the Medieval Warm Period (MWP).

To fill the gap between the Arabian Sea region and southern China, we present two high-resolution stalagmite records from northeastern India. The location of our cave north of the BoB, close to the source region for northwest- and northeastward migrating cyclones, make it an ideal study site for recording ISM variability. Using the stalagmites oxygen isotopic signature we reconstruct past moisture source variability (Araguás-Araguás et al., 1998; Breitenbach et al., in prep. a) and the potential influence of the amount effect (Dansgaard, 1964; Aggarwal et al., 2004). Additionally, we use the carbon isotopic signature, and grey-scale variability to monitor changes in duration and intensity of the dry season. We compare our results with summer monsoon reconstructions from Asia to reveal similarities and differences between the ISM branches and the ASM. Finally, we test the relationship between the ISM, the Indian Ocean Dipole (IOD), and ENSO.

3.2 Environmental setting

The ISM is the most important climate feature in terms of recurring seasonal winds and rainfall for the agricultural India. With its onset in May to June, the southwesterly winds of the both ISM branches; Arabian Sea and BoB transport moist air from the Indian Ocean to the continent (Fig. 3.1). While the Arabian Sea branch reaches into NW India, the BoB branch is directed over Bangladesh and NE India, to split at the foot of the Himalaya. One arm travels along the Ganges river valley northwestward, the other penetrates northeastward onto the southern Tibetan Plateau. The ISM depends to some extent on the snow conditions in Central Asia and in the Himalaya in the preceding winter and spring (Blanford, 1884; Walker, 1918; Gadgil, 2003). Winters with anomalous snow cover thickness and extent in Eurasia are related to drought years in India (Dash et al., 2005). Today, the ISM is considered as an integral part of the ITCZ (Fleitmann et al., 2007). When the winter high pressure system over Central Asia and Tibet decays the ITCZ – and with it the ISM – can enter the Indian sub-continent. The seasonal migration of this rainfall belt is a major factor determining the strength of the ISM. The ISM rainfall amount is modulated by oceanic conditions in the Indian and Pacific Oceans. The two governing factors here are the IOD (Abram et al., 2007; Saji et al., 1999) in the equatorial Indian Ocean, and the ENSO in the Pacific, although their influence on the ISM varies and is not fully understood (Krishna Kumar et al., 1999).

For the present study we selected two samples from Krem Umsynrang Cave in NE India (25°13' N, 92°21' E; 825 meters above sea level (m a.s.l.), Fig. 3.1). The cave is located at the south-facing ridge of the Meghalaya Plateau, where rainfall is governed by the seasonal recurrence of the ISM (Fig. 3.2). The site is characterized by extremely seasonal ISM
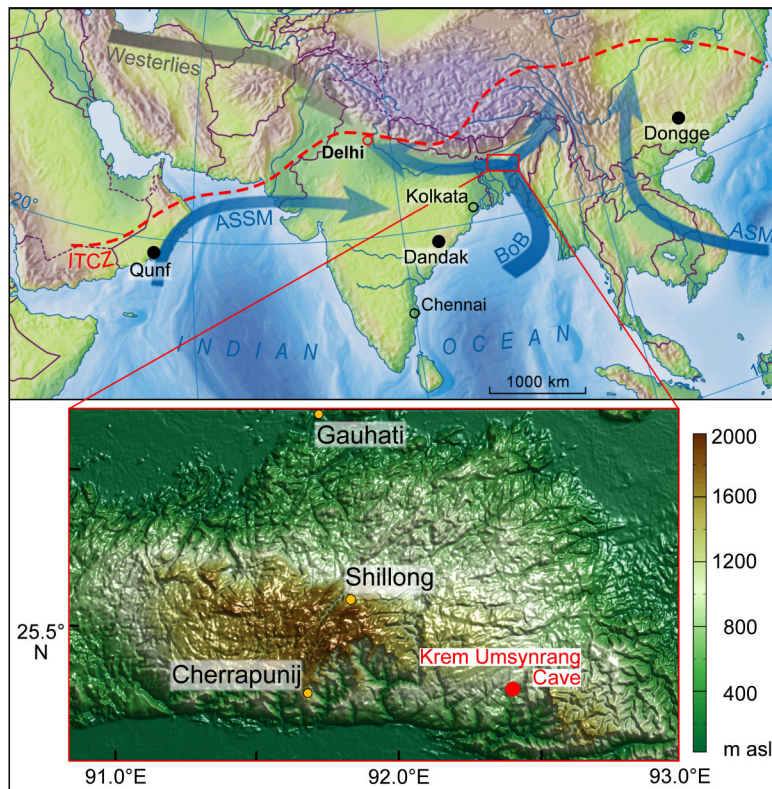
Figure 3.1: Map showing Krem Umsynrang cave location (red dot in enlarged map), Qunf (Oman), Socotra (Fleitmann et al., 2007) and Dongge cave sites (Wang et al., 2005) in black. Arrows denote the Arabian Sea and BoB summer monsoon branches, the Asian Summer Monsoon and the Westerlies. The approximate July ITCZ position over S Asia is shown as red dashed line.

climate; during summer (mid-May to mid-October) the region receives >75 % of its annual rainfall from the BoB. At Cherrapunji, located ∼65 km W of the cave, the worldwide highest mean annual rainfall (11,439 mm/yr) has been recorded (Prokop and Walanus, 2003). In contrast, during the dry season (November to May) the rainfall reaches a minimum of <200 mm/month. The plateau above the cave is covered mainly with grassland. Tropical forest is bound to wet dolines and rock cliffs, seemingly due to deforestation.

The 5.6 km long horizontal cave has developed beneath ∼40 m of Eocene lime- and sandstone with interbedded ∼0.5 m of coal (Fig. 3.3). The sampling site is several hundred meters away from the narrow entrance and ventilation is restricted. Cave air temperature was monitored between March 2006 and March 2007 using a HOBOware U22 Water Temp Pro v2 logger and is stable at 20.6±0.6°C. The relative humidity (rH) measured during two winter field campaigns reached ∼85–90 %. Measured dripwater δ^{18}O ranges from -5‰ to -6‰ VSMOW (Vienna Standard Mean Ocean Water, Tab. 3.1). Seasonal drought in the area implies that percolation water is effectively fed by ISM rainwater; hence δ^{18}O$_{dripwater}$ is likely strongly weighted towards ISM rainfall. The partial CO$_2$ pressure (pCO$_2$) in soil (Khiewtam and Ramakrishnan, 1993) and cave air is high during the ISM, promoting equi-
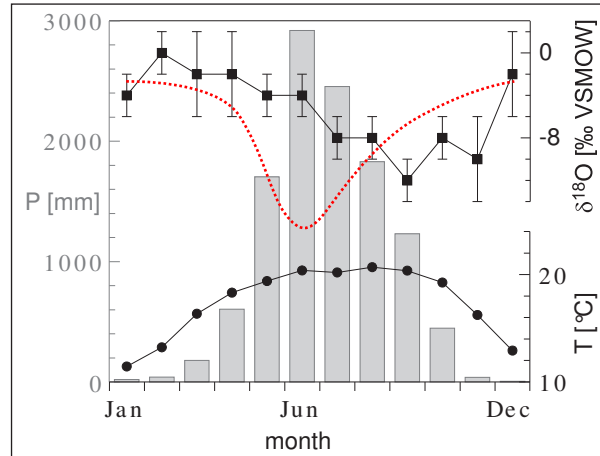
Figure 3.2: Precipitation-δ^{18}O relationship in the monsoonal tropics. Monthly means for precipitation and temperature are given for the period 1961–1990 (Prokop and Walanus, 2003). The modeled $\delta^{18}O_{rainwater}$ values are taken from the GNIP database (IAEA/WMO, 2001). The red line is a hypothetical representation for $\delta^{18}O_{rainwater}$ if governed by the amount effect (Dansgaard, 1964). Model results (black cubes) show distinct differences in the timing of the δ^{18}O minimum (IAEA/WMO, 2001). The causes for the observed delay of the δ^{18}O minimum are discussed in Breitenbach et al., (in prep. b). $\delta^{18}O_{rainwater}$ decreases with the development of a freshwater plume in the BoB during the ISM. Runoff and moisture source dynamics govern the isotopic signal at Cherrapunji. Rainfall amount is probably only a minor factor influencing δ^{18}O in precipitation.
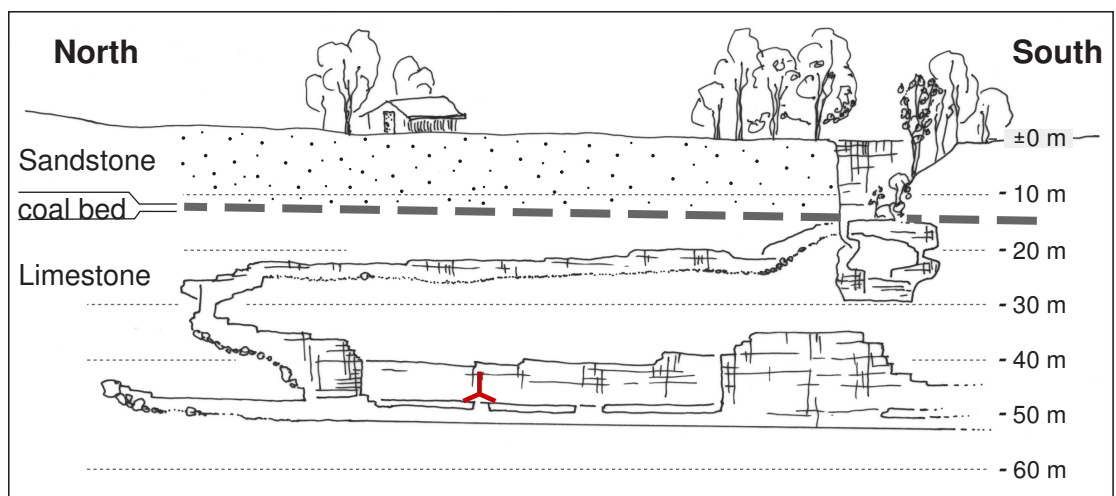
Figure 3.3: Profile of Krem Umsynrang cave (original map courtesy of H. D. Gebauer, 2007). The red star denotes the location of the taken stalagmites. Depth scale is relative to the entrance (at 825 m a.s.l.).

Table 3.1: Drip water stable isotopes (δ^{18}O and δD) from Krem Umsynrang Cave. $*$ measured at UFZ Halle

sampling rate	Lab. Nr.	δ^{18}O [‰ SMOW]	δD [‰ SMOW]	d excess	sample type
19.03.06	AWI 29555	-5.34	-30.6	12.1	D$_{fast}$
19.03.06	AWI 29556	-5.35	-30.4	12.4	D$_{fast}$
19.03.06	AWI 29557	-5.33	-30.4	12.2	D$_{fast}$
03.03.07	AWI 1776	-5.10	-30.0	10.8	R
03.03.07	AWI 1777	-5.08	-29.6	11.0	R
03.03.07	AWI 1778	-5.20	-29.8	11.7	D$_{fast}$
03.03.07	AWI 1780	-5.20	-30.4	11.2	D$_{slow}$
03.03.07	AWI 1781	-5.17	-29.5	11.9	P
03.03.07	AWI 1783	-5.14	-29.9	11.3	D$_{fast}$
13.03.07	AWI 1784	-5.14	-29.6	11.6	D$_{slow}$
03.03.07	UFZ #2 $*$	-5.4	-27.7	–	D$_{slow}$

librium conditions in the cave. The ISM season in Meghalaya is characterized by high rH and temperature.

3.3 Material and Methods

3.3.1 Material

Two actively growing stalagmites KRUM-3 (65 cm long) and KRUM-1 ($\sim$180 cm long, both $\sim$5 m apart) were collected from Krem Umsynrang cave in 2006. The candle-stick shaped stalagmites and a host rock sample were collected from the middle cave level which is not affected by flooding (Fig. 3.3). Both stalagmites were actively fed by soda straw stalactites; the dripwater fall height is for KRUM-1 and KRUM-3 $\sim$0.5 m and $\sim$1.5 m respectively. For analysis the stalagmites were cut along their growth axes. Micro X-ray diffraction (μXRD, Bruker AXS D8) and optical microscopy revealed that both stalagmites consist of aragonite. Visible growth banding in both stalagmites was analyzed using reflected normal light and near-UV light microscopy. Optically visible growth density changes are manifested by alternation of opaque elongated needle-shaped crystals and dense translucent microcrystalline material, resulting in micrometer-scale bright (porous) and dark (dense) growth layers.

3.3.2 U/Th chronology and layer counting

The chronologies for both samples were established using U/Th disequilibrium dating. By initial testing (using a PerkinElmer/SCIEX DRC-e inductively coupled mass spectrometer) high U concentrations of 5–20 ppm and very low initial ^{230}Th were found. Sub-samples

of 30–160 mg were drilled parallel to growth layers for dating. Each sample was spiked with a mixed ^{236}U–^{229}Th spike solution before treatment with standard techniques for U and Th separation. Isotope compositions of the sample fractions were analyzed with a Finnigan 'Neptune' multi-collector inductively coupled plasma mass spectrometry (MC-ICP-MS) at Caltech, Pasadena. Measured ^{232}Th concentrations and estimates for detrital ^{230}Th/^{232}Th ratios obtained from isochrons from both stalagmites were used to account for initial ^{230}Th. Unpolished slabs of KRUM-3 were scanned with a flat-bed scanner at a resolution of 4800 dpi (i.e. 5.3 μm/pixel). Grey values, sub-parallel to the stable isotope profile, were extracted and processed with the ImageJ software (Rasband, 2008). Layer counting was performed for the uppermost 380 mm (Fig. 3.4), based on grey-scale results. Grey-scale maxima (bright laminae) were identified, counted, and individual laminae thicknesses calculated. Additionally, we took advantage of the relation between grey intensity change and crystallography (bright layers – porous, dark layers – dense) and utilized the grey-scale profile as a potential aridity proxy (see below). Banding is observed also in KRUM-1; however, due to the complex and porous crystal structure no grey-scale analysis was performed.

3.3.3 Stable isotopes

For stable isotope analysis both stalagmites were sampled every 0.2–5.0 mm (discrete holes, $\varnothing$ 0.2 mm) along their growth axes with a Sherline® precision mill stage. The host rock limestone was sampled using the same technique. From KRUM-3 a total of 1439 samples were taken, resulting in a temporal resolution of 5–55 years. 565 samples were analyzed from KRUM-1, the temporal resolution ranging from 1 to 10 years. Stable isotopes were analyzed on a Finnigan DeltaMAT253 mass spectrometer with attached Kiel IV device at the GeoForschungsZentrum (GFZ) Potsdam. NBS19 was used as reference material, with isotope ratios (^{18}O/^{16}O and ^{13}C/^{12}C) reported in Delta notation relative to the Vienna Pee Dee Belemnite (‰ VPDB) standard. The analytical precision for both, δ^{13}C and δ^{18}O is better than 0.06‰.

Dripwater samples, collected in 2006 and 2007, were analyzed for stable isotopes (δD and δ^{18}O) on a Finnigan MAT Delta-S mass spectrometer equipped with two equilibration units for online determination of hydrogen and oxygen isotopic composition at the Alfred Wegener Institute for Polar and Marine Research (AWI), Potsdam. External errors of long-term standard measurements for hydrogen and oxygen are better than 0.8‰ and 0.10‰, respectively (Meyer et al., 2000). One drip sample has been analyzed at Umwelt-ForschungsZentrum Halle (S. Weise) according to the method of Gehre et al. (2004).

3.3.4 Spectral analysis

Spectral analysis was performed on the stable isotope and grey-scale data using the programs REDFIT (Schulz and Mudelsee, 2002), and Matlab®. A Lomb-Scargle Fourier trans-
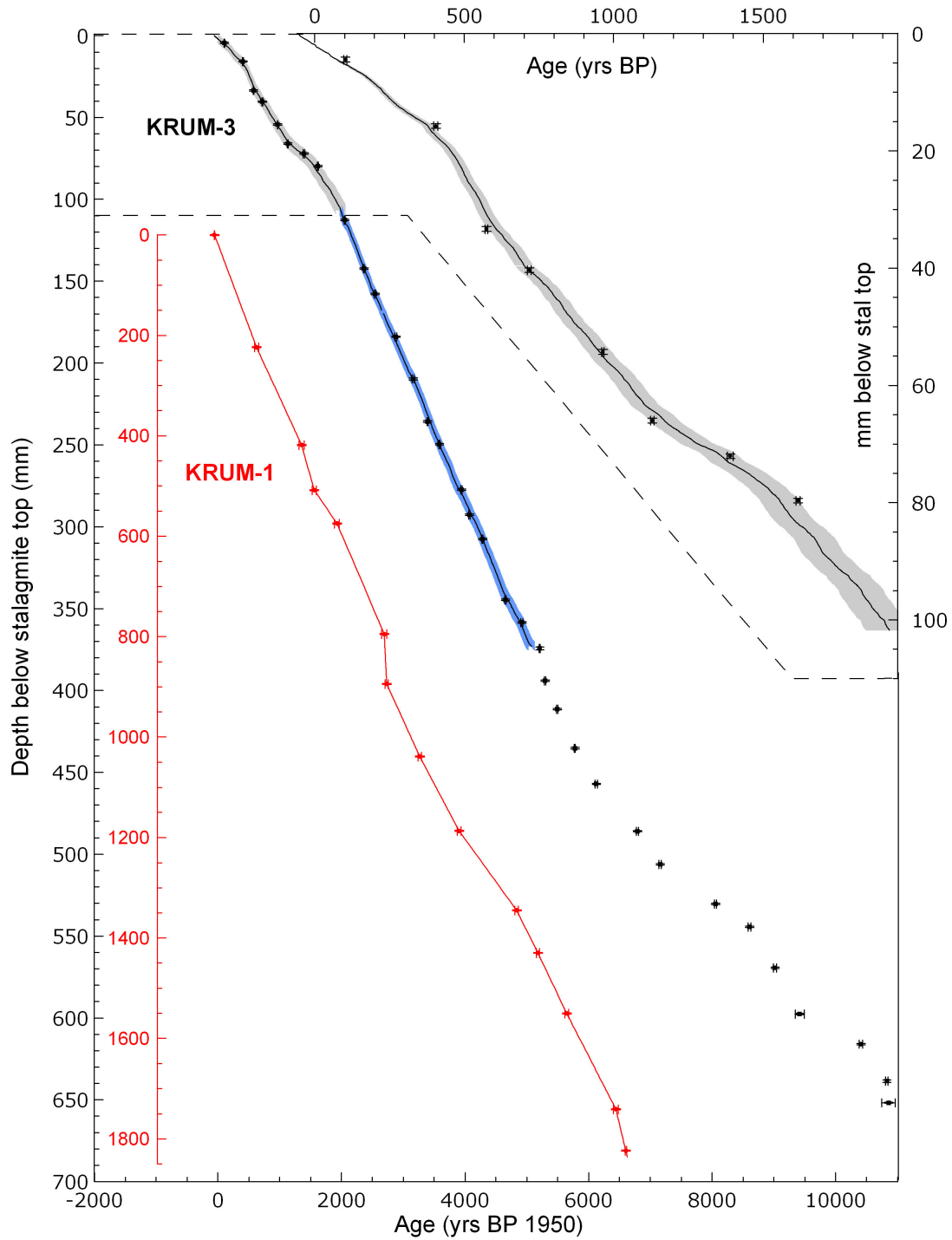
Figure 3.4: Age versus depth plot of KRUM-3 (in black) and KRUM-1 (in red) U/Th dates. Points with 2σ error bars indicate U/Th dates. The zoomed in part (upper 110 mm) shows the U/Th dating compared to layer counting results (black line). The layer counting chronology of the top 110 mm agrees within 4 % estimated counting error (grey shading) with the U/Th dating, while the counting between 110 and 380 mm agrees within 1 % estimated counting error (blue shading).

form for unevenly sampled data, with a Hanning window and the Welch-Overlapped-Segment-Averaging procedure was employed (Schulz and Mudelsee, 2002). We computed 5000 Monte-Carlo simulations in order to bias-correct the input spectra.

3.4 Results

3.4.1 Chronology and grey-scale-based layer counting

All U/Th results and ages are given in table 3.1 and reported in years (yr) or thousand years (kyr) before present (BP = 1950). The depth-age plots in Figure 3.4 depict the chronologies for KRUM-1 and KRUM-3. The KRUM-3 age model is based on linear interpolation between 34 radiometric dates, with two additional isochrons of 4 and 5 sub-samples. KRUM-3 grew continuously between ~11,000 years BP and 2006 AD. The growth rate ranges between 0.015 and 0.21 mm/yr. All ages are in stratigraphic order within their dating uncertainties. 2σ errors are typically in the range of ± 20 years. Uncertainties of 0.2–1.5 % (for the 2σ interval) result from high ^{238}U concentrations, low δ^{234}U values (140‰ to 225‰), and low detrital ^{232}Th content (0.2–80 pmol/g). Independently, layer counting based on the grey-scale data of the uppermost 380 mm was performed. Ages are assigned based on the assumption that a couplet of one dark and one bright layer corresponds to one year (Genty and Quinif (1996), and discussion below). As separation between dark and bright layers was impracticable, the thickness between two subsequent bright layers was taken as a 'growth year'. The layer counting results agree within 1 and 4 % counting error with the U/Th dating (Fig. 3.4). With each pixel representing 5.3 μm, and the distance between two adjacent bright peaks (representing 1 year) ranging from 15 to >200 μm, the grey-scale record is of sub-annual resolution. The age model for replicate stalagmite KRUM-1 is based on 13 U/Th ages. In total, 21 U/Th samples were analyzed, including two isochrons with 4 sub-samples each. KRUM-1 grew rapidly since ~6.7 kyr BP until AD 2006 (Fig. 3.4). Growth rates range from ~0.2 to 0.8 mm/yr. All dates are in stratigraphic order and show typical errors of ± 11–40 years within the 2σ interval.

3.4.2 Stable isotope profiles ($\delta^{18}O$ and $\delta^{18}O$)

Figure 3.5 shows the δ^{13}C and δ^{18}O time series for the analyzed stalagmites KRUM-1 and KRUM-3, which represents the first continuous stalagmite record from India covering the entire Holocene.

The δ^{18}O time series of both stalagmites show a similar narrow range between -6.8 and -4.1‰. In both records the amplitude variation of δ^{18}O is typically 0.5‰, with several event-like fluctuations reaching 1‰ within a few years. KRUM-3 has a higher sampling rate and reaches longer back in time; therefore we chose this record as the master time series. KRUM-1 serves for replication purposes. KRUM-3 δ^{18}O values decrease from 11 kyr BP until the Holocene thermal maximum (HTM) 9.4 kyr BP (Fig. 3.5a) (the timing for

Table 3.1: U/Th dating results from stalagmites KRUM-1 and KRUM-3 from Krem Umsynrang Cave, India. Uses an initial $^{230}Th/^{232}Th$ value of 4±4 ppm [atomic]. Final age errors are the combination of the ^{232}Th correction and the measured $^{230}Th/^{238}U$ ratio.

Sample ID	Depth [mm below top]	^{238}U [ppb]	^{232}Th [pmol/g]	$\delta^{234}U(T)$ [act]	$^{230}Th/^{238}U$ $\times 10^{-3}$	U/Th yrs [corrected]	Age [yrs BP]	$\delta^{234}U^*$
KRUM-3								
LU02	4.43	10118.7±31.8	1.8±0.2	-230.3±2.0	1.1±0.03	158	102 5	-230.38
LW26	15.76	14885.5±58.8	0.9±0.6	-224.9±0.5	3.3±0.05	461	405±7	-225.24
LU06	33.32	15390.6±51.9	0.5±0.2	-221.6±1.6	4.5±0.03	630	574±5	-222.02
LW29	40.32	15213.9±54.2	0.8±0.5	-219.1±0.3	5.5±0.05	774	718±6	-219.56
LU05	54.3	20606.2±65	1.8±0.2	-222.6±1.2	7.2±0.03	1020	964±4	-223.24
LU11	66	15804.3±52.6	0.3±0.2	-217.6±1.5	8.4±0.04	1185	1129±6	-218.38
SJ14	72.09	17112.5±41.9	1.8±0.5	-220.4±0.3	10.3±0.07	1446	1390±10	-221.34
LU03	79.66	13944.6±51.2	0.3±0.2	-217.8±1.9	11.9±0.05	1672	1616±7	-218.80
LW02	112.61	13872.3±52.1	1±0.6	-220.7±0.4	14.9±0.06	2105	2049±9	-222.03
LW07	142.3	19477.6±71	0.4±0.5	-222.1±0.5	17.0±0.05	2418	2362±7	-223.58
LW21	157.74	12387.6±42.5	0.9±0.5	-216.1±0.4	18.4±0.07	2597	2541±10	-217.72
SJ06	183.9	13549.5±46.1	1.2±0.7	-212.5±0.3	20.9±0.12	2937	2881±17	-214.24
SJ02	209.62	13026.2±38.9	1.3±0.6	-214.2±0.2	22.8±0.11	3214	3158±16	-216.20
LW19	235.62	15233.7±51.3	0.4±0.5	-210.6±0.3	24.5±0.06	3447	3391±9	-212.68
LW15	249.51	16431.8±54.7	0.6±0.5	-211.4±0.4	25.8±0.06	3639	3583±8	-213.58
LW06	277.36	15590±53.6	0.5±0.5	-210.9±0.4	28.3±0.07	3997	3941±10	-213.29
LW01	292.59	13223.3±41.3	0.5±0.5	-209.8±0.4	29.3±0.07	4128	4072±10	-212.23
LW30	307.44	16512±61.5	0.8±0.6	-205.8±0.4	30.9±0.06	4337	4281±9	-208.30
LW09	344.5	13532.1±44.2	0.8±0.5	-210.8±0.4	33.2±0.08	4707	4651±11	-213.60
SJ03	358.4	15783.8±52.2	1.1±0.6	-204.9±0.3	35.3±0.11	4973	4917±15	-207.80
LW28	374.26	19244.6±65.5	0.4±0.5	-200.0±0.4	37.6±0.06	5263	5207±9	-203.02
LW03	393.93	15792.8±55	0.6±0.5	-206.0±0.4	37.9±0.07	5352	5296±10	-209.10
LW13	411.29	14174.5±49.3	1.3±0.5	-204.9±0.4	39.3±0.07	5547	5491±10	-208.10

Table 3.2: U/Th dating results from stalagmites KRUM-1 and KRUM-3 from Krem Umsynrang Cave...continued from the last page

Sample ID	Depth [mm below top]	^{238}U [ppb]	^{232}Th [pmol/g]	δ^{234}U(T) [act]	^{230}Th/^{238}U $\times10^{-3}$	U/Th yrs [corrected]	Age [yrs BP]	δ^{234}U*
LW24	435.23	15901.9±55.4	0.7±0.5	-203.8±0.4	41.3±0.07	5831	5775±9	-207.16
SJ05	457.0	11876.7±37.2	1.8±0.6	-197.3±0.3	44.1±0.14	6179	6123±19	-200.73
LW18	485.95	9625±32.4	0.8±0.5	-181.3±0.4	49.6±0.12	6846	6790±16	-184.86
LW05	506.18	5828.7±21.3	1.7±0.6	-174.4±0.5	52.7±0.16	7214	7158±22	-177.97
LW25	530.29	7173.4±25.1	0.2±0.5	-175.6±0.5	58.9±0.13	8108	8052±18	-179.65
LW16	544.3	6487.4±23.1	11.2±0.5	-168.8±0.4	63.3±0.15	8660	8604±24	-173.01
SJ01	569.39	8663.1±25.1	0.8±0.6	-162.8±0.4	66.6±0.18	9071	9015±24	-167.00
LW08	597.52	5357.6±17.8	52.8±0.5	-157.8±0.5	70.3±0.17	9471	9415±74	-162.09
LW27	615.95	4907.7±16.7	0.6±0.5	-156.7±0.6	76-8±0.20	10464	10408±27	-161.43
LW10	638.52	6885.4±17.1	10.4±0.4	-141.9±0.4	81-4±0.12	10902	10846±20	-146.34
SJ04	651.71	5529.9±16.4	82.4±0.6	-136.1±0.4	81-9±0.27	10799	10743±110	-140.31
KRUM-1								
SJ23	223.8	12376±86.7	1.5±1.3	-178.1±0.5	5.0±0.26	681	625±36	-178.40
SJ22	418.5	12243.3±98.5	3.5±1.5	-160.6±0.5	1.05±0.30	1410	1354±41	-161.24
SJ28	508.4	9899.4±56.7	1.5±1.1	-163.9±0.5	1.19±0.27	1614	1558±36	-164.66
SJ25	574.5	11314±80.2	2.4±1.4	-157.8±0.6	1.47±0.29	1983	1927±39	-158.69
SJ24	794.8	10900.2±76.2	0.5±1.3	-161.7±0.5	2.02±0.30	2748	2692±41	-162.89
SJ26	894.1	16186.3±106.3	0.8±1.3	-149.0±0.4	2.09±0.19	2788	2732±26	-150.12
SJ27	1038.4	14949±99.6	0.6±1.3	-160.9±0.4	2.45±0.21	3322	3266±29	-162.33
SJ21	1187	15762.2±116.7	4.4±1.4	-159.5±0.5	2.91±0.23	3960	3904±31	-161.28
SJ07	1345	14026.2±92.9	2.5±1.3	-155.2±0.4	3.52±0.23	4779	4723±31	-157.25
SJ20	1429.8	17825±115.1	5.6±1.2	-154.8±0.4	3.85±0.18	5235	5179±24	-157.04
SJ29	1550.3	15965.5±120.5	7.2±1.4	-137.3±0.5	4.27±0.24	5700	5644±32	-139.46
SJ13	1741	12039.3±96.4	2.3±1.5	-152.9±0.5	4.51±0.31	6153	6097±43	-155.46
SH28	1823.7	13039.5±13.3	13.9±0.1	-146.4±0.4	5.05±0.06	6657	6601±11	-149.16

* no error was propagated for δ^{234}U

the HTM is adopted from Wanner et al. (2008). Rapid positive shifts of $\sim$0.5‰ took place at 10.4 and 10.2 kyr. A longer positive excursion is recorded between $\sim$9.8 to 9.4 kyr BP. Lowest for the entire Holocene $\delta^{18}O$ values ($\sim$-6.25‰) are found between $\sim$9.4 and $\sim$8.6 kyr BP. It follows a 400-year long two-pronged-structured event between 8.4–8.0 kyr with maximum values $\sim$-5.2‰. Conditions remained variable around an average of -5.5‰ until $\sim$6 kyr BP with positive shifts at 7.2 and 6.4 kyr BP. At $\sim$6 kyr BP a gradual shift to less negative $\delta^{18}O$ values occurs, with several superimposed events at 5.1, 3.9, 3.5, 1.4–1.2, 0.7, and 0.3 kyr BP (Fig. 3.5b). Two strong events at 4.3 and 4.1 kyr BP appear in the $\delta^{18}O$ record, interrupted by an 80 year period of enriched $\delta^{18}O$. The past $\sim$2 kyr experienced the highest $\delta^{18}O$ variability of the whole record. At $\sim$1.2, $\sim$0.8, and $\sim$0.3 kyr BP strong $\delta^{18}O$ excursions up to values of -4‰ reach well above the modern value (-4.6‰). The two stalagmite $\delta^{18}O$ series show some differences on decadal-scales, with higher variability in the faster growing KRUM-1. After $\sim$3.5 kyr BP the $\delta^{18}O$ in KRUM-1 diverges from KRUM-3 by $\sim$+0.28‰.

The $\delta^{13}C$ values vary between -1‰ and +7‰ in KRUM-3 and -1.3‰ and +3.4‰ in KRUM-1 (Fig. 3.5a). While the millennial-scale trend is similar in both records, changes on centennial timescales show some disagreement. Decadal-scale variations reach 3‰. The KRUM-3 $\delta^{13}C$ record reveals multiple event-like increases up to +4‰ at 10.6, 10.4 and 10.2 kyr BP corresponding to higher $\delta^{18}O$ values. After a decrease to 0‰ a very pronounced $\sim$2‰ shift to more positive $\delta^{13}C$ values occurs around 9.3 to 9.0 kyr BP. After a decadal-scale decrease, the $\delta^{13}C$ profile gradually increases until 8.3 kyr BP. The onset of the 8.2 ka event is clearly reflected in the $\delta^{13}C$ profile with an increase of more than 1‰ within only $\sim$10 years. Around 6.9 kyr BP an increase of similar magnitude is found, whereafter the $\delta^{13}C$ values decrease to above 0‰ at 6 kyr BP. Starting at $\sim$6.2 kyr BP, the $\delta^{13}C$ profile shows a striking $\sim$1,200-year cyclic saw-tooth pattern (discussion below). A $\sim$200 year rapid $\delta^{13}C$ decrease of $\sim$1.5‰ is repeatedly followed by a gradual 1000 year increase, followed again by a rapid increase. Between 6.2 and 2.2 kyr BP this pattern appears very pronounced. A cycle from 1.3 kyr BP to 0.3 kyr BP shows similar behaviour, but is strongly enhanced in its $\delta^{13}C$ increase.

Isotopic equilibrium conditions were tested with 15 Hendy tests, conducted on both stalagmites (Fig. 3.6; Hendy (1971)). Minor $\delta^{18}O$ variation (<0.4‰) along lighter multi-layer intervals indicates near-equilibrium conditions during deposition in KRUM-3. Slightly higher variability found in darker multi-layer intervals may reflect slight evaporation or prolonged CO_2 degassing due to longer residence of individual drops on the stalagmite surface at reduced drip rate, likely resulting from short-lived non-equilibrium conditions. Disequilibrium fractionation effects are believed to play only a minor role on the isotopic differences. A value for modern $\delta^{18}O_{aragonite}$ was calculated using a calcite–water equilibrium fractionation factor of $(2.78 \times 10^6 / T^2)$-2.89 (O'Neil et al., 1969) and the following parameters: a cave air temperature of 19.8°C, a mean $\delta^{18}O_{dripwater}$ of -5.17‰ (Tab. 3.1),
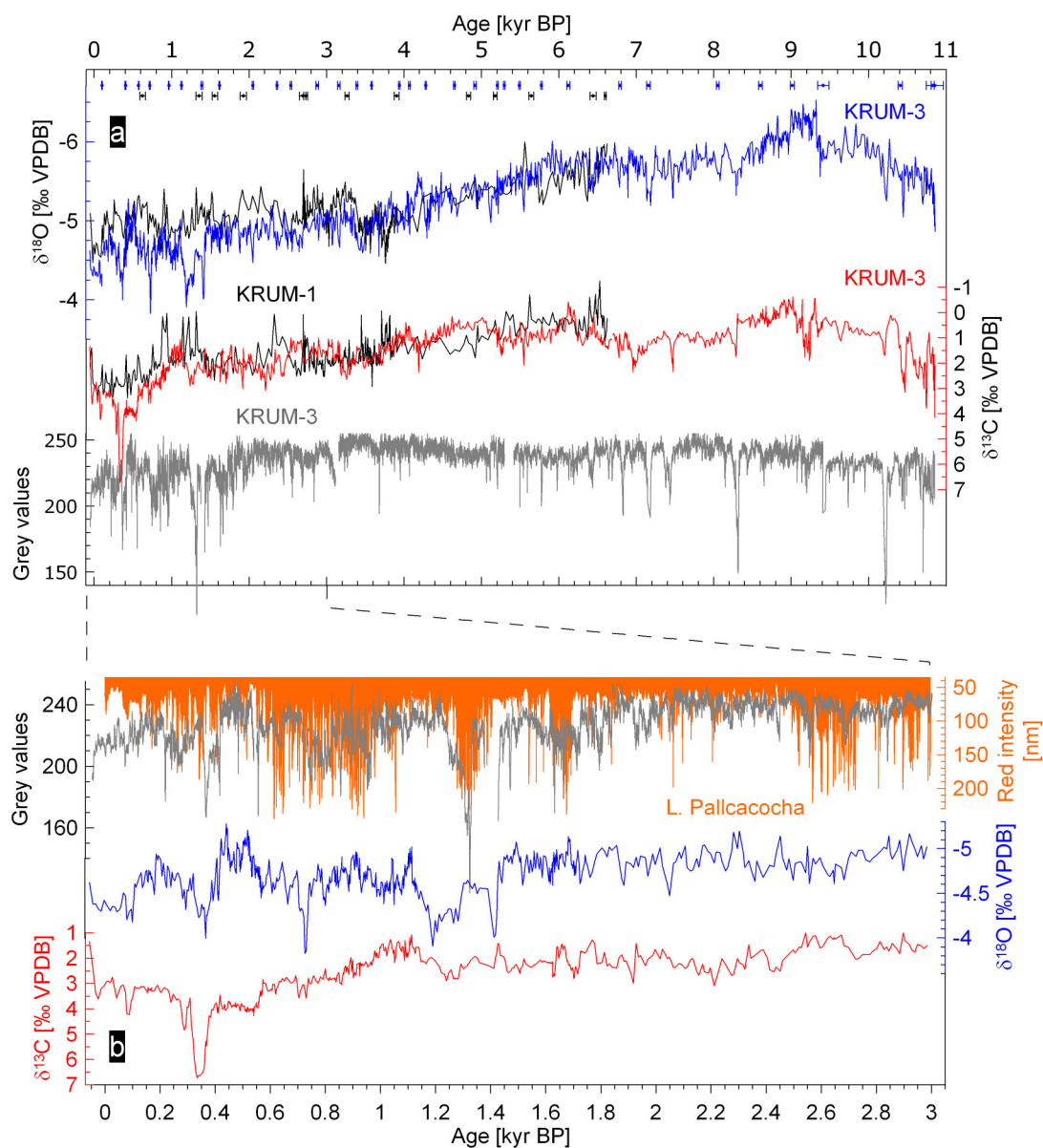
Figure 3.5: a) Holocene stable isotope time series of KRUM-3 (in blue and red) and KRUM-1 (in black) and the grey-scale record from KRUM-3 (in grey). Black and blue dots denote dating points with 2σ errors of the respective stalagmite record. **b)** Grey values from KRUM-3 (in grey) compared to red intensity (in orange) from Laguna Pallcacocha, Ecuador (Moy et al., 2002), and stable isotopes from KRUM-3. A general anticorrelation between grey values and red intensity is found. Stronger and more frequent ENSO events appear parallel to weak ISM. The grey-scale record is based on linear interpolation between U/Th ages.
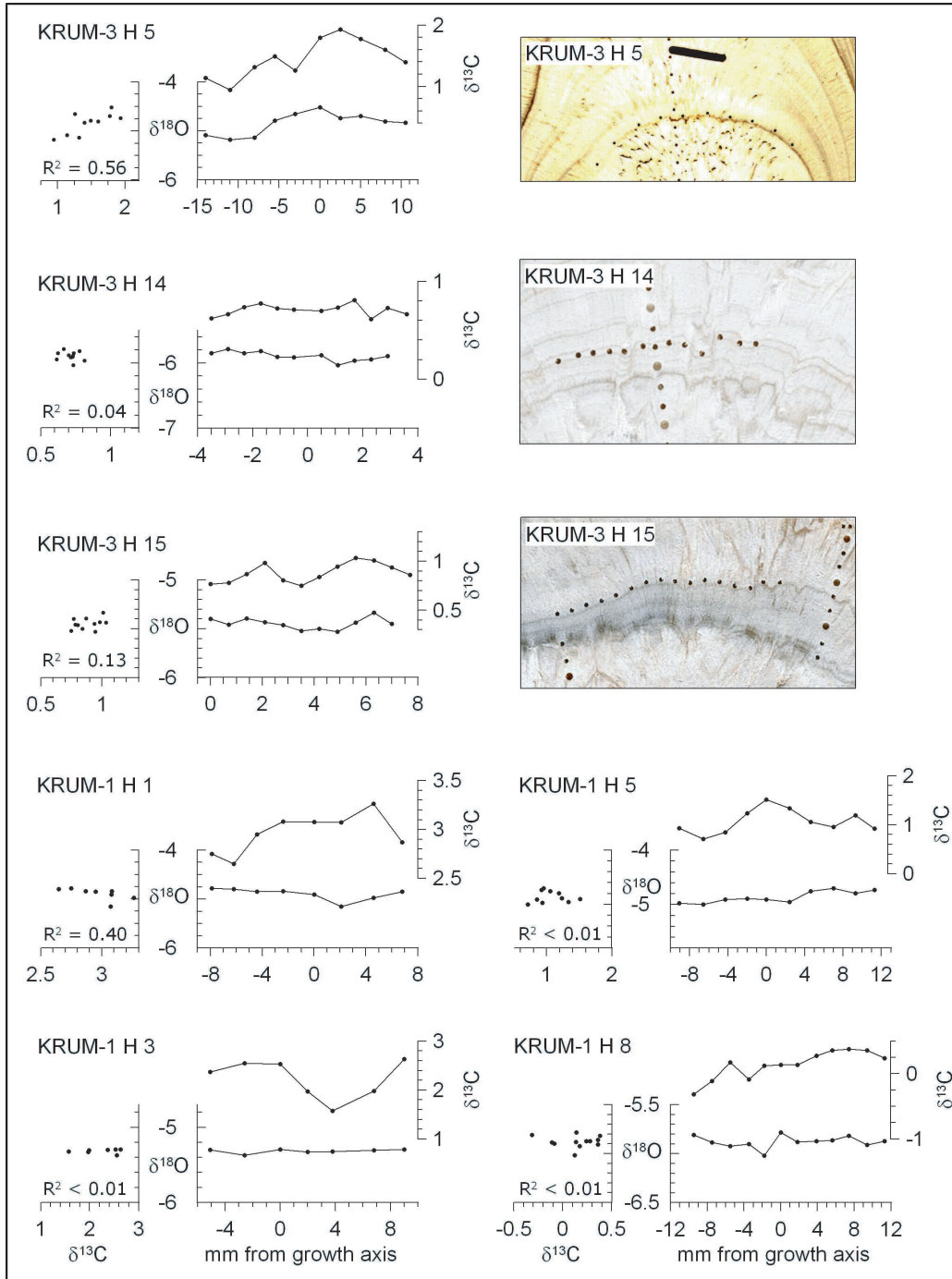
Figure 3.6: Selected Hendy tests taken from KRUM-3 (H5, H14, H15) and KRUM-1 (H1, H3, H5, H8). All isotope ratios are given in ‰ VPDB. For comparison, 3 images show the position of H5 – H15, respectively. Minor $\delta^{18}O$ variation of <0.4‰ supports the assumption of the cave microclimate supporting equilibrium conditions and that most of the $\delta^{18}O$ variability reflects $\delta^{18}O_{dripwater}$ and hence hydrological conditions.

and a $+0.8‰$ enrichment of aragonite relative to calcite (Kim et al., 2007). The obtained value of $-4.61‰$ is in excellent agreement with values found at the top of KRUM-3 ($-4.60±0.07‰$, n=6). We are confident that equilibrium conditions prevailed during the latest growth of KRUM-3; but we note these might have changed with time.

3.4.3 Grey-scale analysis

The KRUM-3 grey-scale profile reveals distinct changes towards lower grey values on centennial to decadal timescales during the Holocene (Fig. 3.5). Ages for the grey-scale proxy record were assigned by linear interpolation between U/Th dates. The highest grey-scale variability is recorded during the past $\sim$2 kyr. Observed events normally last <100 years and coincide with high $\delta^{18}O$ and $\delta^{13}C$ values (e. g. at $\sim$8.3 kyr BP).

The sub-annual grey-scale record reveals remarkable changes over the Holocene (Fig. 3.5). Grey-scale variability is relatively low between 10.8 and 2 kyr BP, with values between 220 and 250; however, some rapid decadal-scale events with minimum values below 180 are superimposed on this long-term stability. Major excursions are found at 10.2, 8.3, and 7.4 kyr BP. Minima are also seen $\sim$7.2, 6.8, 6.4, $\sim$3, and $\sim$2.6 kyr BP. After 2 kyr BP, the internal variability of the grey-scale record increases, showing two very pronounced minima between 1.7 and 1.2 kyr and 0.5–0.3 kyr BP. These events coincide with $\delta^{18}O$ maxima and with events recorded in Laguna Pallcacocha sediments (Fig. 3.5b, Moy et al. (2002).

3.4.4 Spectral analysis

The 11 kyr stable isotope record has an average sampling resolution of $\sim$8 yrs, so the lowest reliable periodicity that can be detected is $\sim$16 yrs. For the highest resolved interval (the last $\sim$2 kyr), characterized by an average sampling resolution of $\sim$4 yrs, the lowest periodicity is 8 yrs. We performed statistical experiments to identify correlations between the $\delta^{18}O$ profile and other published isotope records as well as between our grey-scale time-series and the red intensity of the ENSO proxy record provided by Moy et al. (2002). Figures 3.7a and 3.7c show the results from the spectral analysis of the entire 11 kyr record ($\delta^{18}O$ and $\delta^{13}C$); Figures 3.7b and 3.7d the last 2 kyr of the KRUM-3 record, which were evaluated separately. Periods of 43, $\sim$35, 28, and 15.5 years are significant at the 99 % confidence level and dominate both $\delta^{18}O$ and $\delta^{13}C$ complete Holocene records. Additional periodicities on decadal-scale were found in the high-resolution part of the KRUM-3 $\delta^{18}O$ record (Fig. 3.7b). The high-resolution $\delta^{13}C$ record (Fig. 3.7d) confirms the presence of the 21.5 and 15 years periodicities at the 95 % level. Evolutionary spectral analysis of the sub- annually resolved grey-scale record reveals increasing high-frequency variability during the late Holocene (Fig. 3.8). ENSO frequencies between 8.5 and 2.5 years are found in the late Holocene (Fig. 3.8).
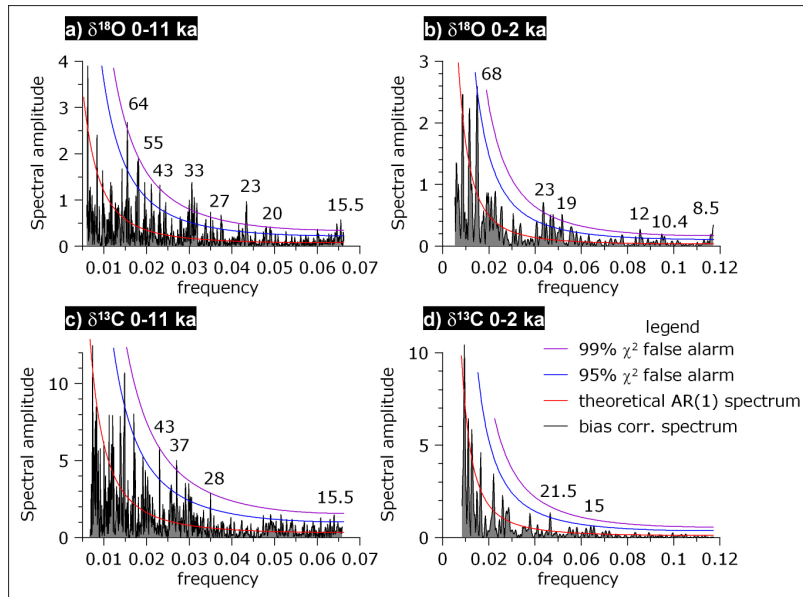
Figure 3.7: Results of univariate spectral analysis for δ^{18}O and δ^{13}C from KRUM-3. The theoretical AR-1 spectrum is shown as red line. As red noise estimates, the 95 % in blue and the 99 % in violet chi-squared bounds of the AR (1) process are given. Numbers above spectral peaks indicate years of significant cycles. **a**) spectral peaks, found for the complete (lower resolution) 11kyr δ^{18}O record, and significant at the 99 % level, have been identified at 64, 43, 33, 27, 23, and 15.5 yrs. The high-resolution part (<2 kyr) of KRUM-3 δ^{18}O (**b**) shows significant frequencies at 23, 19, 12, and 8.5 yrs. Spectral results for δ^{13}C time series are given in c) and d). In the 11 kyr record for δ^{18}O **c**), significant peaks are found at 37, and possibly at 28 years. **d**) For the high-resolution record (<2 kyr) however, no peak appears to be significant at the 99 % level.

3.5 Discussion

The quality of the palaeoclimate interpretation depends on the reliability and reproducibility of the data. Therefore we put the produced records to the test regarding two crucial issues: a) equilibrium conditions during growth (see above) and b) the differences between the main (KRUM-3) and the replicate (KRUM-1) records. Despite a similar general trend the two stalagmite isotope profiles show decadal-scale discrepancies in both, δ^{13}C and δ^{18}O (Fig. 3.5). These differences likely result from the very different growth rates, suggesting the two stalagmites were not fed by the same hydrological system. The influence of different dripwater feeders on stalagmite growth has been discussed in Fairchild et al. (2007). KRUM-1 is likely supplied by fast flow through fracture pipes, while KRUM-3 is rather fed by slow matrix seepage water. KRUM-1 could react faster on rainfall events, while KRUM-3 reflects a slower response and an attenuated δ^{18}O signal of the wet season.

Additionally, the different growth rates cause different time integration in the analyzed stalagmites; in KRUM-3 one sample integrates 3–5 years, while in KRUM-1 it may integrate only one year. Hence, KRUM-3 data are smoothed by sampling integration. Considering

The evolutionary spectrogram for the KRUM-3 grey scale record is based on simple periodograms with a Hanning window. Each spectrogram represents 500 year long intervals. Only significant periods are shown.
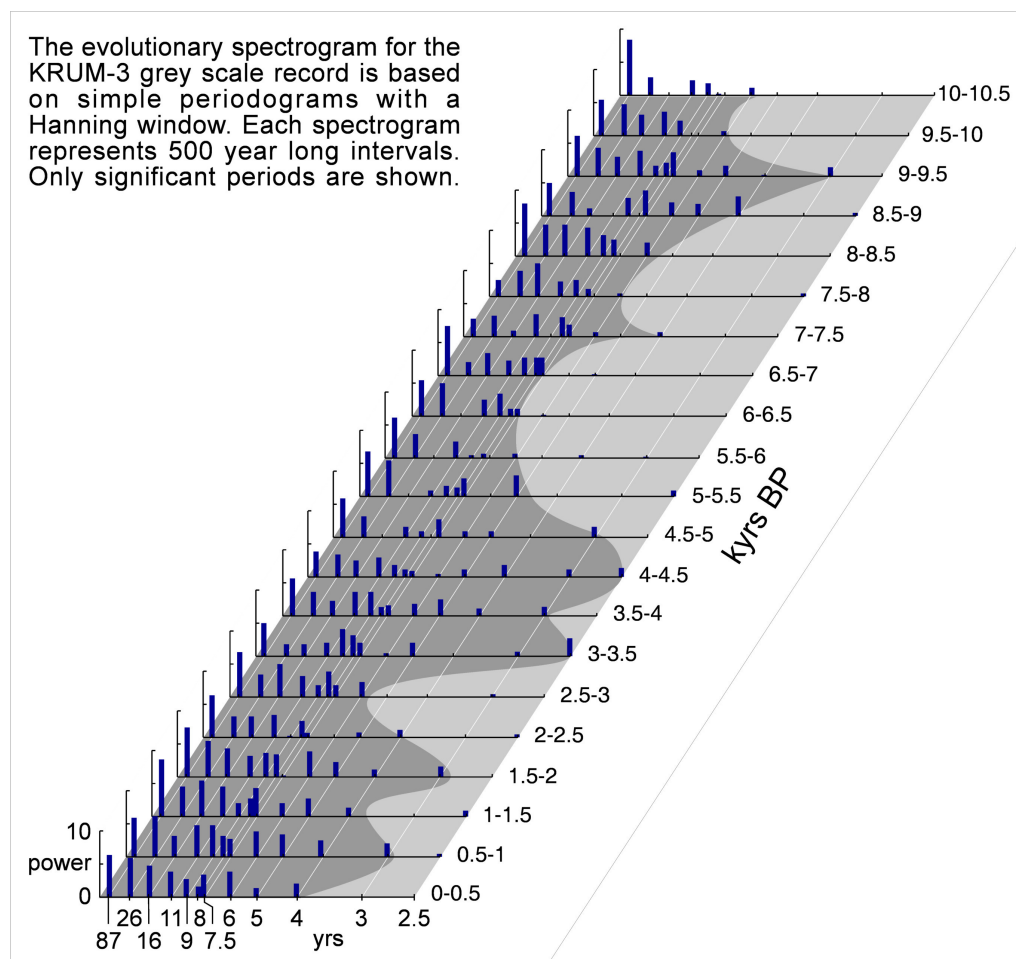
Figure 3.8: Evolutionary power spectra for the grey-scale record in KRUM-3. Only significant periods are shown. Between 10.5 and 5 kyr BP, high-frequency variability is reduced and no significant periods below 5–6 years is found, with the exception of the period 9.5 to 8.5 kyr BP. After 5.0 kyr BP, a tendency to higher frequencies is apparent. The periods of 2.5 to 6 years may be attributed to ENSO variability, pointing to an increasing influence of ENSO on the ISM since ∼5 kyr BP.

the aforementioned, the KRUM-3 is taken as the more robust of the two records and its palaeoclimatic information will be discussed below.

3.5.1 Interpretation of stable isotope and grey-scale records

The δ^{18}O from subtropical stalagmites is often used as a proxy for the amount of the monsoonal rainfall (Fleitmann et al., 2003a; Wang et al., 2008). Ongoing monitoring in the study region is not yet advanced enough to declare the amount effect (the negative correlation between rainfall amount and δ^{18}O$_{rainwater}$; Dansgaard, 1964), the major factor governing the stalagmite δ^{18}O. Preliminary results suggest that the amount effect may play a role during the early ISM while during late ISM the isotopic composition of rainfall is modulated by the isotopic composition of the BoB surface water (Fig. 3.2). The isotopic composition of BoB surface water is strongly influenced by river runoff during the ISM. Increased rainfall, enhancing runoff, leads to build-up of a freshwater plume and consequently isotopic depletion of a moisture source; this 'plume effect' is described in Breitenbach et al., (in prep. b). A strong 'plume effect' on δ^{18}O$_{rainwater}$ is expressed in the observed discrepancy between maximum rainfall and minimum δ^{18}O$_{rainwater}$ values. With the beginning of the dry season, the freshwater plume diminishes and rain- and dripwater δ^{18}O shift to higher values. Hence, we interpret more negative oxygen values as reflecting a larger BoB freshwater plume and increased ISM rainfall (Fig. 3.2).

δ^{13}C in stalagmites can be influenced by the type of vegetation (C$_3$ versus C$_4$ photosynthetic plants), density of vegetation, soil microbial activity, and the type of host rock. Except the latter, all these factors are primarily dependent on effective moisture and temperature. Temperature variability – negligible in the sub-tropics – can be excluded as influencing factor at our site. Changes in C$_3$/C$_4$ vegetation would lead to values oscillating between -12‰ and -6‰ (as end members, if the plant cover was the only δ^{13}C-influencing factor). Measured host rock δ^{13}C ranges between +1‰ and +2‰. Apparently, high δ^{13}C values (up to +6.8‰) observed in our record are best explained as the host rock baseline signal modulated by isotopic fractionation of carbon. Such process would oppress any vegetation imprint on the δ^{13}C signal. The carbon signal is likely influenced by kinetic enrichment during dry periods due to a lowered hydraulic head, causing diminished winter drip rates. This in turn can lead faster to δ^{13}C fractionation. Similarly, longer residence time of water on stalagmite surfaces and reduced cave air rH might lead to additional evaporation of drip water (Fairchild and McMillan, 2007). Mühlinghaus et al. (2007) found that a slight drip rate decrease indeed results in strong positive enrichment of stalagmite δ^{13}C. Since via the drip rate dependence the δ^{13}C signal can be directly related to the moisture availability we will further use it as a proxy for winter aridity.

The general trend in the grey-scale record corresponds to dry episodes revealed in the stable isotope profiles (Fig. 3.9). Due to the different resolution (sub-annual for grey-scale and >5 yrs for stable isotopes) the exact assignment of grey-scale values to stable isotope profiles is not possible. However, δ^{13}C values are significantly enriched where stable isotope samples

were taken from multi-year dark layers (not shown). This long-term relationship should be valid also on seasonal scale. With the moisture availability depending on the season (Fairchild et al., 2007; Genty and Quinif, 1996), climatic and hydrologic changes likely result in crystal-growth variations. We assume that the dark dense layers were formed during the dry winter season when drip rate was low. Based on this assumption we interpret our grey-scale record as winter aridity proxy. Concerning the millimeter-scale intervals visually dominated by dark color it is likely that they represent multiple annual layers deposited during very dry conditions (drought). Comparison of layer counting and U/Th chronology together with the parallel occurrence of thick dark layers during weak ISM events (e.g. at 8.3 kyr BP) support this interpretation. We argue that thick dark intervals represent prolonged droughts.

To test correlations between the grey-scale and isotope records, we interpolated to a common resolution of 2 years unfiltered $\delta^{18}O$ and grey-scale profiles and calculated correlation-coefficients. We find that the grey-scale values do not follow the isotope records in general, but correlate significantly if only low $\delta^{18}O$ values are considered. Therefore, we applied a threshold of -5.3‰ to the $\delta^{18}O$ data and calculated the correlation-coefficient between grey values and $\delta^{18}O$, which are lower than the threshold. At this threshold a maximum correlation of -0.53 is found (95 % significance level). The correlation between grey values and $\delta^{13}C$ is strongest at threshold values around +0.85‰ (r^2=-0.36, p=0.05). The $\delta^{18}O$ and $\delta^{13}C$ profiles of KRUM-3 show periods of strong anti-correlation. Increased summer rainfall can be reconciled with severely dry winters if enhanced seasonality is taken into consideration. Increased seasonality during high-insolation periods (Ohgaito and Abe-Ouchi, 2007) stands in a good agreement with our interpretation. Higher air temperatures are likely to cause higher frequency and intensity precipitation (Allan and Soden, 2008). Intensified seasonality with shorter but stronger ISM and severe and more frequent winter droughts could trigger the $\delta^{13}C$ to anti-correlate with the $\delta^{18}O$ signal. Following this argument enhanced winter drought is recorded by $\delta^{13}C$ while multi-year aridity can be reflected in all, $\delta^{18}O$, $\delta^{13}C$, and grey-scale records.
The agreement between grey-scale and stable isotope records leads us to conclude that drought conditions recurred during the entire Holocene. However, the ISM experienced higher drought intensities after ∼4.8 kyr BP and aridity reached a maximum around 1.3 kyr BP.

3.5.2 Holocene climate change in northeastern India

On millennial timescales, KRUM-3 $\delta^{18}O$ shows gradual changes reflecting a coupling of ISM intensity to summer insolation and to the insolation-related movement of the ITCZ (Fig. 3.9a and g), as suggested by Haug et al. (2001) and Fleitmann et al. (2003a). Higher summer insolation in the Northern Hemisphere would push the ITCZ northward, resulting in stronger ISM and enhanced runoff. The millennial-scale ISM weakening during the mid and late Holocene observed in our record corresponds to a southward displacement of the

mean ITCZ position, caused by insolation changes (Wang et al., 2005). Other records from the monsoonal realm also reflect this Holocene pattern (Fleitmann et al., 2007; Wang et al., 2005). As today's climate in the study area is influenced by large scale atmospheric circulation patterns (Krishna Kumar et al., 1999; Dash et al., 2005) we explain centennial to decadal-scale variations in δ^{18}O, superimposed on an insolation-related trend as indirectly linked (via the Tibetan High) to the European climate realm, and to the IOD and ENSO (see below).

After 11 kyr BP, decreasing δ^{18}O values until the beginning of the HTM $\sim$9.2 kyr BP may reflect enhanced BoB freshwater plume build-up and increasing ISM rainfall. This ISM strengthening is interrupted by periods of weaker ISM conditions, lasting $\sim$20 to $\sim$150 years. A first event at 10.6 kyr BP is most pronounced in the δ^{13}C record, but minor excursions are also found in δ^{18}O and grey intensity. The severe anomalies found at 10.4 and 10.2 kyr, reflected by δ^{18}O and δ^{13}C increases and very low grey values, are possibly related to cooler conditions in Tibet (Thompson et al., 1997) and Europe (von Grafenstein et al., 1999) (Fig. 3.9). Enhanced snow cover in winter and spring over Central Asia and a stronger Tibetan High leads to stronger dry air mass transport into northern India, thus directly influencing the duration and/or intensity of winter drought in northern India (Dash et al., 2005). The HTM from $\sim$9.2 to 8.6 kyr BP is characterized by very high δ^{18}O values suggesting higher ISM rainfall, while δ^{13}C reflects increased winter aridity (Fig. 3.9). This behaviour differs from reported monsoonal variations in China (Dykoski et al., 2005) and Oman (Fleitmann et al., 2007). The strong δ^{13}C shift to drier conditions $\sim$9.3–9.0 kyr BP is in agreement with the 9.2 ka event reported by Fleitmann et al. (2008). One explanation for divergence of stable isotopes records might be, as already mentioned, increased seasonality, with higher ISM rainfall and enhanced winter drought. On the other hand, the δ^{18}O minimum may reflect extreme meltwater influx from the Tibetan Plateau, resulting in strong changes in BoB surface water isotopy. This scenario is also imaginable without a strong increase of summer rainfall.

The HTM was followed by ISM deterioration, culminating in a $\sim$400-year long two-pronged-structured period of droughts between 8.4–8.0 kyr, corresponding to the 8.2 kyr event found elsewhere (Baldini et al., 2002; Ellwood and Gose, 2006; von Grafenstein et al., 1999; Wang et al., 2005). Until $\sim$6 kyr BP, relatively stable conditions were interrupted only by decadal to centennial droughts at 7.4, 7.2 and 6.4 kyr BP. At $\sim$6 kyr BP increasing δ^{18}O values reflect a gradual decline in ISM strength, likely forced by insolation changes. While δ^{18}O reveals several ISM events after 6 kyr BP, δ^{13}C reflects interesting winter changes of a cyclic saw-tooth pattern. Several major glacier advances recorded on the Tibetan Plateau (Wanner et al., 2008; Yang et al., 2008) coincide with severe multi-year droughts (e.g. 3.2, 1.4, 0.4, and 0.32 kyr BP) revealed by our data. We propose that the unique saw-tooth pattern is related to glacier dynamics on the Tibetan Plateau (Fig. 3.9c). The age control of Tibetian Plateau glacier advances does not match our age model but we speculate

that gradual advances culminating in glacier high-stands might lead to prolonged and/or enhanced migration of dry air into northern India reflected in high δ^{13}C values. Rapid melting would lead to shorter and/or less severe winter conditions over NE India and would shift δ^{13}C back to more negative values. If our hypothesis is correct the reasons for cyclic behaviour of glaciers is worth further investigation.

The monsoonal variations associated with the '4.2 event' agree with conditions in China and Oman (Fleitmann et al., 2007; Wang et al., 2005), but differ from records further west (Arz et al., 2006; Cullen et al., 2000; Drysdale et al., 2005; Staubwasser and Weiss, 2007). The past ∼2 kyr witnessed a declining ISM, with the weakest ISM of the entire Holocene at ∼1.4–1.1 kyr BP, coinciding with strong ENSO activity (Fig. 9h). During the early Little Ice Age (LIA, timing after Wanner et al. (2008) and Haug et al. (2001)) the δ^{13}C record shows an increase in concert with the cooling onset. On the contrary δ^{18}O indicates a stronger ISM; weakening only ∼250 years later. Following our line of argument the lag in the δ^{18}O record may reflect that cooling in Tibet has a strong immediate effect on winter aridity in Meghalaya, while it need longer to effect the ISM rainfall.

Strongly enhanced δ^{13}C at ∼0.5 kyr BP can likely be associated with the LIA and reflect hydrological changes in NE India, similar to findings by Sinha et al. (2007) in a stalagmite from Dandak Cave, central India (Fig. 3.1). The driest conditions in our record appear to happen between 390 and 320 yrs BP, simultaneous with a prominent glacier advance on the Tibetan Plateau and the Late Ming Weak Monsoon period in China (Yang et al., 2008; Zhang et al., 2008). The late Holocene ISM was highly variable, with strong droughts indicated by above modern δ^{18}O values. With such enhanced variability the ISM rainfall recurrence is less reliable, with severe consequences for rural Indian societies (Bhatia, 1991; Dyson, 1991).

3.5.3 Atmospheric teleconnections

Instrumental data reveal that weak or failing ISM frequently occurs parallel to El Niño events (Fig. 3.9). Krishna Kumar et al. (2006) and Webster et al. (1998) proposed to link these two phenomena by the mechanism of the Walker circulation, yet the mechanism of the connection between ISM and ENSO is not fully understood. Negative precipitation anomalies, recorded in the Tibetan Guliya ice core, are found to significantly correlate with ENSO events Yang et al. (2000). Within the last 2 kyr, changes in the KRUM-3 grey-scale record correspond to the red intensity record from Laguna Pallcacocha, a proxy for El Niño activity Moy et al. (2002); Figs. 3.5b and 3.9). Low grey-scale values often coincide with higher red intensity and enhanced El Niño activity respectively, supporting a link between ISM and ENSO. Moreover, a significant negative correlation (-0.25, p=0.05) has been found between the grey-scale and red intensity records. This correspondence supports our assumption that dark laminae in KRUM-3 represent dry periods. Evolutionary spectral analysis provides evidence for a relation since ∼4.5 kyr BP (Fig. 3.8), whereafter
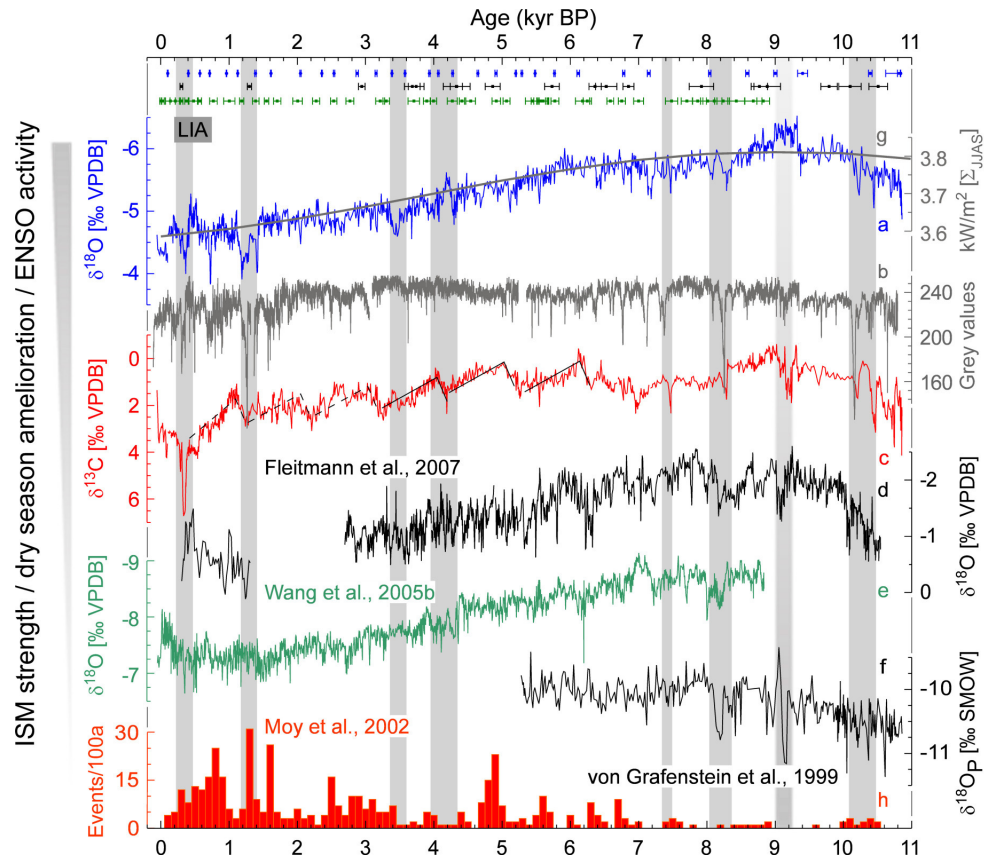
Figure 3.9: Juxtaposition of selected climatic records spanning the Holocene.
(**a**) δ^{18}O, (**b**) grey values, based on linear interpolation between U/Th ages, and (**c**) δ^{13}C from KRUM-3, are compared to other proxy records: (**d**) Oman stalagmite Q5, and (**e**) Dongge DA stalagmite δ^{18}O records, both representing monsoonal rainfall; (**f**) δ^{18}O of mid-European precipitation inferred from lake Ammersee; (**g**) sum of summer (JJAS) insolation at 30°N; (**h**) number of ENSO events in Ecuador, derived from a red intensity record. Dating errors for the different records are color-coded. Grey bars indicate major features found on centennial to decadal timescales. Black lines in the KRUM-3 δ^{13}C record visualize cyclic pattern discussed in the main text. The timing for the LIA is adopted from (Wanner et al., 2008).

the grey-scale record is characterized by high-frequency variability, with periods typical for ENSO (3 to 6 years). The timing agrees well with a stronger El Niño and enhanced ENSO variability since about 4 kyr BP, as found by Haug et al. (2001). Some disagreement between the red intensity and grey-scale records suggests that on centennial time scales also additional factors influence the ISM. The IOD, characterized by east-west sea surface temperature (SST) anomalies, plays an important role on Indian Ocean climate. Within the last 150 years, IOD events were found to correlate with El Niño events Chang et al. (2006); Abram et al. (2008); Meyers et al. (2007). It was suggested that IOD and ENSO modulate the ISM variability in the eastern Indian Ocean (Abram et al., 2008; Saji et al., 1999; Webster et al., 1999). The IOD characteristics could account for decadal to centennial-scale differences between records from Meghalaya and China (Fig. 3.9, Wang et al. (2005, 2008): while south China receives higher rainfall during positive IOD events,

NE India and Bangladesh likely receive less rain (Chang et al., 2006; Abram et al., 2008). We argue that large positive IOD events, especially when in phase with strong El Niño events, weaken the ISM. Enhanced ISM variability with severe droughts is likely linked to increased IOD and El Niño activity since ∼2 kyr BP – and possibly since ∼3 kyr BP.

Spectral analysis provides support for a Pacific influence on the study area. Several of the spectral peaks found in our record are similar to results from Pakistan (von Rad et al., 1999), and China (Dykoski et al., 2005). High frequencies found in the δ^{13}C record at 43 and 37 years (Fig. 3.7c) agree with results from sediments from the Arabian Sea and the Santa Barbara basin (von Rad et al., 1999), suggesting some ENSO influence on the dry season length and the ISM. The 15 year periodicity has been related to ENSO (Mann and Park, 1994). Also the 8.5 year cycle points to ENSO as an influencing factor, similar to stalagmite records from China (Dykoski et al., 2005). A trend to higher frequencies after about 5 ka BP is apparent in the grey-scale evolutionary spectra (Fig. 3.8), supporting our finding of enhanced influence from the Pacific during the late Holocene. Periodicities of 23 to 20 years have been associated with solar output variations (Neff et al., 2001). The 21.5 yr cycle (Fig. 3.7d) might correspond to the 22 yr cycle in the global temperature record, reflecting sun spot activity. The 10.4 yr cycle can be related to the Schwabe cycle.

KRUM-3 reflects rapid decadal-scale changes towards dry conditions centered at ∼10.450 and 10.230 years BP. Both events are interpreted as droughts and are very similar to changes in the δ^{18}O of precipitation in Europe, which were interpreted as short weakenings of the thermohaline circulation in the Atlantic (von Grafenstein et al., 1999). The correspondence between two distant regions suggests that in NE India the early Holocene ISM was influenced indirectly by North Atlantic atmospheric circulation changes, associated with changes of the Tibetan High (Dash et al., 2005; Krishna Kumar et al., 1999). A northern Hemisphere cooling strengthens the winter high pressure cell on the Tibetan Plateau. Associated enhanced snow cover length this may lead to a delay of the weakening of the Tibetan High in spring, and ultimately a delayed and/or weakened ISM. Such linkage could cause ISM failure during North Atlantic cold events (Krishna Kumar et al., 1999). A North Atlantic influence has also been suggested on the Chinese ASM (Dykoski et al., 2005). During the mid-Holocene the strengthening of the ENSO system likely led to a shift of the major western influence (Europe) to a south-eastern (Pacific, eastern Indian Ocean). On the basis of our data we conclude that the millennial-scale trend in our δ^{18}O record can be explained by decreasing insolation on the northern hemisphere. The early to mid Holocene (11–6 kyr BP) ISM centennial to decadal-scale variability was likely governed by changes of the westerlies and the Tibetan High. The late Holocene ISM seem to have experienced changes associated with the onset of the modern ENSO and IOD conditions in the Pacific and Indian Ocean respectively.

3.6   Conclusions

Our stalagmites constitute a first terrestrial absolute-dated high-resolution record from India covering the entire Holocene. δ^{18}O and δ^{13}C are interpreted as ISM-induced runoff and dry season aridity proxy, respectively. The grey values represent changes in stalagmite growth rate and as such are considered as an aridity proxy. While winter aridity is reflected only in the δ^{13}C and grey-scale data, multi-year aridity (drought) is recorded additionally in the δ^{18}O record. We draw three main conclusions from our Holocene record.

- Similar to other regions in the monsoonal realm the ISM experienced millennial-scale changes related to regional insolation changes. Strong ISM, associated with the northward extent of the ITCZ during the early and middle Holocene weakened ∼5 kyr BP.

- Centennial to decadal-scale events superimposed on the general trend of the ISM often show dramatic shifts to weaker ISM conditions which seem to be related to cold phases recognized in the Northern Hemisphere. Our data suggest that while in the early to mid Holocene (11–6 kyr BP) westerlies and the Tibetan High had a very strong influence on NE Indian climate, in the late Holocene the onset of the modern ENSO and IOD conditions in the Pacific and Indian Ocean seems to take control over the ISM variability.

- During the last two millennia NE India experienced its most variable and driest ISM conditions in the past ∼11 kyr. A parallel enhancement of ENSO variability compounds the notion of an indirect link between ISM and ENSO. In-phase occurrence of El Niño and positive IOD events weakens the ISM. The linkage between grey-scale and a Central American record shows weak ISM periods to be coincident with enhanced El Niño activity during the past ∼2 kyr.

Though our record constitutes an important contribution in reconstructing Indian Holocene climate, we note a demand to establish a dense network of well-dated palaeoclimate records in order to reach a comprehensive picture of temporal and spatial monsoonal dynamics.

4 Palaeoclimatic significance of element concentrations determined by LA-ICP-MS in a high resolution speleothem record from NE India

Sebastian F. M. Breitenbach[1,2,*], Mattias B. Fricker[3], Birgit Plessen[1], Norbert Marwan[4], Beat Aeschlimann[3], David Lund[5], Diego P. Fernandez[5,†], Hedi Oberhänsli[1], Jess F. Adkins[5], Detlef Günther[3], Gerald H. Haug[2,6]

[1] *Helmholtz Zentrum Potsdam, Deutsches GeoForschungsZentrum, 5.2 Climate Dynamics and Landscape Evolution, 14473 Potsdam, Germany*

[2] *DFG-Leibniz Center for Surface Process and Climate Studies, Institute for Geosciences, Potsdam University, 14476 Potsdam, Germany*

[*] *corresponding author: sebastian.breitenbach@gfz-potsdam.de, tel: ++47(0) 331 288 1347, fax: ++47(0) 331 288 1302*

[3] *Laboratory of Inorganic Chemistry, ETH Zürich, 8093 Zürich, Switzerland*

[4] *Potsdam Institute for Climate Impact Research (PIK), 14412 Potsdam, Germany*

[5] *California Institute of Technology, GPS Division, 1200 E. California Blvd., Pasadena, CA 91125, USA*

[†] *present address: Department of Geology and Geophysics, University of Utah, UT 84112, USA*

[6] *Geological Institute, Department of Earth Sciences, ETH Zürich, 8092 Zürich, Switzerland*

Keywords: laser ablation, ICP-MS, trace element, Indian summer monsoon, stalagmite, palaeoclimate

Abstract

We present a stalagmite element concentration record from NE India, covering the past 1500 years. Laser ablation inductively coupled plasma mass spectrometry is used to reconstruct a high-resolution element profile from a U-series dated aragonite stalagmite. Strontium, barium, uranium, and copper concentrations are positively correlated and are compared to δ^{18}O and grey values to reconstruct local rainfall variability. We develop a conceptual model for seasonal element variations and their linkage to climatic parameters at our study site. Comparison with instrumental data and other records suggests that both, element mobilization and inclusion into the stalagmite are governed by rainfall variability. Our record points to strong rainfall changes during the past 1500 years, with enhanced rainfall during the medieval period (820 to 1540 AD). Additionally, we provide tentative evidence that volcanic forcing also plays a role in element mobilization. Therefore, our stalagmite

element proxy record may archive volcanic eruptions.

4.1   Introduction

Seasonally varying precipitation is a key issue which the agriculture of sub-tropical coun-
tries has to deal with. The Indian summer monsoon (ISM), bringing rainfall to the Indian
sub-continent, is influenced by oceanic and atmospheric conditions in the Indian and Pacific
Oceans (Krishna Kumar et al., 1999; Saji et al., 1999). Detailed investigation is vital to
understand the variables that govern ISM dynamics, and to provide a reliable prognosis on
future monsoon changes. Existing instrumental records of precipitation present two major
difficulties. First, there are large spatial differences in rainfall distribution; droughts might
occur in central India, while the lowlands of Bangladesh are flooded. Second, available
instrumental records, many of which are discontinuous, cover a time span of ∼150 years
which is insufficient to represent implicitly the natural variability of precipitation.

To reach a comprehensive picture of past seasonal changes the compilation of instrumen-
tal and palaeoclimate data is essential. However, few well-dated Holocene high-resolution
palaeoclimate records are available from India so far (Sinha et al., 2007; Breitenbach et al.,
in prep. a). Additionally, the interpretation of palaeo-proxies, often based on assumptions,
is only an approximation of complex multidimensional processes. These include trans-
mission and storage of a global or regional climate signal interwoven with influences of
site-specific conditions. Adequate understanding of the different factors contributing to
palaeoclimate records requires long-term monitoring of the chosen sampling sites.

Cave microclimate has been used for record calibration and quantification (Fairchild et al.,
2007; Fairchild and Treble, 2009; Mattey et al., 2008b). Unfortunately, and mostly due to
logistic difficulties, in many parts of the world, like Asia, cave monitoring is still under-
represented. Stalagmites offer undisturbed long-term high-resolution climate profiles with
unique chronological control (Henderson et al., 2006; Overpeck and Cole, 2008). With
typical growth rates of 10–100 μm/year, and instrumental advances in recent years, they
provide palaeoclimate information on sub-decadal to sub-annual resolution. Geochemical
proxy records from stalagmites play an increasingly important role for reconstructions of
past climate (Fairchild and Treble, 2009).

Laser Ablation-Inductively Coupled Plasma-Mass Spectrometry (LA-ICP-MS) mapping is
becoming a popular method of analysis in various fields such as environmental sciences
due to fast analyses with high spatial resolution of major and trace elements (Woodhead
et al., 2007). Additionally, LA-ICP-MS offers a wide dynamic range and multi-isotope
capabilities, together with very low limits of detection (LoD). The advantages of the laser
ablation techniques are relativised when applied to cave deposits. The interpretation of
high-resolution element records in terms of climatic and meteorological variability is often
hampered, due to limited insight into hydrological and Karst processes at the study sites
(Desmarchelier et al., 2006; Fairchild and Treble, 2009; Johnson et al., 2006; Treble et al.,
2003).

Changes in element concentration in a stalagmite can record effective moisture availability during the late Holocene in NE India. The study site in Meghalaya is sensitive to monsoonal rainfall variability. This region receives enormous rainfall during the ISM, whereas the winter season experiences aridity. The pronounced seasonality makes our study site a key location for delineating seasonal climate variability, recorded over thousands of years. Understanding precipitation and runoff in the vulnerable region of Meghalaya might eventually help to make prognoses on flood or drought. Sub-annual to decadal scale reconstruction on past ISM could support forecast modeling and shed light on the rapidity and amplitude of climate changes.

We aim to reconcile high-resolution stalagmite elemental data with meteorological records of precipitation. Our arguments are presented in two steps: a) a conceptual model is used to describe how the climatic signal is transmitted into the cave environment, taking important local factors into account. b) further, we explain, based on this concept, the observed patterns of element concentration in the context of precipitation changes documented in instrumental data. The chronological limit for such comparison is given by the instrumental data sets. Assuming the governing factors for element dynamics remained unchanged; we reconstruct qualitatively the hydrological changes since about 500 AD.

4.2 Regional setting and site description

The sub-tropical Meghalaya Plateau is strongly affected by the ISM (Fig. 4.1a). Jowai, the nearest meteorological station and ca. ∼30 km NW from the cave site, receives 3445 mm of annual rainfall (Fig. 4.1b), 80 % of which is received during the ISM (May–September). During the winter season, less than 70 mm/month are recorded. On the Meghalaya plateau water is poorly retained, leading to dry season water shortage. On the other hand, runoff from Meghalaya is a major source for floods in northern Bangladesh (Murata et al., 2008).

The vegetation above Krem Umsynrang cave (25°13' N, 92°21' E, 825 m above sea level (m a.s.l.), Fig. 4.1a), is represented by C_4 grasses; tropical forest covers dolines and shadowy rock cliffs. The ∼40 m thick hostrock overburden consists of sandstone at the top, intercalated by a ∼50 cm thick coal layer. The overlying rock and the cave limestone belong to the Lakadong member of the middle Eocene Shella formation (Gebauer, 2008; Singh and Singh, 2000). The cave consists of a semi-active, sub-horizontally developed maze with three levels. The mean cave air temperature is lower than the mean air temperature in the region, with 20.5±0.7°C (monitored from March 2006 to September 2008) compared to ∼25°C at Jowai (Fig. 4.1b). Cave air temperature varies seasonally about 1.5°C, while mean air temperature at the surface varies 10°C between winter and summer. In the absence of local instrumental data, we use relative humidity (rH, ranging from ∼40 to 95 %) data provided by the National Centers for Environmental Prediction and the National Center for Atmospheric Research (NCEP/NCAR) reanalysis database (Kalnay et al., 1996). The vegetation activity follows seasonally changing soil moisture conditions (Khiewtam and Ramakrishnan, 1993). Hashimoto et al. (2007) and Khiewtam and Ramakrishnan (1993)
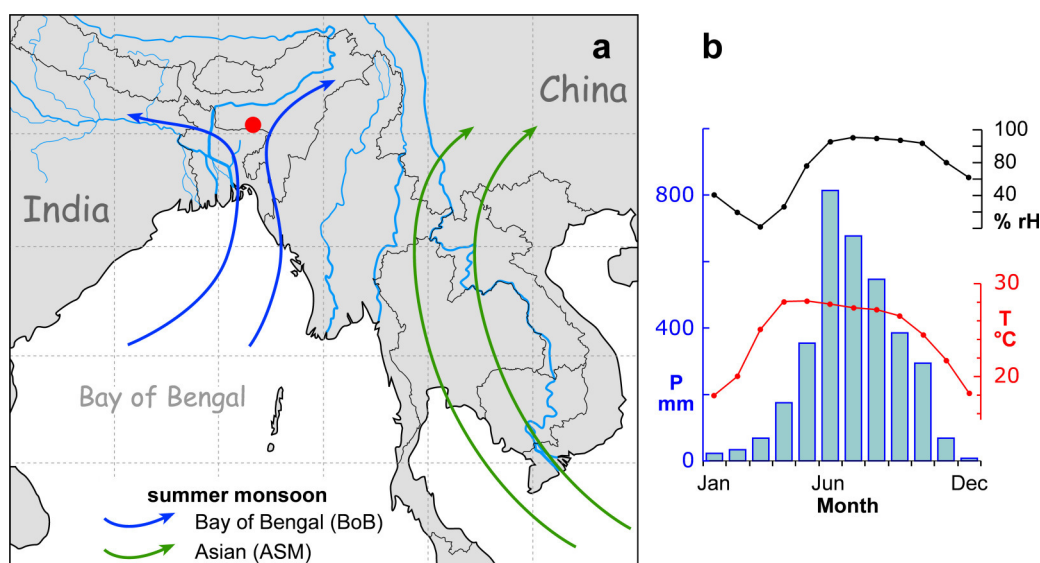
Figure 4.1: Map of the study area (**a**). Location of Krem Umsynrang Cave is marked as red dot. The location north of Bangladesh is ideal for studying the BoB branch of the ISM. The diagram in (**b**) shows rainfall for the nearest meteorological station Jowai (25°25'59.9" N, 92°12'1.7" E, 1334 m a.s.l.), based on monthly means for the period 1901–1930; air temperature and rH (1961–1990 monthly means) are calculated for the study area using NCEP/NCAR reanalysis data (Kalnay et al., 1996).

observed highest $p\mathrm{CO}_2$ levels in soil during the ISM season.

4.3 Material and Methods

The ∼64 cm long aragonitic stalagmite KRUM-3 covers the past ∼11,000 years (Breitenbach et al., in prep. a). KRUM-3 was broken in three pieces, and cut along the growth axis. Unpolished central slabs of approximate dimensions of 29×9×230 mm each were sampled for $\delta^{18}\mathrm{O}$ and $\delta^{13}\mathrm{C}$ (Breitenbach et al., in prep. a). Here, we discuss the element concentrations of the uppermost 73 mm, while the entire length of KRUM-3 will be presented in a future contribution. Micro X-ray diffraction (μXRD) is used for element concentration analysis on coal sample. 12 g of powdered sample were mixed with 3 g of Hoechst wax C and a pill with 40 mm diameter was pressed with 25 t. We used a PANalytical Axios advanced instrument and Pro-Trace software for the μXRD analysis. The employed instruments comprise a 193 nm ArF excimer laser by Lambda Physik (Göttingen, Germany), coupled to a quadrupole ICP-MS, ELAN 6100 DRCII by Perkin Elmer (Massachusetts, USA) (see Fig. 4.2 for operating conditions). An ablation cell was designed and in-house built to fit long stalagmite slabs without further sample size reduction. Prior to acquisition scanning, cleaning scans were performed with different settings (Fig. 4.1). Element concentrations were measured along line scans, (sub-) parallel to the growth axis and isotope sampling holes. Table 4.1 shows the list of the analyzed elements. Concentrations were calculated using a calibration protocol by Longerich et al. (1996) with NIST-610 SRM as external standard and $^{42}\mathrm{Ca}$ as internal standard. A detailed description of the analytical

Table 4.1: Mean element concentrations for the past 1500 years, limit of detection (LoD) for the elements discussed, and mean element concentrations in the coal analyzed by μXRD, with analytical error.

Method		^{65}Cu [ppm]	^{66}Zn [ppm]	^{88}Sr [ppm]	^{137}Ba [ppm]	^{238}U [ppm]
LA-ICP-MS	Mean	22	14	5306	55	17
LA-ICP-MS	MeanLoD	2.0	1.9	0.13	0.23	0.02
μXRD	Mean	15	11	37	<10	3.1
μXRD	Error (2σ)	2	2	2	3	1

method can be found in Fricker et al., in prep..
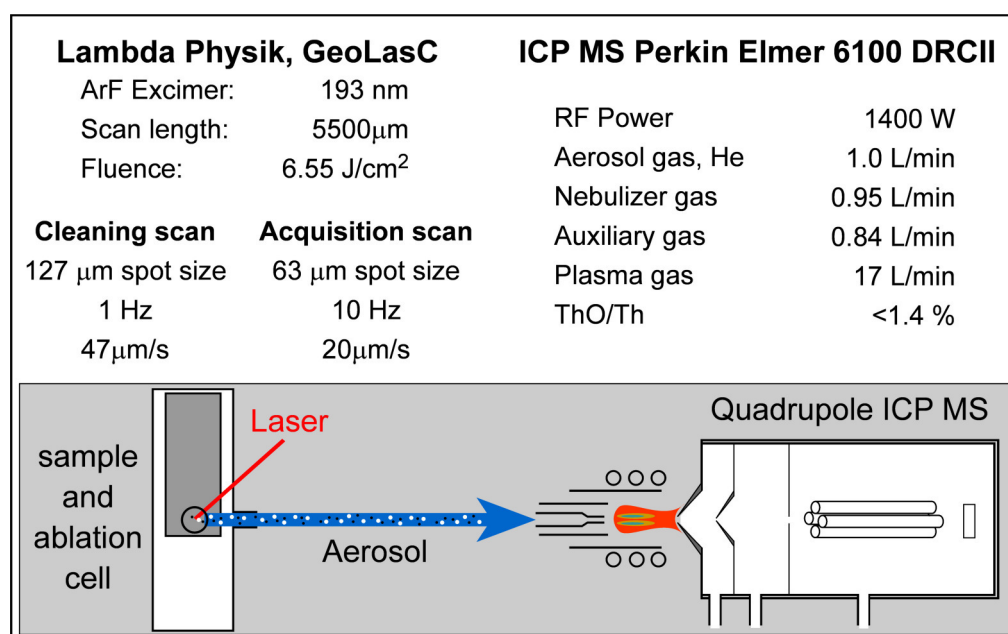
Figure 4.2: Summary of the operating conditions of the instruments used in this study.

4.4 Chronology

The interpretation of the element concentration changes as climate proxy requires a robust chronology. The age model for the 1500 year long KRUM-3 element record presented here is based upon linear interpolation between 7 discrete U/Th ages (Fig. 4.3). High U concentration of 10 to 20 ppm allows for very precise ages with errors as small as 0.4 %, as is seen in Table 4.2. The uranium concentration from U/Th ages are confirmed by the laser ablation data. Details on the multi-collector ICP-MS U/Th dating can be found in Breitenbach et al., (in prep. a). All ages are given in calendar years AD.

Table 4.2: U/Th dating results from stalagmites KRUM-3 from Krem Umsynrang Cave, India. For the calculations, an initial 230/232 value of 4±4 ppm (atomic) is used. Final age errors are the combination of the ^{232}Th correction and the measured ^{230}Th/^{238}U ratio. Errors are given as 2σ. There is no error propagated from the δ^{232}U uncertainty.

| Sample ID	Depth [mm below top]	^{238}U [ppb]	^{232}Th [pmol/g]	δ^{234}U(T)	^{230}Th/^{238}U [act] $\times 10^{-3}$	Age corrected [U/Th yrs]	Age [yrs BP]	δ^{234}U
LU02	4.2	10118.7±32	1.8±0.2	-230.3±2	1.13±0.03	158	102±5	-230.38
LW26	15.1	14885.5±59	0.9±0.6	-224.9±0.5	3.27±0.05	461	405±7	-225.24
LU06	31.4	15390.6±52	0.5±0.2	-221.6±1.6	4.48±0.03	630	574±5	-222.02
LW29	38.4	15213.9±54	0.8±0.5	-219.1±0.3	5.51±0.05	774	718±6	-219.56
LU05	53.6	20606.2±65	1.8±0.2	-222.6±1.2	7.23±0.03	1020	964±4	-223.24
LU11	65.1	15804.3±53	0.3±0.2	-217.6±1.5	8.44±0.04	1185	1129±6	-218.38
SJ14	70.1	17112.5±42	1.8±0.5	-220.4±0.3	10.52±0.07	1446	1390±10	-221.34

no error was propagated for δ^{234}U
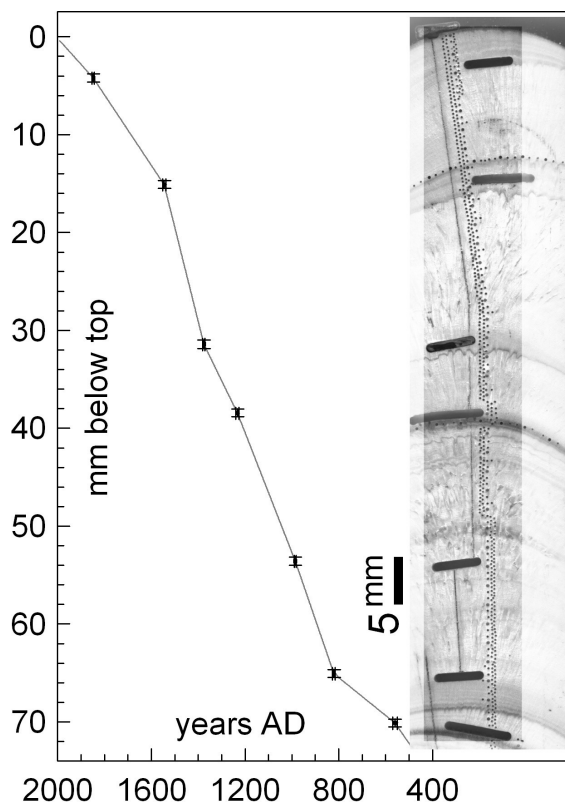
Figure 4.3: Age model for the 1500 year element concentration profile from stalagmite KRUM-3. The U/Th ages (black dots) are given with 2σ error. Fast growth with growth rates between 20 and 100 μm/year allow sub-annual laser ablation sampling. The scan shows the sub-samples for dating (black trenches) and stable isotopes (black dots). The laser transect is not visible, but parallel on the right hand side of the grey pencil line to the left of the stable isotope samples.

4.5 Results and Interpretation

Our stalagmite profile reflects strong variability of several major and trace elements. Here, we focus on those elements (Tab. 4.1) that are highest correlated to each other. All elements discussed here show a positive co-variation during the 1500 year period (Fig. 4.4) and increase together with increasing growth rate. μXRD analyses revealed that the coal is likely only a minor source for elements (Tab. 4.1), and we assume that the major contribution of elements stems from the arcosic sandstone.

4.5.1 Growth rate and signal resolution

KRUM-3 grew during the past 1500 years with a growth rate of 30–100 μm/year; with enhanced growth between 800 and 1550 AD (Fig. 4.5h). Evaluation of depth-age information of KRUM-3 reveals that the stalagmite grew several dozens of micrometer (μm) per year. Changing growth rates lead to varying time resolution at a given crater size (63 μm). Additionally, slight sample smoothing is expected from the aerosol transport.
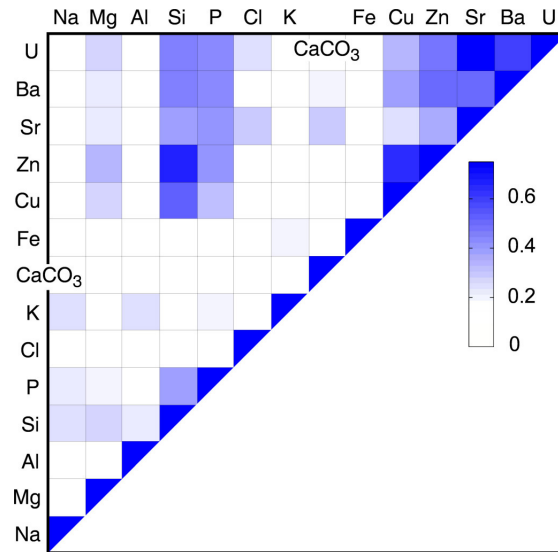
Figure 4.4: Element-element cross correlation plot. Included are the elements for the past 1.5 kyr. All shown elements are positively correlated, except Fe which shows no correlation with any element.

The observed amplitudes in element concentrations and comparison with the age model support our assumption that we achieve sub-annual resolution. High growth rates of up to 100 μm/year result in sub-annual time resolution, assuming that a final datapoint integrates over $\sim$13 μm. Growth rates of less then 30 μm/year before 800 AD and after 1550 AD allow only seasonal time resolution. Still, annual resolution is found and inter-annual changes can be reconstructed with confidence.

4.5.2 The proxy record during the past 1500 years

The element profiles reflect three periods of different characteristics (Fig. 4.5). The first interval from 500 AD to $\sim$820 AD is a relatively quiet phase, followed by a second period of high element variability between 820 and 1540 AD. A third interval started after 1540 AD, and very alike the first, is relatively stable with low element concentration variability. Additionally to the element profiles we take advantage of KRUM-3 δ^{18}O and grey scale data, which are described in detail for the entire Holocene in Breitenbach et al., (in prep. a). δ^{18}O reflects past hydrological conditions in the northern Bay of Bengal (BoB) and summer (ISM) rainfall amount. We interpret lower δ^{18}O values as intensified ISM rainfall and a larger BoB freshwater plume (Breitenbach et al., in prep. b). Higher δ^{18}O values in turn reflect drier summer conditions and weak ISM and we refer to drier or wetter conditions when δ^{18}O is above or below the modern value (-4.6‰), respectively (Fig. 4.5a). We interpret the grey scale values as proxy for drought intensity; lower grey scale values reflect intensified drought conditions (Breitenbach et al., in prep. a; Fig. 4.5b). The grey scale values generally correspond to the oxygen isotope record; some differences are likely due to the influence of winter conditions on the sub-annual grey scale record, which are not present in the δ^{18}O record.
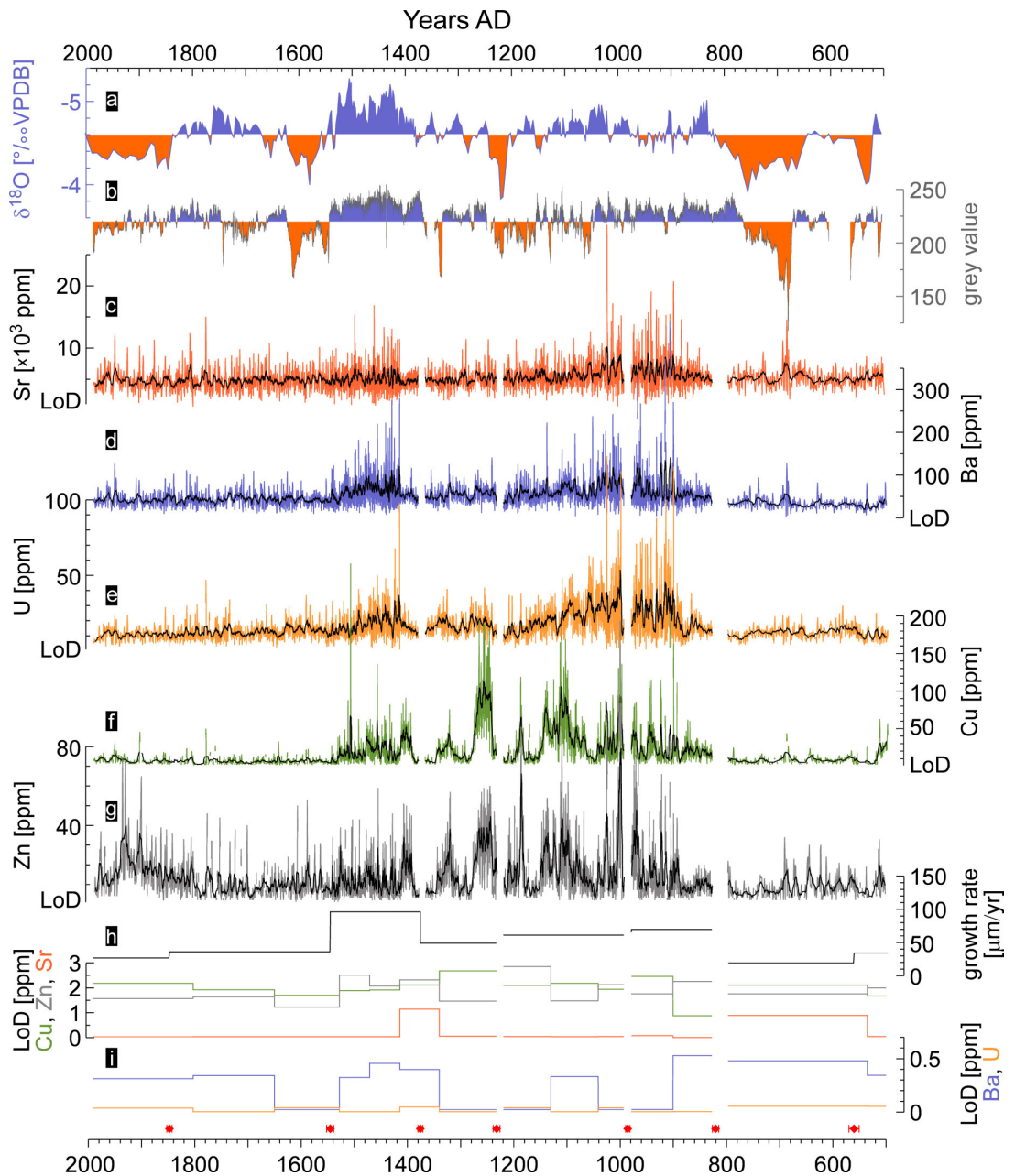
Figure 4.5: Element profiles from KRUM-3 for the past 1500 years. δ^{18}O reflects ISM variability (Breitenbach et al., in prep. a) (**a**). Blue filling shows periods wetter, orange filling drier than today. The grey scale record follows broadly the δ^{18}O profile and is interpreted as aridity proxy (**b**) . Lower grey values are expected during dry periods. The color coding is similar to, but chosen arbitrarily for best correspondence with (a). Sr variation (**c**) shows large variability and is very similar (Fig. 4.4) to Ba (**d**), and U concentration (**e**). Cu reacts very pronounced on changes in the soil and hydrological system above the cave (**f**). Zn is, together with Cu, a potential proxy for volcanic aerosol sulfate flux (**g**). The black curves in c) to f) represent a 15 point running averages. The period of element increases between 820 AD and 1550 AD also shows higher growth rates (**h**). Red diamonds with error bars are U/Th dates. In **i**) we show the LoD for the different elements and laser scans.

4.5.3 The period 500–820 AD

The first interval is characterized by low element variability and above modern $\delta^{18}O$ values reflect drier ISM conditions. From 780 AD onwards an increase in rainfall is found in both, $\delta^{18}O$ and grey scale values (Fig. 4.5b). The Sr and Ba records are very similar, but the concentration is with 1000 to 25000 ppm one order of magnitude higher than Ba (Fig. 4.5c and d). Between 500 and 800 AD, Sr shows relatively low variability around a mean value of 5195 ppm. A single peak is found in both records at 685 AD, when Sr concentration increases for ~5 to 10 years to 15000 ppm, while Ba peaks at 100 ppm. Uranium is found at a mean concentration of 12 ppm, reflecting only low variability in this early part of the record (Fig. 4.5e). Until 520 AD, the Cu concentration (Fig. 4.5f) decreases from 30 ppm and remains low with a mean concentration of 11.6 ppm. Zinc shows decadal scale variation between 10 and 20 ppm, unlike the above mentioned elements (Fig. 4.5g).

4.5.4 The period 820–1540 AD

The second time interval of our record reflects highly variable conditions. $\delta^{18}O$ points to wet conditions, except for a 40 year long dry interval between 1200 and 1240 AD. Several rapid changes to dry conditions took place within two to five years and are followed by about 30 years of intense ISM. These repeated fluctuations give the record a characteristic see-saw pattern. Between 1000 and 1350 AD the ~30 year periodicity is very pronounced. Wettest conditions are recorded between 1420 and 1540 AD. The grey values also point to generally moist conditions (Fig. 4.5b), with observed higher variability between 1050 and 1240 AD. Sr values of up to 25000 ppm are found between 820 and 1200 AD, with very strong fluctuations. Some anomalies, like the 4 events between 900 and 920 AD are coeval with Ba maxima. In 1010 AD, a short-lived Sr maximum is found which correlates with a Ba anomaly. Until 1200 AD, Sr concentration decreases by ~50 %. After a stable interval until ~1400 AD, Sr starts to fluctuate again, but not as pronounced as in the Ba or Cu profiles (Fig. 4.5d and f). Ba concentration reached 250 ppm around 900 AD, 10 years later 300 ppm. The following 300 years reflect elevated Ba concentration and variability. Although not reaching the earlier maxima, high Ba values are observed ~1100 AD, parallel to very high concentrations in Cu. No significant anomalies are recorded from 1200 to 1400 AD, but between 1240 and 1280 AD Ba increases to ~70 ppm. A last decadal scale Ba increase is recorded between 1400 and 1540 AD, with a rapid rise to ~300 ppm and a gradual decrease, in concert with depleted $\delta^{18}O$ values. Uranium rapidly increases to ~80 ppm around 880 AD (Fig. 4.5e). The concentration remains elevated, with rapid fluctuations, until 1050 AD. A relatively gradual decline back to the mean concentration of 12 ppm follows 1200 AD. Between 1240 and 1360 AD two events of elevated concentration are registered. Very similar to the variability of Ba and Sr, but less structured then the Cu profile, a large event with enhanced U concentration is observed, starting around 1400 AD. This event is gradually terminated during the 16th century. The Cu concentration fluctuates dramatically between 820 and 1550 AD. The mean concentration increases for

this interval to 28.3 ppm, but maxima reach almost 200 ppm. After 820 AD, Cu increases stepwise to ∼60 ppm around 1000 AD. This peak is followed by a 50-year decrease to about 12 ppm and another rise to a second maximum at 1100 AD, similar to the first peak. A rapid decline is interrupted by a 20 year long event, whereafter very low concentrations are reached within only 10 years at 1140 AD. Forty years later a short-term peak is found, reaching 115 ppm. The most pronounced Cu increase is observed between 1240 and 1280 AD, together with an increase in Zn (Fig. 4.5g), followed 30 years later by a minor peak. The last period of enhanced Cu variability is observed between 1390 and 1540 AD, with maximum concentrations of ∼90 ppm. Zn almost mirrors the Cu pattern, although maxima reach only about 100 ppm.

4.5.5 The period 1540–2000 AD

After 1540 AD the low variability low element concentrations are almost reached again, similar to the early part of the record. Drought, lasting from 1550 to 1670 AD, is recorded in the δ^{18}O and grey scale records (Fig. 4.5a and b). The period from 1670 to 1840 AD was apparently slightly wetter than today, while the last 150 years seem to have been relatively dry. Unlike the other elements, Sr concentration starts to vary with a ∼20 year periodicity after 1830 AD, clearly visible in the 15 point running average (Fig. 4.5c). Ba is relatively stable around a mean of ∼45 ppm. The U record shows only low variability around a mean value of 12.2 ppm, similar to the early part of the record. Cu concentration in this late phase is as low as during the early interval, except for a short increase around 1900 AD. Zn (Fig. 4.5g) however shows a different picture. Between 1600 and 1800 AD, it shows several short lived peaks. From 1800 to 1940 AD, an increase is found, with two maxima up to 70 ppm at 1900 and 1935 AD. The latest period finds again decreasing Zn concentrations.

4.6 Discussion

4.6.1 Seasonal climate signal transmission into the cave — a conceptual model

In Figure 4.6 we present a conceptual model of seasonal variability for some of the factors that govern provenance, transport, and incorporation of elements into the stalagmite. This concept is the basis for our interpretation of the element profiles reconstructed from KRUM-3. Element mobilization depends on the biological and hydrological characteristics above the cave. Fairchild and Treble (2009) discuss potential element sources, including dust, wet atmospheric deposition, sediment and bedrock. Dissolution is focused on the zone of regolith where pCO$_2$ is highest; therefore the primary element and calcium source is likely the soil and upper bedrock (Fairchild and Treble, 2009). Our cave is overlain by sandstone with a thin soil, underlain by coal and limestone. In Meghalaya, the biological activity peaks during the summer monsoon (Ramakrishnan and Ram, 1988). The associated litter decomposition reaches a maximum with early ISM rainfall resulting in enhanced
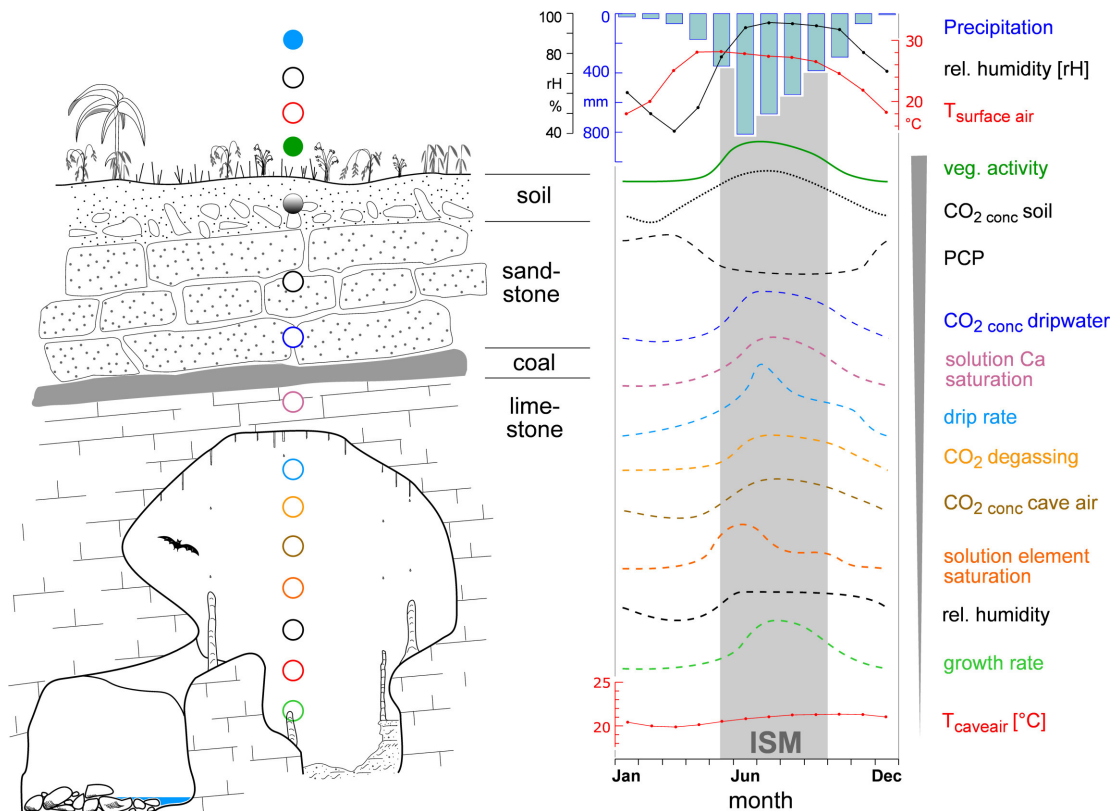
Figure 4.6: Factors influencing element concentration changes in stalagmites in seasonal context at Krem Umsynrang Cave. Cave air temperature was monitored from March 2006 to August 2008. Rainfall, air temperature, and rH are given for station Jowai as in Fig. 4.1b. Normal and dotted lines represent published parameter (see main text for discussion and references). Dashed lines show hypothetical behavior of the factors at the study site.

pCO$_2$ in soil (Hashimoto et al., 2004) during the (early) wet season and increased element loss from the soil, due to rapid leaching (Khiewtam and Ramakrishnan, 1993). The excess moisture during ISM refills conduits in the percolation system, impeding prior calcite precipitation (PCP). Due to high soil pCO$_2$ during ISM, CO$_2$ concentration in infiltrating water is likewise enhanced, resulting in higher Ca and element dissolution rates in the hostrock and probably in higher drip water Ca saturation. Additionally, sea salt components likely increase during ISM, due to higher sea spray production in summer (Begum et al., 2004; Shrestha et al., 1997).

Element transport is divided into three modes, **a**) particle, **b**) colloid, and **c**) solutes (Fairchild and Treble, 2009). We did not observe residues in U/Th samples in KRUM-3 and assume that particle-bound transport is insignificant in our case. Borsato et al. (2007) found enhanced colloid transport during high infiltration times. The major transport modes for the elements presented here are likely solutes and possibly to some extent colloids (Zhang et al., 2005).

Element concentration in percolating water peaks probably with the first infiltration events

during pre-monsoon and somewhat delayed in drip water, when easily leached elements are flushed into the cave. The arrival of the peak depends on the reservoir response time, and element concentration should remain elevated until the early dry season (October–November). Drip rate follows probably fairly closely the rainfall pattern, but with a lag, dependent on infiltration response time. With higher hydraulic head, drip rate should peak after initial refill of the percolation system, and is subsequently likely to remain elevated due to fast accumulation of infiltration water in the bedrock. With ceasing rainfall it gradually lowers, reflecting the reservoir draining.

The incorporation of elements into aragonite is more complicated than for calcite, due to the orthorhombic crystallization (Fairchild and Treble, 2009), and can result in lateral element variability, as reported by Finch et al. (2003). Additionally to the availability of trace elements in the feeding drip water, the incorporation is controlled by crystal structure Reeder et al. (1999). Ba and Sr likely substitute for Ca in the carbonate (Fairchild and Treble, 2009; Finch and Allison, 2007). We follow Borsato et al. (2007) and Zhang et al. (2005) in that Cu can be deposited as colloids during high infiltration periods. Cu, archived in stalagmites, can possibly serve as proxy for volcanic eruptions with large sulfur emissions (Frisia et al., 2005). The factors that govern the incorporation work probably in parallel since all our elements are positively correlated.

Elements vary on a seasonal scale in KRUM-3, with higher concentrations probably during bright layer deposition (ISM period). Faster growth seems to allow more Sr to be included (Borsato et al., 2007). We observe growth laminae with different grey scale values; dark grey translucent layers are thin and microcrystalline, while bright layers are showing elongated and porous crystallization. The different crystallization results likely from variable growth rates (Breitenbach et al., in prep. a). $CaCO_3$ deposition (and hence growth rate) is bound to climate dependent parameters, such as amount of seepage water, Ca saturation state of the drip water and CO_2 degassing (Fairchild et al., 2007). Growth rate is probably highest during the wet season (Fig. 4.6), as Ca saturation is one limiting factor for crystal growth. CO_2 degassing from the wet stalagmite surface influences carbonate deposition, so that maximum growth is likely found before maximum CO_2 concentration in the cave air is reached (early ISM). CO_2 degassing is possibly enhanced during summer due to a stronger gradient between drip water and cave air pCO_2. This should lead to a slightly lagging CO_2 concentration peak in cave air. We note that highest CO_2 degassing could also occur during the winter, due to lower pCO_2 in cave air (Fairchild and McMillan, 2007); however, evidence from the carbon isotope and grey value data supports the concept proposed here (see Breitenbach et al., in prep. a for details). Faster growth is prone to increase the number of lattice defect sites and the porosity, which can be filled interstitially with transported elements (Fairchild et al., 2001; Fairchild and McMillan, 2007).

In the cave, rH was measured at 80–90 % during dry season field campaigns in 2006 and 2007. These low values probably reflect variable rH conditions above the cave (Fig. 4.6). During the ISM season, cave rH values close to 100 % are very likely due to excessive water

availability. Cave air temperature is relatively stable and assumed not to influence element incorporation into $CaCO_3$ in Krem Umsynrang Cave.

The causal connection between the different factors is simplified for our study site. At different cave locations the coherence has to be established very carefully. Until monitoring of the variability of the parameters shown in Figure 4.6 is carried out, this schematic is only seen as preliminary. Longer-term element variability is certainly influenced by changes in all, the atmo-, bio-, and pedosphere. Volcanic eruptions for example might change atmospheric aerosol loading, and subsequently rainfall pattern, which in turn impacts vegetation and biotic activity in the soil. Additionally, such events would acidify the soil and enhance element mobilization.

While certainly several superposed factors control the element concentration variations in KRUM-3, disentangling the different acting parameters has to await detailed long-term observations of dripwater chemistry. The observed changes in element concentration are interpreted as reflecting mainly rainfall variability. Here, we will propose an outlook with the hypothesis that changes in the soil water can be associated with volcanic eruptions.

4.6.2 Comparison of element concentration with instrumental data

Comparison of elemental variations with regional precipitation (Cherrapunji and Jowai meteorological stations) shows that maximum Ba and U concentrations often match August rainfall peaks (Fig. 4.7). Strontium seems to follow Jowai ISM rainfall. Strict statistical correlation does not give meaningful results, due to the distance between the stations and the study site, too short instrumental records, and age uncertainties in the element proxy record. The concentration changes for the elements likely mirror the seasonal pulse of high- element loading in the percolating water. We assume that an initial element peak is derived from the first heavy rainfalls during the early ISM. Finding the peak concentration coinciding with August rainfall may point to a response time of the drip water of several weeks, a lag not surprising in a hostrock reservoir of ∼40 to 50 m (Fairchild and Treble, 2009). We assume that slight temperature changes observed in the cave have only limited influence on element variability, due to the subtropical location. Even on glacial to interglacial timescales, temperature changes were found to be of minor influence on element variations, compared to rainfall (Cruz Jr et al., 2005).

4.6.3 Rainfall variability in NE India

We interpret our $\delta^{18}O$ record as a proxy for rainfall and ISM strength (Breitenbach et al., in prep. a). The oxygen profile shows similarities to the oxygen record from Dandak Cave, despite large age uncertainties (Fig. 4.8) (Sinha et al., 2007). Their central Indian $\delta^{18}O$ record shows values below modern during the period 940 to 1340 AD, and between 1400 and 1520 AD, interpreted as increased rainfall. The disagreement between the Dandak cave and our $\delta^{18}O$ record can be explained by both regional differences of monsoonal rainfall
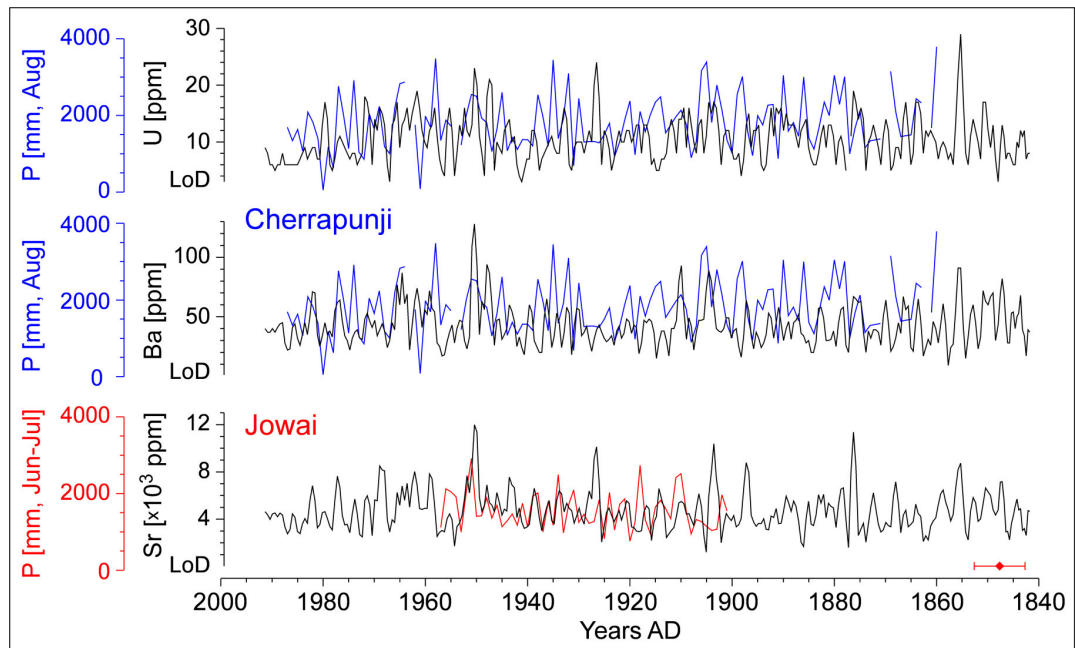
Figure 4.7: Comparison between KRUM-3 element data and meteorological observations. Two available meteorological datasets are shown; Jowai (in red) is the closest station available, while Cherrapunji (in blue) is shown as one available longer record. Barium and uranium concentration in KRUM-3 seem to increase with monsoonal rainfall. Strontium is found to correlate with main monsoonal rainfall (June–July) at Jowai. However, strict correlation is hampered by the limited meteorological data available and the age uncertainty in the element record. The red diamond represents U/Th age with 2σ error.

and chronological uncertainties. Taking these records as proxies for rainfall amount, we observe above modern precipitation in the period 820 to 1540 AD. This interval is approximately coincident with the Medieval Warm Period (MWP, $\sim$900 to 1300 AD) (Wanner et al., 2008). High element concentrations and lower $\delta^{18}O$ values (Fig. 4.8) reflect wetter conditions in NE India during the MWP, compared to the LIA (1300 to 1850 AD). The MWP has been described in various other archives from the Indo-Pacific domain. Staubwasser (2006) re-evaluated a varve thickness record from the Arabian Sea, found enhanced rainfall during the MWP ($\sim$800 to 1550 AD), supporting our argument. He interpreted enhanced varve thickness as reflecting reduced runoff, in contrast to earlier interpretation (Lückge et al., 2006).

The ISM rainfall is not independent of large-scale atmospheric changes. The seasonal recurrence of the ITCZ is a possible driver for ISM rainfall variations on millennial timescales. Enhanced and/or prolonged northward migration of this rainfall belt into the Asian continent can strengthen the ISM and allow for higher rainfall (see Breitenbach et al., in prep. a for detailed discussion). However, as Haug et al. (2001) pointed out, the position of the ITCZ is not independent of sea surface temperatures (SST) in the Pacific. El Niño events are characterized by above normal SST and a more southerly ITCZ position.

Breitenbach et al., (in prep. a) find evidence that El Niño events affect ISM strength together with the Indian Ocean Dipole (Saji et al., 1999). Stronger and more frequent El
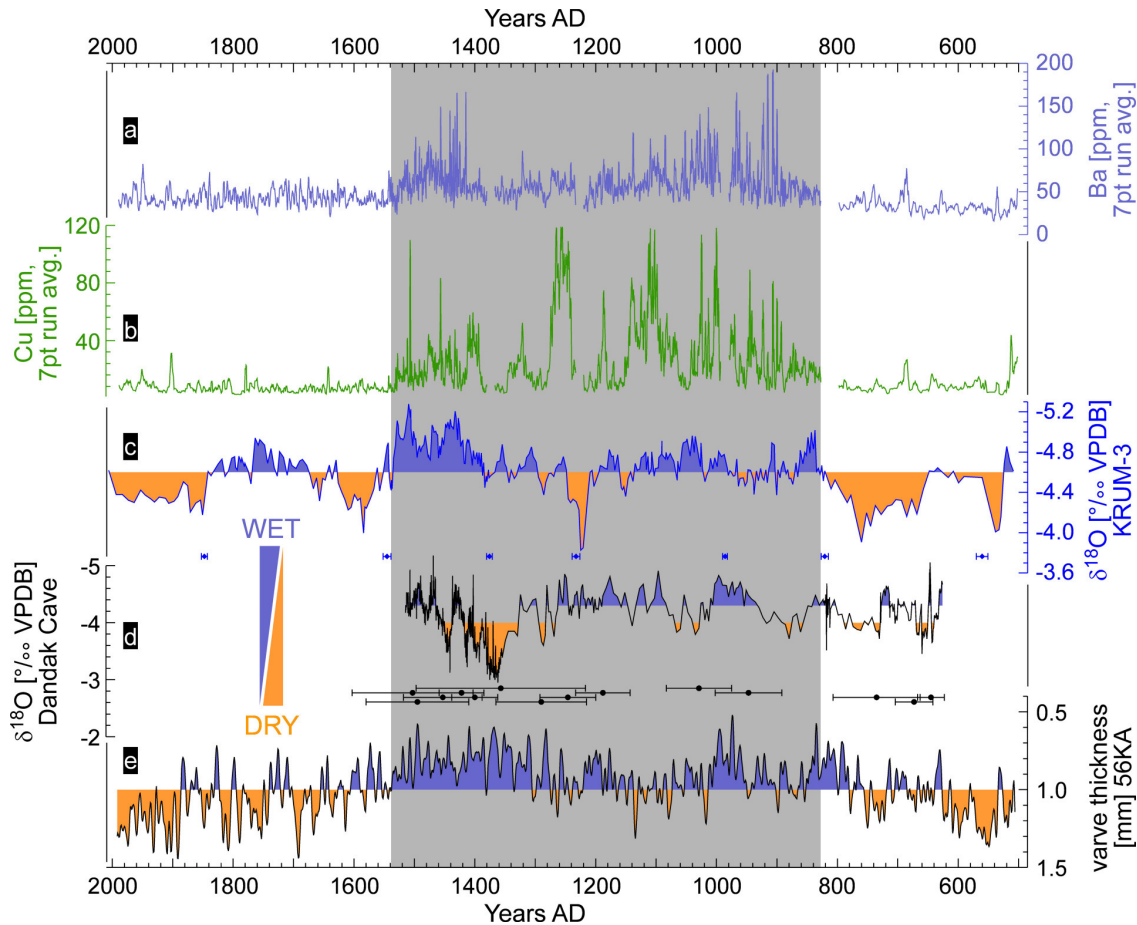
Figure 4.8: KRUM-3 elements and stable oxygen ratios compared to regional palaeoclimate records. KRUM-3 Ba concentration (**a**) is compared to **b**) copper concentration, **c**) δ^{18}O of KRUM-3 **d**) δ^{18}O from Dandak Cave, central India (Sinha et al., 2007), and **e**) varve thickness from sediment core 56KA, recovered from the northern Arabian Sea (Lückge et al., 2006; Staubwasser and Weiss, 2007). Blue diamonds with error bars represent the U/Th dates taken from KRUM-3, while black dots with error bars assign the U/Th dates from the Dandak Cave stalagmite. The cut-off value, separating the blue and orange filling in the KRUM-3 δ^{18}O is the modern value of -4.6‰. For the Dandak Cave record, the filling is adopted from the original authors. For the sediment flux record (e), an arbitrary cut-off value is chosen that fits the profile to the KRUM-3 proxy records. Grey shading shows wettest conditions in our record, corresponding with the 'Medieval Climate Anomaly', found by Wanner et al. (2008) and Sinha et al. (2007). However, our element and stable isotope record reflects wet conditions to sustain 200 years longer then elsewhere, contradictory to the Little Ice Age, found in central India and elsewhere.

Niño events, especially if coinciding with positive IOD events are likely to weaken the ISM. The absence of strong El Niño's might allow for enhanced ISM rainfall. Such interpretation is in agreement with records from America. Rein et al. (2004) describe El Niño weakening between 800 and 1250 AD. Laird et al. (1996), using lake sediments, and Stine (1994), evaluating relict tree stumps, reported very strong droughts in Northern America for the MWP interval. These droughts point to lowered El Niño recurrence and possibly La Niña conditions.

4.6.4 Speleothem element variations as potential recorders for volcanic eruptions

Understanding the impact of volcanic eruptions on climate is of importance to disentangle natural and anthropogenic climate forcing (Gao et al., 2008). This impact depends on many variables such as plume height, geographical position, eruption duration, and magma composition (Parfitt and Wilson, 2008). Eruptions at tropical locations and producing large amounts of sulfuric acid over a long period have certainly much stronger effects on global climate than short-term, low-productivity events at higher latitudes. Zielinski et al. (1995), Zielinski (2000) and de Silva and Zielinski (1998) analyzed the chemical composition in ice cores and show increases of sulfur loadings during large eruptions and link them to climate changes. Gao et al. (2008) reconstruct sulfate aerosol loading for the past 1500 years based on 54 ice cores from both hemispheres. These authors show that aerosol exchange between the hemispheres is limited, while tropical aerosol injections will be distributed globally. Therefore, they reconstruct the sulfate loading individually for each hemisphere, and as a global mean. One finding of Gao et al. (2008) is that in the 13th century the atmospheric sulfate flux was 2 to 10 times higher than in any other century within the past 1000 years. Speleothems potentially serve as recorders for past global volcanic activity, although such cutting-edge investigations still face many difficulties (Fairchild and Treble, 2009; Frisia et al., 2005). Volcanic sulfur emissions can strongly influence the soil chemistry and hence the mobilization of elements from the soil and host rock (Wynn et al., 2008). The rapid changes in the Cu and Zn records (Fig 4.5f and g) and visual correspondence with volcanic sulfate injections, reconstructed by Gao et al. (2008) give evidence that element concentration might be altered by eruptions. Both, Cu and Zn increase at times of enhanced volcanism (Fig. 4.9). Copper goes readily into solution as Cu sorption is pH dependent (Borsato et al., 2007; Marshall and Fairbridge, 1999). Cu concentration increases in dripwater are probably due to acidification of soil waters. However there is ambiguity in the timing of the element increases if forced by soil acidification.

Given that our interpretation that the Zn and Cu concentrations depend on volcanic forcing and associated soil chemistry changes is correct, we can clearly see that many unknown eruptions with large aerosol injections took place in medieval times (Fig. 4.9). As examples for major eruptions, we label some of the possible resulting element peaks using information provided by Gao et al. (2008) and the compilation of large historical events of the Global Volcanism Program of the Smithsonian National Museum of Natural His-
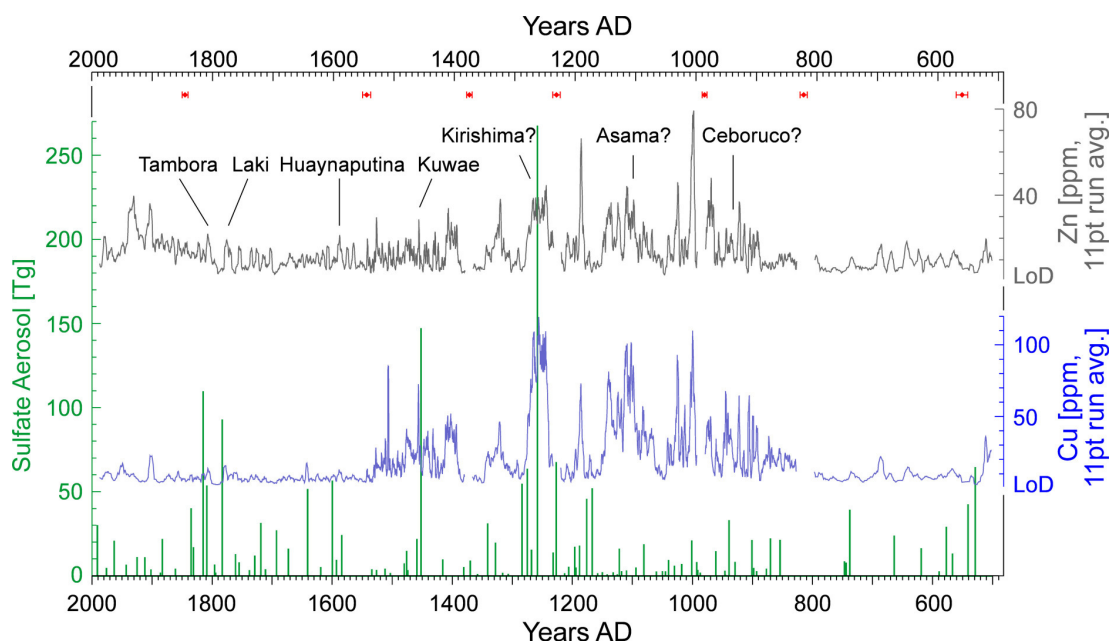
Figure 4.9: Element mobilization may potentially be forced by volcanic sulfate aerosol loading. Red diamonds with 2σ error bars indicate KRUM-3 U/Th dates. Both, Zn (in grey) and Cu (in blue) increase rapidly when atmospheric sulfate loading increases, as reconstructed from ice cores by Gao et al. (2008) (in green). We interpret such characteristics as changes in soil acidity and subsequently in element mobilization due to sulfuric acid fallout. Record comparison shows the increasingly problematic assignment of individual eruptions to element peaks with increasing age. Please see main text for discussion of the difficulties in data interpretation.

tory (data available on http://www.volcano.si.edu/world/largeeruptions.cfm). The large Cu anomaly may result from the 1259 AD Unknown event, which has been reported from both hemispheres (Emile-Geay et al., 2008). This eruption may well have been a Kirishima eruption in Japan, which begun the 25 January 1235 (after historical records and AMS ^{14}C results, Okuno et al. (1998). The end of this event is not known. However, to firmly assign atmospheric sulfate spikes and stalagmite element peaks to individual eruptions, additional geochemical and tephrochronological information for historical eruptions is required. Providing a quantitative reconstruction of eruption intensity or an improved timescale for unknown eruptions is beyond the scope of our study.

The complex changes in stalagmite element concentration forced by volcanic eruptions are difficult to delineate. Sulfuric acid produced during tropical eruptions will certainly be precipitated within a few years, but the induced changes in soil and host rock might buffer the acidification, with prolonged element leaching over decades. This effect is likely enhanced when multiple quasi-simultaneous eruptions lead to cumulative H_2SO_4 flux from the atmosphere. Furthermore, aerosols, serving as condensation nuclei in the troposphere, might have enhancing effects on monsoonal rainfall intensity, especially when atmospheric aerosol loading is enhanced during pre-monsoon (Lau and Kim, 2006; Lau et al., 2008). Other authors find volcanic aerosols of strong volcanic eruptions to have a positive effect

on the occurrence of El Niño events (Adams et al., 2003; Emile-Geay et al., 2008). To understand the competing forcings, additional studies are necessary. For example, the sulfur isotope ratio $\delta^{34}S$ might be a powerful proxy to distinguish the different natural and anthropogenic sources that contribute to the total S concentration in stalagmites (Wynn et al., 2008).

4.7 Conclusions

This study presents a 1500 year long high-resolution element concentration record from a U/Th dated stalagmite collected in northeastern India. LA-ICP-MS element data shows significant changes within this time interval. A conceptual model is proposed for a variety of influencing factors that could force concentration changes in the stalagmite profile. This model and from comparison of element concentrations and instrumental data lead us to conclude that element variations are governed by summer rainfall variability.

When compared to other climate proxies, our element record provides insight into regional ISM changes. While between 850 AD and 1550 AD element concentration is much enhanced, reflecting higher effective rainfall, the time before and after this interval does not show anomalies. There is evidence from the behaviour of Cu and S in our record that element mobilization is further enhanced by higher volcanic activity during this period, with subsequent changes in the soil cover and hydrochemistry. We propose the about 700 year long wet period as characterized by enhanced and more variable rainfall. Such ISM behaviour corresponds to the MCA, as found in different parts of the world.

Multiple and possibly superposed factors hamper quantitative rainfall reconstruction from element concentration. The seasonal to sub-decadal resolution merit further investigation and geochemical and microclimatic monitoring at our study site. Using advanced analytical methods and promising proxies, such as $\delta^{34}S$, the presented record may prove valuable for reconstructions of atmospheric changes, induced by volcanic activity and/or human pollution.

5 Summary

5.1 Main results

I present my thesis as a cumulative work composed of three separate manuscripts, each concerned on a specific problem. The major target of my project, the interpretation of geochemical proxies derived from stalagmites depends on the degree of understanding of the parameters that influence these proxies. In order to disentangle the factors that influence stalagmite oxygen isotopes in the sub-tropics, I started to sample rainwater in 2007 in the study region. Initial results led to a hypothesis, how the interaction of the source effect, the amount effect and local rainfall conditions affect the rainfall isotopy (*Manuscript 1*). The monitoring of hydrological conditions proved essential to interpret the stalagmite stable isotope records described in another manuscript (*Manuscript 2*). Compilation of δ^{18}O and δ^{13}H and grey scale data, compared with other records from the monsoonal domain provoked discussion on forcing mechanisms and possible teleconnections. I used the conclusions drawn from the second study to delineate the complex nature of different elements (Cu, Zn, Sr, Ba, U), incorporated into the stalagmites carbonate (*Manuscript 3*). The conceptual model presented in the last manuscript explains how different environmental parameters are likely to contribute to the variability observed in chemical and physical properties of the analyzed stalagmite. Here, I summarize the most important results.

The isotopes (δ^{18}O and δ^{2}H) measured in rainwater collected near Cherrapunji, NE India, show a clear annual cycle, with lowest values during the late summer monsoon and higher values during the dry winter. As stable isotopy of rainfall in this area was assumed to be influenced mainly by the amount effect (Dansgaard, 1964; Rozanski et al., 1993), finding no clear (anti-)correlation between rainfall amount and its δ^{18}O was, at first, surprising. In turn, comparison of the δ^{18}O signature of rainwater with corresponding air mass trajectories suggests that the most prominent factor governing the isotopic composition of the rainfall is the seasonality of the isotopic signature of the Bay of Bengal surface water. Analyses of backward and forward air mass trajectories confirm that the main source region for water vapor is the Bay of Bengal; only occasionally, a subordinate contribution to winter rainfall may originate from SE Asia. The isotopic composition of the Bay of Bengal surface water is influenced by sea surface salinity, together with the intensity of fluvial runoff from the Ganges-Brahmaputra river system. Highest runoff occurs during August and September when isotopically depleted runoff stems largely from meltwater and rainfall at high altitudes in the Himalaya and Tibet. The theoretical premise of the high summer runoff is that the summer period will be characterized by lowest δ^{18}O and δ^{2}H values in the Bay of Bengal surface water. The consequent assumption that in this way an inherited signal may likely be recycled in subsequent rainfall is the base for a novel concept of the 'plume effect'. It appears that the δ^{18}O signature of Meghalayan stalagmites represents a combination of a plume and amount effect.

Except for the general features common to palaeoclimate records from the monsoonal domain, high resolution $\delta^{18}O$, $\delta^{13}C$ and grey scale results from the KRUM-3 stalagmite display millennial to sub-annual scale changes of the ISM. High U concentration (>80 ppm) allow for highly precise and accurate MC-ICP-MS U/Th dating on small samples. The linearly interpolated age model confirmed that KRUM-3, growing continuously during the past $\sim$11,000 years provides, insofar, the most detailed documentation of Indian Holocene climate change.

The general trend in the $\delta^{18}O$ record suggest that the long-term ISM variability was guided by changes in insolation, while the $\delta^{18}O$ excursions point to centennial to decadal scale changes resulting from interactions between atmospheric conditions on the Asian continent (Tibetan High) and the in the Pacific and Indian oceans (ENSO and IOD). On the intra-annual timescale, ISM likely follows its seasonal latitudinal oscillation of the ITCZ. How fast and how deep the ITCZ–ISM system can penetrate onto the Asian continent is partly determined by the snow cover length in Central Asia and Tibet, and the strength of the Tibetan High. Temperature and vegetation changes, the two most common factors which can influence $\delta^{13}C$ in stalagmites, seem to have a negligible effect on the KRUM-3. However, a tentative comparison between the KRUM-3 $\delta^{13}C$ profile and advances of Tibetan glaciers suggest a relation between high $\delta^{13}C$ values and cold conditions on Tibetan Plateau. The stronger the Tibetan High, the more likely are dry cold northeasterly winds (winter monsoon) in NE India. It is known, that very high $\delta^{13}C$ values result from reduced drip rates – a situation expected during prolonged dry periods. Additional evidence for high $\delta^{13}C$ reflecting drought winter conditions comes from a comparison with grey-scale data. Grey-scale values depend on crystallography; lower grey values characterize dense dark crystallization, while high grey values reflect milky-white porous one. The growth rate determines the density of the stalagmite carbonate; fast growth during wet conditions leads to low density, porous crystallization, while slow growth during dry periods results in precipitation of dense crystals. High $\delta^{13}C$ values observed during the intervals characterized by low grey scale values confirm that both parameters may be used as aridity indicators. Analyzing a summer rainfall ($\delta^{18}O$) and winter aridity ($\delta^{13}C$, grey scale) proxies recorded within the same archive is a great advantage as it allows for inferring seasonality changes. Comparison of $\delta^{18}O$, $\delta^{13}C$ and grey scale profiles from KRUM-3 with the proxies for ENSO intensity, and considering modern meteorological analogues for ENSO and IOD behavior reveals that a negative influence on the ISM rainfall in NE India derives from positive IOD events, especially when in parallel with El Niño conditions in the Pacific. La Niña events, negative IOD conditions, and early snow thaw in Central Asia support early onset and above normal ISM rainfall in NE India.

The early Holocene in Meghalaya was characterized by an increase in ISM rainfall and progressively moister winter conditions. These conditions prevailed until the Holocene

Thermal Maximum when seasonality was seemingly enhanced. During this period, the ISM further increased, while the winter season probably became drier. The change in insolation weakened the ISM during the following millennia. Starting 4.5 kyr BP, grey values and partly also δ^{18}O records suggest an increasing influence of the ENSO system, coincident with higher insolation on the southern hemisphere. An important finding is that the ISM variability increased although the rainfall amount continued to diminish and consequently, the last ∼2 kyr were the driest period that NE India witnessed during its Holocene history.

The excellent age model of the KRUM-3, together with the well established high-resolution isotope and grey scale proxy records encouraged the analysis of element concentrations at ultrahigh resolution. The element concentrations for the last 1500 years were measured with the LA-ICP-MS at ETH Zürich, in a special, in-house build ablation cell allowing for the first time for measuring oversized samples (230×29×9mm). The obtained results reflect changes in carbonate element concentrations, directly related to dripwater chemistry. Cu, Zn, Sr, Ba, and U are positively correlated and are likely leached from soil and hostrock during times of enhanced water supply. The composition of the dripwater is dependent on a multitude of factors. The complexity of this problem is depicted as a conceptual model tracing some of these factors from the atmosphere into the cave environment and explaining how the seasonal variability can be reconstructed. The interpretation of initial results shows that the wettest period Meghalaya experienced during the last 1500 yr (840–1540 AD) fairly corresponds to the European Medieval Warm Period. However, there is evidence that during this time not only the ISM rainfall varied, but soil chemistry changed: peaks in Cu and Zn concentration seem to correspond to large tropical volcanic eruptions which might have led to increased soil acidity and subsequently enhanced element mobilization. Thus, similar to ice cores, element changes in stalagmites may potentially trace past volcanism. Though element concentration results are site-specific they seem to be very promising for detection of unknown and chronologically uncertain eruptions and their impact on climate.

5.2 Conclusions and implications beyond the main scope of the study

The paleoclimatic investigation presented in my thesis demonstrates the potential of Meghalayan stalagmites for palaeoenvironmental reconstructions. The combination of rainwater isotopy monitoring, air mass trajectory tracing, and traditional and novel stalagmite proxies brought up insofar the most comprehensive picture of Holocene climate change in NE India. Some of the outcomes of my work can be considered of overregional significance.

- The example of Meghalayan rainwater isotopy depicts that the amount effect is likely not the only process influencing the isotopic composition in subtropical regions. Ad-

mittedly, the sampling interval was rather short (two years only) but assuming that the argumentation presented in Manuscript 1 is correct, the isotopy of the moisture source can change in a seasonal cycle. Consequently, the 'plume effect' could probably be observed in other sub-tropical and tropical regions (e. g. Mekong delta), given seasonally variable continental runoff from high alpine mountain ranges, located at short distance from the river mouth. Concerning the Bay of Bengal case study, the shape, the spatial and temporal dynamics of the freshwater plume, and the variability of runoff isotopy are not well understood and worth detailed investigation.

- A first high-resolution stable isotope and grey scale record from NE India shows that during the Holocene, the ISM was nothing but stable. Throughout the last 11 kyr the ISM strength followed the pattern of northern hemisphere insolation changes. When insolation weakened ∼4 kyr ago, maritime conditions in the Indian and Pacific oceans won the control and significantly increased the ISM variability, while the overall ISM rainfall continued to decrease. In the light of the ongoing discussion on climate change and global warming this dependence may prove a serious issue for rainfall predictability. It seems that in future ISM rainfall could become of more sporadic nature, with more frequent 'extreme events' of heavy precipitation over a very short time period and prolonged periods of severe drought. In short, the frequency of high amplitude ISM changes might escalate and this would have serious consequences for Indian agriculture.

- An attempt to understand the incorporation of trace elements into the stalagmite carbonate lattice initiated a conceptual model of the temporal development of different factors influencing stalagmite proxy records in an annual cycle. The suggested model envisages mechanisms transmitting environmental signals into the cave and further into the stalagmites. Accordingly, the signal which originates in the atmosphere is carried by a medium (dripwater) and modulated along the way by a suite of physical and chemical processes starting in the soil and ending in the cave. The application of such a model approach, taken with care as each cave is a unique and specific environment, can greatly improve our understanding of interactions, relations and positive and negative feedbacks between different processes governing stalagmite palaeoclimatic records. The mark of a successful scientific model/theory is that it makes specific predictions that can be validated. Therefore, the best and most recommended way to evaluate the conceptual model introduced in manuscript 3 is setting up a natural laboratory integrating cave monitoring and meteorological observations.

5.3   Outlook

Despite the successful qualitative reconstruction of past ISM conditions, many interesting problems remain unanswered. Here I consider some issues worth future investigation, focusing on already ongoing work, and discussing potential regions of interest and ap-
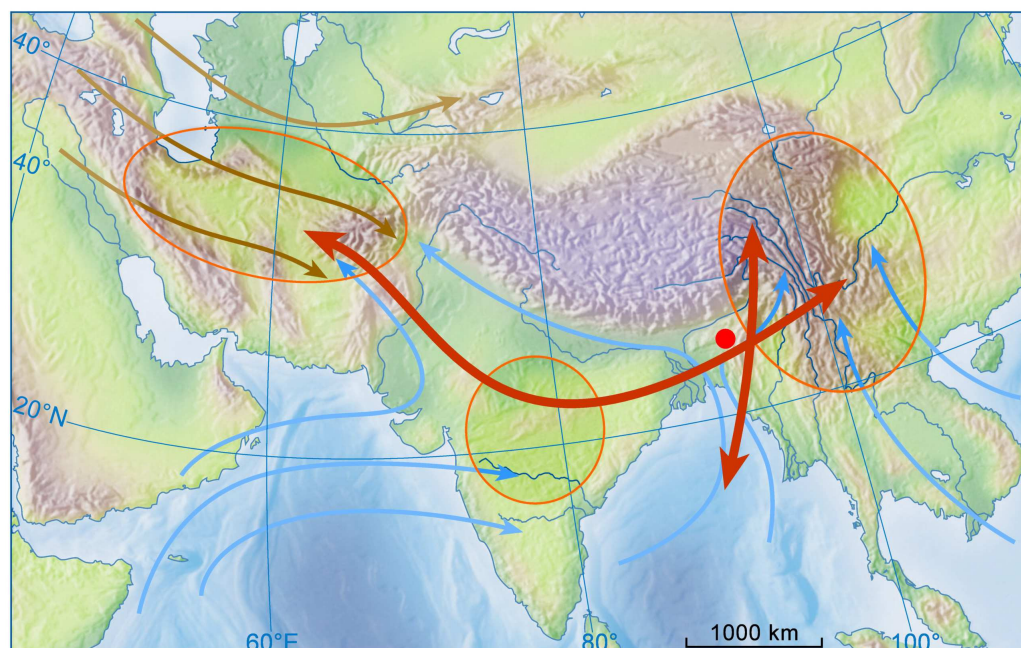
Figure 5.1: Key regions of interest in orange circles and the proposed transects as orange arrows on a schematic map of atmospheric circulation patterns. The red dot denotes the location of Krem Umsynrang Cave. Blue and brown arrows represent the Indian and Chinese summer monsoon and the westerlies, respectively.

plicable methods. Stalagmites provide a unique opportunity to analyze a multitude of proxies in one and the same sample. Combined ^{14}C, ^{10}Be, and ^{36}Cl analysis[1] will foster detailed investigation of production rate changes of these cosmogenic isotopes and subsequently variations in solar activity (Lundblad, 2006). Moreover, I will utilize the ^{14}C and ^{10}Be deposited in marine sediments and ice-cores for comparison with studied sub-tropical archives (Beer et al., 1990, 2002; Wagner et al., 2000; Muscheler et al., 2005). By matching radio-isotope records from different archives I hope to provide insight into the differences of climate signals between the poles and the sub-tropics. Further, correlation of ice-core, marine, and stalagmite profiles will help to assess phase relations in the different climate archives. Accurate dating of ^{14}C plateaus and excursions by means of U/Th routines can greatly improve radiocarbon chronologies in a time window where the ^{14}C-calibration is still ambiguous (Beck et al., 2001).

To seize the regional extent of climate changes in India and beyond, additional Indian and south Asian localities with high time-resolution records should be investigated – in the optimal case as zonally and meridionally oriented transects (Fig. 5.1). Establishing a westward transect into the mountainous Central Asian region[2] would help to understand

---

[1]The analysis of ^{14}C, ^{10}Be, and ^{36}Cl is performed in collaboration with Irka Hajdas at the AMS facility of the ETH located at Zurich, Switzerland.

[2]Suitable study sites are already at hand in Iran and Kurdistan (northern Iraq). In both cases, future

the dynamics in the interaction zone of the ISM and the westerlies (Fig. 5.1). An eastward extension of such transect would be beneficial for disentangling the contribution of the BoB branch of the ISM to the Asian Summer Monsoon in South Asia[3]. A meridional transect from northernmost Bangladesh into the Himalaya, taking into account sites located at different altitudes is equally important. It will reveal the altitude effect that forces $\delta^{18}O$ and δD changes in rainfall during its way onto the Tibetan Plateau. In perspective, it will help to comprehend the mechanisms that force ISM changes and the shifting of climatic zones (Lachniet, 2009). Sample material and methods listed below offer ways to establish this proposed network of study sites.

During field work in northeastern India, I retrieved several stalagmites that cover several thousand years within Marine Isotope Stage (MIS) 3 and MIS 6. Extensive U/Th dating and stable isotope work on additional samples will eventually lead to the construction of a stacked palaeo-monsoon record for the last ∼200 kyrs.

Preliminary screening shows that the already collected stalagmites are suitable samples for laser ablation studies and the reconstruction of element records on sub-decadal to sub-annual timescales, reaching far into the last glacial period. The detailed investigation of the characteristics of major elements (e.g. Sr, Ba, Mg, U) could allow for disentangling the complex relation in the atmosphere-vegetation-soil system. Furthermore, the combination of sulfur concentration and $\delta^{34}S$ analysis might prove a powerful tracer for volcanic and anthropogenic impacts on atmospheric composition. Similarly, analyses of carbonate associated organic N and nitrate in stalagmites is an innovative approach towards understanding the ecosystem response to precipitation changes. The unusual crystal growth in samples like KRUM-1 make them very interesting specimen for crystallographic studies. Using synchrotron micro-XRF methods[4] we will investigate the incorporation of elements into crystal lattice and element concentration changes. These, in turn, may be related to seasonally varying growth conditions and as such may provide climate information on sub-annual scale.

The ultimate goal of the planned work is to analyze the characteristics of the Indian climate and its reaction on regional and global climate excursions. The aforementioned samples and techniques at hand, we can broaden the scope of palaeoclimate information for the monsoonal realm. Interpreting the obtained palaeo-data in their meteorological context can only be achieved by monitoring the microclimate and the geochemical factors that govern the archives growth. To delineate the seasonal dependence of stalagmite growth on climatic factors and drip water chemistry, I started to monitor microclimatic parameters

---

collaboration with local scientists will allow sampling and monitoring alike.

[3]A stalagmite project, recently started by Gideon Henderson (Oxford, Great Britain) in Laos will give an additional location for such transect.

[4]Together with Silvia Frisia (Newcastle, Australia), a project has been started at the European Synchrotron Radiation Facility (ESRF Grenoble) to investigate the elemental composition in stalagmites from India at very high resolution.

in Krem Umsynrang cave in 2005. In collaboration with the cave monitoring expert David Mattey (London, Great Britain) we intent to enlarge our monitoring program. A variety of parameters, such as pCO$_2$, T$_{air}$, drip rates and element concentrations, are likely to give deep insights into the relation of the cave's microclimate to regional surface conditions (Mattey et al., 2008b). Monitoring gives a way to establish transfer functions between proxy records from stalagmites and meteorological data. In the optimal case, it may facilitate calibrated and quantitative reconstructions of monsoonal variability.

Bibliography

Abram, N., Gagan, M. K., Cole, J. E., Hantoro, W. S., and Mudelsee, M. (2008). Recent intensification of tropical climate variability in the Indian Ocean. *Nature Geoscience*, Advanced Online Publication:1–5.

Abram, N. H., Gagan, M. K., Liu, Z., Hantoro, W. S., McCulloch, M. T., and Suwargadi, B. W. (2007). Seasonal characteristics of the Indian Ocean Dipole during the Holocene epoch. *Nature*, 445:299–302.

Adams, J. B., Mann, M. E., and Ammann, C. M. (2003). Proxy evidence for an El Niño-like response to volcanic forcing. *Nature*, 426:274–278.

Aggarwal, P. K., Froehlich, K., Kulkarni, K. M., and Gourcy, L. L. (2004). Stable isotope evidence for moisture sources in the asian summer monsoon under present and past climate regimes. *Geophysical Research Letters*, 31:L08203.

Agrawala, S., Barlow, M., Cullen, H., and Lyon, B. (2001). The drought and humanitarian crisis in central and southwest Asia: A climate perspective. *IRI special report*, 01-11:1–20.

Aizen, V. B., Aizen, E. M., Joswiak, D. R., Fujita, K., Takeuchi, N., and Nikitin, S. A. (2006). Climatic and atmospheric circulation pattern variability from ice-core isotope/geochemistry records (Altai, Tien Shan and Tibet). *Annals of Glaciology*, 43:49–60.

Allan, R. P. and Soden, B. J. (2008). Atmospheric Warming and the Amplification of Precipitation Extremes. *Science*, 321:1481–1484.

Araguás-Araguás, L., Froehlich, K., and Rozanski, K. (1998). Stable isotope composition of precipitation over southeast Asia. *Journal of Geophysical Research*, 103(D22):28,721–28,742.

Arz, H. W., Lamy, F., and Pätzold (2006). A pronounced dry event recorded around 4.2 ka in brine sediments from the Northern Red Sea. *Quaternary Research*, 66:432–441.

Baldini, J. U. L., McDermott, F., and Fairchild, I. J. (2002). Structure of the 8200-Year Cold Event Revealed by a Speleothem Trace Element Record. *Science*, 296:2203–2206.

Bates, B. C., Kundzewicz, Z. W., Wu, S., and Palutikof, J. P., editors (2008). *Climate Change and Water. Technical Paper of the Intergovernmental Panel on Climate Change.* Intergovernmental Panel on Climate Change, Geneva.

Beck, J. W., Richards, D. A., Edwards, R. L., Silverman, B. W., Smart, P. L., Donahue, D. J., Hererra-Osterheld, S., Burr, G. S., Calsoyas, L., Jull, A. J. T., and Biddulph, D.

(2001). Extremely Large Variations of Atmospheric ^{14}C Concentration During the Last Glacial Period. *Science*, 292:2453–2458.

Beer, J., Blinov, A., Bonani, G., Finkel, R. C., Hofmann, H. J., Lehmann, B., Oeschger, H., Sigg, A., Schwander, J., Staffelbach, T., Stauffer, B., Suter, M., and Wölfli, W. (1990). Use of ^{10}Be in polar ice to trace the 11-year cycle of solar activity. *Nature*, 347:164–166.

Beer, J., Muscheler, R., Wagner, G., Laj, C., Kissel, C., Kubik, P., and Synal, H.-A. (2002). Cosmogenic nuclides during isotope stages 2 and 3. *Quaternary Science Reviews*, 22:1129–1139.

Begum, B. A., Kim, E., Biswas, S. K., and Hopke, P. K. (2004). Investigation of sources of atmospheric aerosol at urban and semi-urban areas in Bangladesh. *Atmospheric Environment*, 38:3025–3038.

Bhatia, B. M. (1991). *Famines in India. A Study in Some Aspects of the Economic History of India with Special Reference to Food Problem 1860–1990.* Konark Publishers, New Delhi, 3 edition.

Bhattacharya, S. K., Froehlich, K., Aggarwal, P. K., and Kulkarni, K. M. (2003). Isotopic variation in Indian Monsoon precipitation: Records from Bombay and New Delhi. *Geophysical Research Letters*, 30(24):2285.

Bhattacharya, S. K., Gupta, S. K., and Krishnamurthy, R. V. (1985). Oxygen and hydrogen isotopic ratios in groundwaters and river waters from India. *Proc. Indian acad. Sci. (Earth Planet. Sci.)*, 94(3):283–295.

Blanford, H. (1884). On the Connexion of the Himalaya Snowfall with Dry Winds and Seasons of Drought in India. *Proceedings of the Royal Society of London*, 37(3):3–22.

Bookhagen, B., Thiede, R. C., and Strecker, M. R. (2005). Abnormal monsoon years and their control on erosion and sediment flux in the high, arid northwest Himalaya. *Earth and Planetary Science Letters*, 231:131–146.

Borsato, A., Frisia, S., Fairchild, I. J., Somogyi, A., and Susini, J. (2007). Trace element distribution in annual stalagmite laminae mapped by micrometer-resolution X-ray fluorescence: Implications for incorporation of environmentally significant species. *Geochimica et Cosmochimica Acta*, 71:1494–1512.

Breitenbach, S. F. M. and Gebauer, H. D. (2007). Die Krem Lawkhlieng, Meghalaya, Indien. *Mitteilungen des Verbandes deutscher Höhlen- und Karstforscher*, 53(1):4–8.

Breitenbach, S. F. M., Meyer, H., Marwan, N., Krishna Kumar, K., Adkins, J. F., and Haug, G. H. (in prep.a). Strong Influence of Water Vapor Source Dynamics on Stable Isotopes in Precipitation Observed in Southern Meghalaya, NE India.

Breitenbach, S. F. M., Plessen, B., Marwan, N., Oberhänsli, H., Lund, D., Fernandez, D., Adkins, J. F., and Haug, G. H. (in prep.b). Holocene History of the Indian Summer Monsoon reconstructed from a Stalagmite from Meghalaya/Eastern India.

Brooks, N. (2006). Cultural responses to aridity in the Middle Holocene and increased social complexity. *Quaternary International*, 151:29–49.

Bryson, R. A. and Swain, A. M. (1981). Holocene Variations of Monsoonal Rainfall in Rajasthan. *Quaternary Research*, 16:135–145.

Burns, S. J., Fleitmann, D., Matter, A., Kramers, J., and Al-Subbary, A. (2003). Indian Ocean Climate and an Absolute Chronology over Dansgaard/Oeschger Events 9 to 13. *Science*, 301:1365–1367.

Butler, S. H. (1908). Famine. In Hunter, S. W., editor, *Imperial Gazetteer of India. The Indian Empire.*, volume III Economic, pages 475–502. Clarendon Press.

Chang, P., Yamagata, T., Schopf, P., Behera, S. K., Carton, J., Kessler, W. S., Meyers, G., Qu, T., Schott, F., Shetye, S., and Xie, S.-P. (2006). Climate Fluctuations of Tropical Coupled Systems—The Role of Ocean Dynamics. *Journal of Climate-Special Section*, 19:5122–5174.

Clark, I. D. and Fritz, P. (1997). *Environmental Isotopes in Hydrogeology.* Lewis Publishers, New York.

Craig, H. (1961). Isotopic Variations in Meteoric Waters. *Science*, 133:1702–1703.

Cruz Jr, F. W., Burns, S. J., Karmann, I., Sharp, W. D., Vuille, M., Cardoso, A. O., Ferrari, J. A., Silva Dias, P. L., and Viana Jr, O. (2005). Insolation-driven changes in atmospheric circulation over the past 116,000 years in subtropical Brazil. *Nature*, 434:63–66.

Cullen, H. M., deMenocal, P. B., Hemming, S., Hemming, G., Brown, F. H., Guilderson, T., and Sirocko, F. (2000). Climate change and the collapse of the Akkadian empire: Evidence from the deep sea. *Geology*, 28(4):379–382.

Dansgaard, W. (1964). Stable isotopes in precipitation. *Tellus*, XVI(4):436–468.

Dash, S. K., Singh, G. P., Shekhar, M. S., and Vernekar, A. D. (2005). Response of the Indian summer monsoon circulation and rainfall to seasonal snow depth anomaly over Eurasia. *Climate Dynamics*, 24:1–10.

Datta, P. S., Tyagi, S. K., and Chandrasekharan, H. (1991). Factors controlling stable isotope composition of rainfall in New Delhi, India. *Journal of Hydrology*, 128:223–236.

de Silva, S. L. and Zielinski, G. A. (1998). Global influence of the AD1600 eruption of Huaynaputina, Peru. *Nature*, 393:455–458.

Delaygue, G., Bard, E., Rollion, C., Jouzel, J., Stievenard, M., Duplessy, J. C., and Ganssen, G. (2001). Oxygen isotope/salinity relationship in the northern Indian Ocean. *Journal of Geophysical Research*, 106(C3):4565–4574.

Desmarchelier, J. M., Hellstrom, J. C., and McCulloch, M. T. (2006). Rapid trace element analysis of speleothems by LA-ICP-MS. *Climate Dynamics*, 231:102–117.

Dorale, J. A., Edwards, R. L., Alexander Jr., C., Shen, C.-C., Richards, D. A., and Cheng, H. (2007). Uranium-series dating of speleothems: current techniques, limits, & applications. In Sasowsky, I. D. & Mylroie, J., editor, *Studies of Cave Sediments. Physical and Chemical Records of Palaeoclimate.*, pages 177–197. Kluwer Academic, New York, 2 edition.

Drysdale, R., Zanchetta, G., Hellstrom, J., Maas, R., Fallick, A., Pickett, M., Cartwright, I., and Piccini, L. (2005). Late Holocene drought responsible for the collapse of Old World civilizations is recorded in an Italian cave flowstone. *Geology*, 34(2):101–104.

Duplessy, J. C. (1982). Glacial to interglacial contrasts in the northern Indian Ocean. *Nature*, 295:494–498.

Dykoski, C. A., Edwards, R. L., Cheng, H., Yuan, D., Cai, Y., Zhang, M., Lin, Y., Qing, J., An, Z., and Revenaugh, J. (2005). A high-resolution, absolute-dated Holocene and deglacial Asian monsoon record from Dongge Cave, China. *Earth and Planetary Science Letters*, 233:71–86.

Dyson, T. (1991). On the Demography of South Asian Famines: Part I. *Population Studies*, 45(1):5–25.

EEDRB (2006). Energy and Environment Data Reference Bank (EEDRB). http://www.iaea.org/inisnkm/nkm/aws/eedrb/data/BD-gd.html. International Atomic Energy Agency.

Ellwood, B. B. and Gose, W. A. (2006). Heinrich H1 and 8200 yr B.P. climate events recorded in Hall's Cave, Texas. *Geology*, 34(9):753–756.

Emile-Geay, J., Saeger, R., Cane, M., Cook, E. R., and Haug, G. H. (2008). Volcanoes and ENSO over the Past Millennium. *Journal of Climate*, 21:3134–3148.

Enzel, Y., Ely, L. L., Mishra, S., Ramesh, R., Amit, R., Lazar, B., Rajaguru, S. N., Baker, V. R., and Sandler, A. (1999). High-Resolution Holocene Environmental Changes in the Thar Desert, Northwestern India. *Science*, 284:125–128.

Fairchild, I. J., Baker, A., Borsato, A., Frisia, S., Hinton, R. W., McDermott, F., and Tooth, A. F. (2001). Annual to sub-annual resolution of multiple trace-element trends in speleothems. *Journal of the Geological Society London*, 158:831–841.

Fairchild, I. J., Frisia, S., Borsato, A., and Tooth, A. F. (2007). *Speleothems.*, pages 200–245. Blackwell, London.

Fairchild, I. J. and McMillan (2007). Speleothems as indicators of wet and dry periods. *International Journal of Speleology*, 36(2):69–74.

Fairchild, I. J. and Treble, P. (2009). Trace elements in speleothems as recorders of environmental change. *Quaternary Science Reviews*, 28:449–468.

Finch, A. A. and Allison, N. (2007). Coordination of Sr and Mg in calcite and aragonite. *Mineralogical Magazine*, 71(5):539–552.

Finch, A. A., Shaw, P. A., Holmgren, K., and Lee-Thorp, J. (2003). Corroborated rainfall records from aragonitic stalagmites. *Earth and Planetary Science Letters*, 215:265–273.

Fleitmann, D., Burns, S. J., Mangini, A., Mudelsee, M., Kramers, J., Villa, I., Neff, U., Al-Subbary, A. A., Buettner, A., Hippler, D., and Matter, A. (2007). Holocene ITCZ and Indian monsoon dynamics recorded in stalagmites from Oman and Yemen (Socotra). *Quaternary Science Reviews*, 26:170–188.

Fleitmann, D., Burns, S. J., Mudelsee, M., Neff, U., Kramers, J., Mangini, A., and Matter, A. (2003a). Holocene Forcing of the Indian Monsoon Recorded in a Stalagmite from Southern Oman. *Science*, 300:1737–1739.

Fleitmann, D., Burns, S. J., Neff, U., Mangini, A., and Matter, A. (2003b). Changing moisture sources over the last 330,000 years in Northern Oman from fluid-inclusion evidence in speleothems. *Quaternary Research*, 60:223–232.

Fleitmann, D., Burns, S. J., Neff, U., Mudelsee, M., Mangini, A., and Matter, A. (2004). Palaeoclimatic interpretation of high-resolution oxygen isotope profiles derived from annually laminated speleothems from Southern Oman. *Quaternary Science Reviews*, 23:935–945.

Fleitmann, D., Mudelsee, M., Burns, S. J., Bradley, R. S., Kramers, J., and Matter, A. (2008). Evidence for a widespread climatic anomaly at around 9.2 ka before present. *Paleoceanography*, 23:PA1102.

Ford, D. and Williams, P. (2007). *Karst Hydrogeology and Geomorphology.* J. Wiley & Sons, Chichester.

Frank, R. and Becher, A. S. (1998). Ein zusammenhängendes Höhlensystem bei Chieruphi (Meghalaya/Nord-Ost-Indien)? *Mitteilungen des Verbandes deutscher Höhlen- und Karstforscher*, 44(3):96–99.

Fricker, M. B., Breitenbach, S. F. M., Aeschlimann, B., Dietiker, R., Haug, G. H., and Günther, D. (in prep.). High resolution trace element analysis of a stalagmite by Laser Ablation ICP-MS with a new ablation cell for large samples.

Frisia, S., Borsato, A., Fairchild, I. J., and Susini, J. (2005). Variations in atmospheric sulphate recorded in stalagmites by synchrotron micro-XRF and XANES analyses. *Earth and Planetary Science Letters*, 235:729–740.

Gadgil, S. (2003). The Indian Monsoon and Its Variability. *Annu. Rev. Earth Planet. Sci.*, 31:429–467.

Gajurel, A. P., France-Lanord, C., Huyghe, P., Guilmette, C., and Gurung, D. (2006). C and O isotope compositions of modern fresh-water mollusc shells and river waters from the Himalaya and Ganga plain. *Chemical Geology*, 233:156–183.

Gao, C., Robock, A., and Ammann, C. (2008). Volcanic forcing of climate over the past 1500 years: An improved ice core-based index for climate models. *Journal of Geophysical Research*, 113:D23111.

Gebauer, H. D. (2008). Resources on the Speleology of Meghalaya State, India. Part 1: Overview. In Laumanns, M., editor, *Berliner Höhlenkundliche Berichte.*, volume 33, page 152. Selbstverlag des Speläoclub Berlin, Rangsdorf.

Gehre, M., Geilmann, H., Richter, J., Werner, R. A., and Brand, W. A. (2004). Continuous flow ^{2}H/^{1}H and ^{18}O/^{16}O analysis of water samples with dual inlet precision. *Rapid Communication in Mass Spectrometry*, 18:2650–2660.

Genty, D. and Quinif, Y. (1996). Annually laminated sequences in the internal structure of some Belgian stalagmites—importance for paleoclimatology. *Journal of Sedimentary Research*, 66(1):275–288.

Goswami, B. N., Venugopal, V., Sengupta, D., Madhusoodanan, M. S., and Xavier, P. K. (2006). Increasing Trend of Extreme Rain Events Over India in a Warming Environment. *Science*, 314:1442–1445.

GRDC (2008). The Global Runoff Data Centre Koblenz. http://grdc.bafg.de/servlet/is/11588/. The Global Runoff Data Centre Koblenz.

Gupta, A. K., Anderson, D. M., and Overpeck, J. T. (2003). Abrupt changes in the Asian southwest monsoon during the Holocene and their links to the North Atlantic Ocean. *Nature*, 421:354–357.

Hardy, R. and Tucker, M. (1988). *X-ray powder diffraction of sediments.*, page 408. Blackwell Scientific Publications, Oxford.

Hashimoto, S., Tanaka, N., Kume, T., Yoshifuji, N., Hotta, N., Tanaka, K., and Suzuki, M. (2007). Seasonality of vertically partitioned soil CO_2 production in temperate and tropical forest. *Journal of Forest Research*, 12:209–221.

Hashimoto, S., Tanaka, N., Suzuki, M., Inoue, A., Takizawa, H., Kosaka, I., Tanaka, K., Tantasirin, C., and Tangtham, N. (2004). Soil respiration and soil CO_2 concentration in a tropical forest, Thailand. *Journal of Forest Research*, 9:75–79.

Haug, G. H., Günther, D., Peterson, L. C., Sigman, D. M., Hughen, K. A., and Aeschlimann, B. (2003). Climate and the Collapse of Maya Civilization. *Science*, 299:1731–1735.

Haug, G. H., Hughen, K. A., Sigman, D. M., Peterson, L. C., and Röhl, U. (2001). Southward Migration of the Intertropical Convergence Zone Through the Holocene. *Science*, 293:1304–1308.

Henderson, G. M., Robinson, L. F., Cox, K., and Thomas, A. L. (2006). Recognition of non-Milankovitch sea-level highstands at 185 and 343 thousand years ago from U–Th dating of Bahamas sediments. *Quaternary Science Reviews*, 25:3346–3358.

Hendy, C. H. (1971). The isotopic geochemistry of speleothems—I. The calculation of the effects of different modes of formation on the isotopic composition of speleothems and their applicability as paleoclimatic indicators. *Geochimica et Cosmochimica Acta*, 35:801–824.

Hinrichs, K., Gensch, M., and Esser, N. (2005). Analysis of organic films and interfacial layers by infrared spectroscopic ellipsometry. *Applied Spectroscopy*, 59:272A.

Hu, C., Henderson, G. M., Huang, J., Xie, S., Sun, Y., and Johnson, K. R. (2008). Quantification of Holocene Asian monsoon rainfall from spatially separated cave records. *Earth and Planetary Science Letters*, 266:221–232.

IAEA/WMO (2001). Gnip maps and animations. `http://isohis.iaea.org`. International Atomic Energy Agency/World Meteorological Organization.

Johnson, K. R., Hu, C., Belshaw, N. S., and Henderson, G. M. (2006). Seasonal trace-element and stable-isotope variations in a Chinese speleothem: The potential for high-resolution paleomonsoon reconstruction. *Earth and Planetary Science Letters*, 244:394–407.

Kalnay, E., Kanamitsu, M., Kistler, R., Collins, W., Deaven, D., Gandin, L., Iredell, M., Saha, S., White, G., Woollen, J., Zhu, Y., Chelliah, M., Ebisuzaki, W., Higgins, W., Janowiak, J., Mo, K. C., Ropelewski, C., Wang, J., Leetmaa, A., Reynolds, R., Jenne, R., and Joseph, D. (1996). The NCEP/NCAR 40-year reanalysis project. *Bulletin of the American Meteorological Society*, 77(3):437–471.

Kharpran Daly, B. D. (2006). *The Caves of Meghalaya.* The Directorate of Information & Public Relations Government of Meghalaya, Shillong.

Khiewtam, R. S. and Ramakrishnan, P. S. (1993). Litter and fine root dynamics of a relict sacred grove forest at Cherrapunji in north-eastern India. *Forest Ecology and Management*, 60:327–344.

Kim, S.-T., O'Neil, J. R., Hillaire-Marcel, C., and Mucci, A. (2007). Oxygen isotope fractionation between synthetic aragonite and water: Influence of temperature and Mg^{2+} concentration. *Geochimica et Cosmochimica Acta*, 71:4704–4715.

Krishna Kumar, K., Rajagopalan, B., and Cane, M. A. (1999). On the Weakening Relationship Between the Indian Monsoon and ENSO. *Science*, 284:2156–2159.

Krishna Kumar, K., Rajagopalan, B., Hoerling, M., Bates, G., and Cane, M. (2006). Unraveling the Mystery of Indian Monsoon Failure During El Niño. *Science*, 314:115–119.

Krishnamurthy, R. V. and Bhattacharya, S. K. (1991). *Stable oxygen and hydrogen isotope ratios in shallow ground waters from India and a study of the role of evapotranspiration in the Indian monsoon.*, volume Special Publication No. 3, pages 187–193. The Geochemical Society.

Kudrass, H. R., Hoffmann, A., Doose, H., Emeis, K., and Erlenkeuser, H. (2001). Modulation and amplification of climatic changes in the Northern Hemisphere by the Indian summer monsoon during the past 80 k.y. *Geology*, 29(1):63–66.

Lachniet, M. S. (2009). Climatic and environmental controls on speleothem oxygen-isotope values. *Quaternary Science Reviews*, 28:412–432.

Laird, K. R., Fritz, S. C., Maasch, K. A., and Cumming, B. F. (1996). Greater drought intensity and frequency before AD 1200 in the Northern Great Plains, USA. *Nature*, 384:552–554.

Lambs, L., Balakrishna, K., Brunet, F., and Probst, J. L. (2005). Oxygen and hydrogen isotopic composition of major Indian rivers: a first global assessment. *Hydrological Processes*, 19:3345–3355.

Lau, K. M. and Kim, K.-M. (2006). Observational relationships between aerosol and Asian monsoon rainfall, and circulation. *Geophysical Research Letters*, 33:L21810.

Lau, K. M., Kim, K.-M., Hsu, C., and Singh, R. P. (2008). Seasonal Co-variability of Aerosol and Precipitation over the Indian Monsoon and Adjecent Deserts. *Global Energy and Water Cycle Experiment News*, 18(1):4–6.

Lawrence, J. R., Gedzelman, S. D., Dexheimer, D., Cho, H.-K., Carrie, G. D., Gasparini, R., Anderson, C. R., Bowman, K. P., and Biggerstaff, M. I. (2004). Stable isotopic composition of water vapor in the tropics. *Journal of Geophysical Research*, 109:D06115.

Lee, J.-E. and Fung, I. (2007). "Amount effect" of water isotopes and quantitative analysis of post-condensation processes. *Hydrological Processes*, pages XXX–XXX.

Liu, Z., Tian, L., Chai, X., and Yao, T. (2008a). A model-based determination of spatial variation of precipitation δ^{18}O over China. *Chemical Geology*, 249:203–212.

Liu, Z., Tian, L., Yao, T., Gong, T., and Yin, C. (2008b). Influence of moisture transport on stable isotopes in precipitation in Yarlungzangbo River basin. *Front. Earth Sci. China*, 2(1):49–57.

Longerich, H. P., Jackson, S. E., and Günther, D. (1996). Laser Ablation Inductively Coupled Plasma Mass Spectrometry Transient Signal Data Acquisition and Analyte Concentration Calculation. *Journal of Analytical Atomic Spectrometry*, 11:899–904.

Lückge, A., Doose-Rolinski, H., Khan, A. A., Schulz, H., and von Rad U. (2006). Monsoonal variability in the northeastern Arabian Sea during the past 5000 years: geochemical evidence from laminated sediments. *Palaeogeography, Palaeoclimatology, Palaeoecology*, 167:273–286.

Lundblad, K. (2006). *Studies of Tropical Palaeo-variation in Climate and Cosmic Ray Influx - Geochemical data from stalagmites collected in Tanzania and northern South Africa.* Thesis, Stockholm University, Stockholm.

Madella, M. and Fuller, D. Q. (2006). Palaeoecology and the Harappan Civilization of South Asia: a reconsideration. *Quaternary Science Reviews*, 25:1283–1301.

Mann, M. E. and Park, J. (1994). Global-scale modes of surface temperature variability on interannual to century timescales. *Journal of Geophysical Research*, 99(D12):25,819–25,833.

Marshall, C. P. and Fairbridge, R. W. (1999). *Encyclopedia of Geochemistry.* Springer, Dordrecht.

Mattey, D., Latin, J. P., and Ainsworth, M. (2008a). Cave monitoring and calibration of a δ^{18}O-climate transfer function for a Gibraltar speleothem. *Pages News*, 16(3):15–17.

Mattey, D., Lowry, D., Duffet, J., Fisher, R., Hodge, E., and Frisia, S. (2008b). A 53 year seasonally resolved oxygen and carbon isotope record from a modern Gibraltar speleothem: Reconstructed drip water and relationship to local precipitation. *Earth and Planetary Science Letters*, 269:80–95.

Mayewski, P. A., Rohling, E. E., Stager, J. C., Karlén, W., Maasch, K. A., Meeker, L. D., Meyerson, E. A., Gasse, F., van Kreveld, S., Holmgren, K., Lee-Thorp, J., Rosqvist, G., Rack, F., Staubwasser, M., Schneider, R. R., and Steig, E. J. (2004). Holocene climate variability. *Quaternary Research*, 62:243–255.

Meyer, H., Schönicke, L., Wand, U., Hubberten, H.-W., and Friedrichsen, H. (2000). Isotope Studies Of Hydrogen And Oxygen In Ground Ice – Experiences With The Equilibration Technique. *Isotopes in Environmental and Health Studies*, 36(2):133–149.

Meyers, G., McIntosh, P., Pigot, L., and Pook, M. (2007). The Years of El Niño, La Niña, and Interactions with the Tropical Indian Ocean. *Journal of Climate*, 20:2872–2880.

Moy, C. M., Seltzer, G. O., Rodbell, D. T., and Anderson, D. M. (2002). Variability of El Niño/Southern Oscillation activity at millennial timescales during the Holocene epoch. *Nature*, 420:162–165.

Mühlinghaus, C., Scholz, D., and Mangini, A. (2007). Modelling stalagmite growth and δ^{13}C as a function of drip interval and temperature. *Geochimica et Cosmochimica Acta*, 71:2780–2790.

Mukherjee, A., Fryar, A. E., and Rowe, H. D. (2007). Regional-scale stable isotopic signatures of recharge and deep groundwater in the arsenic affected areas of West Bengal, India. *Journal of Hydrology*, 334:151–161.

Murata, F., Terao, T., Hayashi, T., Asada, H., and Matsumoto, J. (2008). Relationship between atmospheric conditions at Dhaka, Bangladesh, and rainfall at Cherrapunjee, India. *Natural Hazards*, 44:399–410.

Muscheler, R., Beer, J., Kubik, P., and Synal, H.-A. (2005). Geomagnetic field intensity during the last 60,000 years based on ^{10}Be and ^{36}Cl from the Summit ice cores and ^{14}C. *Quaternary Science Reviews*, 24:1849–1860.

Neff, U., Burns, S. J., Mangini, A., Mudelsee, M., Fleitmann, D., and Matter, A. (2001). Strong coherence between solar variability and the monsoon in Oman between 9 and 6 kyr ago. *Nature*, 411:290–293.

NGRIP members* (2004). High-resolution record of Northern Hemisphere climate extending into the last interglacial period. *Nature*, 431:147–151. *all authors: K. K. Andersen, N. Azuma, J.-M. Barnola, M. Bigler, P. Biscaye, N. Caillon, J. Chappellaz, H. B. Clausen, D. Dahl-Jensen, H. Fischer, J. Flückiger, D. Fritsche, Y. Fujii, K. Goto-Azuma, K. Grøvold, N. S. Gundestrup, M. Hansson, C. Huber, C. S. Hvidberg, S. J. Johnsen, U. Jonsell, J. Jouzel, S. Kipfstuhl, A. Landais, M. Leuenberger, R. Lorrain, V. Masson-Delmotte, H. Miller, H. Motoyama, H. Narita, T. Popp, S. O. Rasmussen, D. Raynaud, R. Rothlisberger, U. Ruth, D. Samyn, J. Schwander, H. Shoji, M.-L. Siggard-Andersen, J. P. Steffensen, T. Stocker, A. E. Sveinsbjörnsdóttir, A. Svensson, M. Takata, J.-L. Tison, Th. Thorsteinsson, O. Watanabe, F. Wilhelms and J. W. C. White.

NOAA (2005). World Ocean Atlas. Vol. 2005. http://www.nodc.noaa.gov/OC5/WOA05/pr_woa05.html. National Oceanographic Administration Agency.

Ohgaito, R. and Abe-Ouchi, A. (2007). The role of ocean thermodynamics and dynamics in Asian summer monsoon changes during the mid-Holocene. *Climate Dynamics*, pages 10.1007/s00382–006–0217–6.

Okuno, M., Nakamura, T., and Kobayashi, T. (1998). AMS ^{14}C dating of historic eruptions of the Kirishima, Sakurajima and Kaimondake volcanoes, southern Kyushu, Japan. *Radiocarbon*, 40:825–832.

O'Neil, J. R., Clayton, R. N., and Mayeda, T. K. (1969). Oxygen Isotope Fractionation in Divalent Metal Carbonates. *The Journal of Chemical Physics*, 51(12):5547–5558.

Oppo, D., Schmidt, G. A., and Le Grande, A. N. (2007). Seawater isotope constraints on tropical hydrology during the Holocene. *Geophysical Research Letters*, 34:L13701.

Overpeck, J. and Cole, J. (2008). The rhythm of the rains. *Nature*, 451:1061–1063.

Parfitt, E. A. and Wilson, L. (2008). *Fundamental of Physical Volcanology*. Blackwell, Malden/Oxford/Carlton.

Pati, S. (1980). Observations on the Hydrography and Inshore Plankton of the Bay of Bengal off Balasore. *Hydrobiologia*, 70:123–132.

Petit, J. R., Jouzel, J., Raynaud, D., Barkov, N. I., Barnola, J.-M., Basile, I., Bender, M., Chappellaz, J., Davisk, M., Delaygue, G., Delmotte, M., Kotlyakov, V. M., Legrand, M., Lipenkov, V. Y., Lorius, C., Pe'pin, L., Ritz, C., Saltzmank, E., and Stievenard, M. (1999). Climate and atmospheric history of the past 420,000 years from the Vostok ice core, Antarctica. *Nature*, 399:429–436.

Phadtare, N. R. (2000). Sharp Decrease in Summer Monsoon Strength 4000–3500 cal yr B.P. in the Central Higher Himalaya of India Based on Pollen Evidence from Alpine Peat. *Quaternary Research*, 53:122–129.

Possehl, G. L. (1997). The Transformation of the Indus Civilization. *Journal of World Prehistory*, 11(4):425–472.

Prasad, S. and Enzel, Y. (2006). Holocene paleoclimates of India. *Quaternary Research*, 66:442–453.

Prokop, P. and Walanus, A. (2003). Trends and Periodicity in the Longest Instrumental Rainfall Series for the Area of most Extreme Rainfall in the World Northeast India. *Geographia Polonica*, 76(2):23–31.

Ramakrishnan, P. S. and Ram, S. C. (1988). Vegetation, biomass and productivity of seral grasslands of Cherrapunji in north-east India. *Vegetatio*, 74:47–53.

Ramesh, R. (2001). High resolution Holocene monsoon records from different proxies: An assessment of their consistency. *Current Science*, 81(11):1432–1436.

Ramesh, R. and Sarin, M. M. (1992). Stable isotope study of the Ganga (Ganges) river system. *Journal of Hydrology*, 139:49–62.

Rasband, W. S. (1997–2008). ImageJ. http://rsb.info.nih.gov/ij/. U. S. National Institutes of Health, Bethesda, Maryland, USA.

Rashid, H., Flower, B. P., Poore, R. Z., and Quinn, T. M. (2007). A ∼25 ka Indian Ocean monsoon variability record from the Andaman Sea. *Quaternary Science Reviews*, 26:2586–2597.

Reeder, R. J., Lamble, G. M., and Northrup, P. A. (1999). XAFS study of the coordination and local relaxation around Co^{2+}, Zn^{2+}, Pb^{2+}, and Ba^{2+} trace elements in calcite. *American Mineralogist*, 84:1049–1060.

Rein, B., Lückge, A., and Sirocko, F. (2004). A major Holocene ENSO anomaly during the Medieval period. *Geophysical Research Letters*, 31:L17211.

Risi, C., Bony, S., and Vimeux, F. (2008). Influence of convective processes on the isotopic composition (δ^{18}O and δD) of precipitation and water vapor in the tropics: 2. Physical interpretation of the amount effect. *Journal of Geophysical Research*, 113:D19306.

Rozanski, K., Araguás-Araguás, L., and Gonfiantini, R. (1993). Isotopic Patterns in Modern Global Precipitation. In Swart, P. K., Lohmann, K. C., McKenzie, J., and Savin, S., editors, *Climate Change in Continental Isotopic Records.*, pages 1–36. Geophysical Monograph 78.

Rozanski, K., Froehlich, K., and W., G. M. (2001). Surface Water. In Mook, W. G., editor, *Environmental isotopes in the hydrological cycle.*, volume 3, page 117. UNESCO/IAEA.

Sachs, L. (1984). *Applied statistics: a handbook of techniques.* Springer, Berlin.

Saji, N. H., Goswami, B. N., Vinayachandran, P. N., and Yamagata, T. (1999). A dipole mode in the tropical Indian Ocean. *Nature*, 401:360–363.

Sarma, J. N. (2008). Fluvial process and morphology of the Brahmaputra River in Assam, India. *Geomorphology*, 70:226–256.

Schulz, M. and Mudelsee, M. (2002). REDFIT: estimating red-noise spectra directly from unevenly spaced paleoclimatic time series. *Computers & Geosciences*, 28:421–426.

Sengupta, D. and Ravichandran, M. (2001). Oscillations of Bay of Bengal sea surface temperature during the 1998 summer monsoon. *Geophysical Research Letters*, 28(10):2033–2036.

Shopov, Y. Y. (2005). 20 Years Palaeoluminescence Techniques for Reconstruction of Past Environmental Changes. In *UIS Contribution. 14th International Congress of Speleology.*, pages 238–245, Athens. Speleological Society Hellas.

Shrestha, A. B., Wake, C. P., and Dibb, J. E. (1997). Chemical composition of aerosol and snow in the High Himalaya during the summer monsoon season. *Atmospheric Environment*, 31(17):2815–2826.

Singh, M., Singh, I. B., and Müller, G. (2007). Sediment characteristics and transportation dynamics of the Ganga River. *Geomorphology*, 86:144–175.

Singh, M. P. and Singh, A. K. (2000). Petrographic characteristics and depositional conditions of Eocene coals of platform basins, Meghalaya, India. *International Journal of Coal Geology*, 42:315–356.

Singh, M. P. and Singh, A. K. (2007). Monsoon Mysteries. *Science*, 318:204–205.

Sinha, A., Cannariato, K. G., Stott, L. D., Cheng, H., Edwards, R. L., Yadava, M. D., Ramesh, R., and Singh, I. B. (2007). A 900-year (600 to 1500 A.D.) record of the Indian Summer Monsoon precipitation from the core monsoon zone of India. *Geophysical Research Letters*, 34:L16707.

Staubwasser, M. (2006). An Overview of Holocene South Asian Monsoon Records – Monsoon Domains and Regional Contrasts. *Journal of the Geological Society of India*, 68:433–446.

Staubwasser, M., Sirocko, F., Grootes, P. M., and Erlenkeuser, H. (2002). South Asian monsoon climate change and radiocarbon in the Arabian Sea during early and middle Holocene. *Paleoceanography*, 17(4):1063.

Staubwasser, M., Sirocko, F., Grootes, P. M., and Segl, M. (2003). Climate change at the 4.2 ka BP termination of the Indus valley civilization and Holocene south Asian monsoon variability. *Geophysical Research Letters*, 30(8):581–584.

Staubwasser, M. and Weiss, H. (2007). Holocene climate and cultural evolution in the late prehistoric–early historic West Asia. *Quaternary Research*, 66:372–387.

Stine, S. (1994). Extreme and persistent drought in California and Patagonia during medieval time. *Nature*, 369:546–549.

Sukumar, R., Ramesh, R., Pant, R. K., and Rajagopalan, G. (1993). A δ^{13}C record of late Quaternary climate change from tropical peats in southern India. *Nature*, 364:703–706.

Takahashi, K. and Arakawa, H. (1981). Climates of Southern and Western Asia. In *World Survey of Climatology.*, volume 9. Elsevier Scientific Publishing Company.

Thompson, L. G., Yao, T., Davis, M. E., Henderson, K. A., Mosley-Thompson, E., Lin, P.-N., Beer, J., Synal, H.-A., Cole-Dai, J., and Bolzan, J. F. (1997). Tropical Climate Instability: The Last Glacial Cycle from a Qinghai-Tibetan Ice Core. *Science*, 276:1821–1825.

Thompson, L. G., Yao, T., Mosley-Thompson, E., Davis, M. E., Henderson, K. A., and Lin, P.-N. (2000). A High-Resolution Millennial Record of the South Asian Monsoon from Himalayan Ice Cores. *Science*, 289:1916–1919.

Tian, L., Masson-Delmotte, V., Stievenard, M., Yao, T., and Jouzel, J. (2001a). Tibetan Plateau summer monsoon northward extent revealed by measurements of water stable isotopes. *Journal of Geophysical Research*, 106(D22):28,081–28,088.

Tian, L. Yao, T., Numaguti, A., and Sun, W. (2001b). Stable Isotope Variations in Monsoon Precipitation on the Tibetan Plateau. *Journal of the Meteorological Society of Japan*, 79(5):959–966.

Treble, P., Shelley, J. M. G., and Chapell, J. (2003). Comparison of high resolution sub-annual records of trace elements in a modern (1911–1992) speleothem with instrumental climate data from southwest Australia. *Earth and Planetary Science Letters*, 216:141–153.

von Grafenstein, U., Erlenkeuser, H., Brauer, A., Jouzel, J., and Johnsen, S. J. (1999). A Mid-European Decadal Isotope-Climate Record from 15,500 to 5000 Years B.P. *Science*, 284:1654–1657.

von Humboldt, A. (1845). *Kosmos. Entwurf einer physischen Weltbeschreibung.* Cotta'scher Verlag, Stuttgart & Tübingen.

von Rad, U., Schaaf, M., Michels, K. H., Schulz, H., Berger, W. H., and F., S. (1999). A 5000-yr Record of Climate Change in Varved Sediments from the Oxygen Minimum Zone off Pakistan, Northeastern Arabian Sea. *Quaternary Research*, 51:39–53.

Wagner, G., Beer, J., Laj, C., Kissel, C., Masarik, J., Muscheler, R., and Synal, H.-A. (2000). Chlorine-36 evidence for the Mono Lake event in the Summit GRIP ice core. *Earth and Planetary Science Letters*, 186:1–6.

Walker, G. T. (1918). Correlation in Seasonal Variations of Weather. *Quaterly Journal of the Royal Meteorological Society*, 44:223–224.

Wang, Y., Cheng, H., Edwards, R. L., He, Y., Kong, X., An, Z., Wu, J., Kelly, M. J., Dykoski, C. A., and Li, X. (2005). The Holocene Asian Monsoon: Links to Solar Changes and North Atlantic Climate. *Science*, 308:854–857.

Wang, Y., Cheng, H., Edwards, R. L., Kong, X., Shao, X., Chen, S., J., W., Jiang, X., Wang, X., and An, Z. (2008). Millennial- and orbital-scale changes in the East Asian monsoon over the past 224,000 years. *Nature*, 451:1090–1093.

Wanner, H., Beer, J., Bütikofer, J., Crowley, T. J., Cubasch, U., Flückiger, J., Goosse, H., Grosjean, M., Joos, F., Kaplan, J. O., Küttel, M., Müller, S. A., Prentice, C., Solomina, O., Stocker, T. F., Tarasov, P., Wagner, M., and Widmann, M. (2008). Mid- to Late Holocene climate change: an overview. *Quaternary Science Reviews*, 27:1791–1828.

Webster, P. J., Magaña, V. O., Palmer, T. N., Shukla, J., Tomas, R. A., Yanai, M., and Yasunari, T. (1998). Monsoons: Processes, predictability, and the prospects for prediction. *Journal of Geophysical Research*, 103(C7):14,451–14,510.

Webster, P. J., Moore, A. M., Loschnigg, J. P., and Leben, R. R. (1999). Coupled ocean-atmosphere dynamics in the Indian Ocean during 1997–98. *Nature*, 401:356–360.

Weiss, H., Courty, M.-A., Wetterstrom, W., Guichard, F., Senior, L., Meadow, R., and Curnow, A. (1993). The Genesis and Collapse of Third Millennium North Mesopotamian Civilization. *Science*, 261:995–1004.

Woodhead, J. D., Hellstrom, J., Hergt, J. M., Greig, A., and Maas, R. (2007). Isotopic and Elemental Imaging of Geological Materials by Laser Ablation Inductively Coupled Plasma-Mass Spectrometry. *Geostandards and Geoanalytical Research*, 31(4):331–343.

Wynn, P. M., Fairchild, I. J., Baker, A., Baldini, J. U. L., and McDermott, F. (2008). Isotopic archives of sulphate in speleothems. *Geochimica et Cosmochimica Acta*, 72:2465–2477.

Yadav, R. K. (2009). Changes in the large-scale features associated with the Indian summer monsoon in the recent decades. *International Journal of Climatology*, 29:117–133.

Yadava, M. G. and Ramesh, R. (2005). Monsoon reconstruction from radiocarbon dated tropical Indian speleothems. *The Holocene*, 15(1):48–59.

Yadava, M. G., Ramesh, R., and Pant, G. B. (2004). Past monsoon rainfall variations in peninsular India recorded in a 331-year-old speleothem. *The Holocene*, 14(4):517–524.

Yancheva, G., Nowaczyk, N. R., Mingram, J., Dulski, P., Schettler, G., Negendank, J. F. W., Liu, J., Sigman, D. M., Peterson, L. C., and Haug, G. H. (2007). Influence of the intertropical convergence zone on the East Asian monsoon. *Nature*, 445:74–77.

Yang, B., Bräuning, A., Dong, Z., Zhang, Z., and Keqing, J. (2008). Late Holocene monsoonal temperate glacier fluctuations on the Tibetan Plateau. *Global and Planetary Change*, 60:126–140.

Yang, M., Yao, T., He, Y., and Thompson, L. G. (2000). ENSO events recorded in the Guliya ice core. *Climate Change*, 47:401–409.

Yoon, J.-H. and Chen, T.-C. (2005). Water vapor budget of the Indian monsoon depression. *Tellus*, 57A:770–782.

Zhang, M., Yang, Y., Chen, B., and Song, F. (2005). Effects of readily dispersible colloid on adsorption and transport of Zn, Cu, and Pb in soils. *Environmental International*, 31:840–844.

Zhang, P., Cheng, H., Edwards, R. L., Chen, F., Wang, Y., Yang, X., Liu, J., Tan, M., Wang, X., J., L., An, C., Dai, Z., Zhou, J., Zhang, D., Jia, J., Jin, L., and Johnson, K. R. (2008). A Test of Climate, Sun, and Culture Relationships from an 1810-Year Chinese Cave Record. *Science*, 322:940–942.

Zhang, X., Jin, H., and Sun, W. (2006). Stable Isotopic Variations in Precipitation in Southwest China. *Advances in Atmospheric Sciences*, 23(4):649–658.

Zhou, T.-J. and Yu, R.-C. (2005). Atmospheric water vapor transport associated with typical anomalous summer rainfall patterns in China. *Journal of Geophysical Research*, 110:d08104.

Zielinski, G. A. (2000). Use of paleo-records in determining variability within the volcanism-climate system. *Quaternary Science Reviews*, 19:417–438.

Zielinski, G. A., Mayewski, P. A., Meeker, L. D., Whiltow, S., Twickler, M. S., Morrison, M., Meese, D. A., Gow, A. J., and Alley, R. (1995). The GISP Ice Core Record of Volcanism Since 7000 B.C. *Science*, 267:255–258.

Selbständigkeitserklärung

Hiermit erkläre ich, dass die Arbeit an keiner anderen Hochschule eingereicht sowie selbständig und nur mit den angegebenen Mitteln angefertigt wurde.

Potsdam, den

Sebastian Breitenbach